UCLEAR ENGINEERING

MASSACHUSETTS INSTITUTE
OF TECHNOLOGY

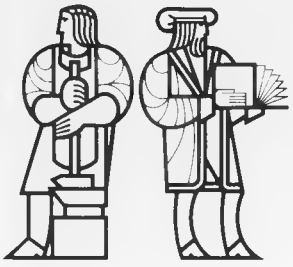

DOE/ET/37240-96TR

DOE/ET/37240--96TR

DE83 003908

FLUID-MIXING STUDIES IN A HEXAGONAL 37-PIN WIRE-WRAPPED ROD BUNDLE

by

Shih-Kuei Cheng and Neil E. Todreas

Report No. DOE/ET/37240-96TR

February 1982

N O T I C E

This report was prepared as an account of work sponsored by the United States Government. Neither the United States nor the Department of Energy, nor any of their employees, nor any of their contractors, subcontractors, or their employees, makes any warranty, express or implied, or assumes any legal liability or responsibility for the accuracy, completeness, or usefulness of any information, apparatus, product or process disclosed or represents that its use would not infringe privately-owned rights.

REPORTS AND PAPERS PUBLISHED UNDER MIT COOLANT MIXING IN LMFBR ROD BUNDLES PROJECT

A. Quarterly Progress Reports

(Available from:
National Technical Information Service
U. S. Department of Commerce
Springfield, Virginia 22151)

COO-2245-1	Period June 1, 1972 - November 30, 1972
COO-2245-2	Period December 1, 1972 - February 28, 1973
COO-2245-3	Period March 1, 1973 - May 31, 1973
COO-2245-6	Period June 1, 1973 - August 31, 1973
COO-2245-7	Period September 1, 1973 - November 30, 1973
COO-2245-8	Period December 1, 1973 - February 28, 1974
COO-2245-10	Period March 1, 1974 - May 31, 1974
COO-2245-13	Period June 1, 1974 - August 31, 1974
COO-2245-14	Period September 1, 1974 - November 30, 1974
COO-2245-15	Period December 1, 1974 - February 28, 1975
COO-2245-23	Period March 1, 1975 - May 31, 1975
COO-2245-25	Period June 1, 1975 - August 31, 1975
COO-2245-26	Period September 1, 1975 - November 30, 1975
COO-2245-28	Period December 1, 1975 - February 29, 1976
COO-2245-30	Period March 1, 1976 - May 31, 1976
COO-2245-31	Period June 1, 1976 - August 31, 1976
COO-2245-34	Period September 1, 1976 - November 30, 1976
COO-2245-38	Period December 1, 1976 - February 28, 1977
COO-2245-50	Period March 1, 1977 - May 31, 1977
COO-2245-53	Period June 1, 1977 - August 31, 1977
COO-2245-60	Period September 1, 1977 - November 30, 1977
COO-2245-63	Period December 1, 1977 - February 28, 1978
COO-2245-64	Period March 1, 1978 - May 31, 1978
COO-2245-65	Period June 1, 1978 - August 31, 1978
COO-2245-66	Period September 1, 1978 - November 30, 1978

COO-2245-69 Period December 1, 1978-February 28, 1979

COO-2245-70 Period March 1, 1979-May 31, 1979

COO-2245-71 Period June 1, 1979-August 31, 1979

COO-2245-72 Period September 1, 1979-November 30, 1979

DOE/ET/37240-75 Period December 1, 1979-February 29, 1980

DOE/ET/37240-76 Period March 1, 1980-May 31, 1980

DOE/ET/37240-85 Period June 1, 1980-August 31, 1980

DOE/ET/37240-89 Period September 1, 1980-November 30, 1980

DOE/ET/37240-90 Period December 1, 1980-February 28, 1981

DOE/ET/37240-91 Period March 1, 1981 - May 31, 1981

DOE/ET/37240-93 Period June 1, 1981 - August 31, 1981

DOE/ET/37240-94 Period September 1, 1981-November 30, 1981

DOE/ET/37240-95 Period December 1, 1981 - February 28, 1982

Reports Issued Under This Contract

B.1 Original Topical Reports (Available from National Technical Information Service, U.S. Department of Commerce, Springfield, VA 22151)

E. Khan and N. Todreas, "A Review of Recent Analytical and Experimental Studies Applicable to LMFBR Fuel and Blanket Assembly Design", COO-2245-4TR, MIT, September 1973.

E. Khan, W. Rohsenow, A. Sonin and N. Todreas, "A Simplified Approach for Predicting Temperature Distribution in Wire Wrapped Assemblies", COO-2245-5TR, MIT, September 1973.

T. Eaton and N. Todreas, "Instrumentation Methods for Interchannel Coolant Mixing Studies in Wire-Wrap Spaced Nuclear Fuel Assemblies", COO-2245-9TR, MIT, June 1974.

Y. B. Chen, K. Ip, N. E. Todreas, "Velocity Measurements in Edge Subchannels of Wire Wrapped LMFBR Fuel Assemblies", COO-2245-11TR, MIT, September 1974.

E. Khan, N. Todreas, W. Rohsenow, A. A. Sonin, "Analysis of Mixing Data Relevant to Wire-Wrapped Fuel Assembly Thermal-Hydraulic Design", COO-2245-12TR, MIT, September 1974.

E. Khan, W. Rohsenow, A. Sonin, N. Todreas, "A Porous Body Model for Predicting Temperature Distributions in Wire Wrapped Fuel and Blanket Assemblies of an LMFBR", COO-2245-16TR, MIT, June 1975.

* E. Khan, W. M. Rohsenow, A. Sonin, N. Todreas, "Input Parameters to the ENERGY Code (To be used with the ENERGY Codes Manual), COO-2245-17TR, MIT, May 1975.

* E. Khan, W. Rohsenow, A. Sonin, N. Todreas, "Manual for ENERGY Codes I, II, III", COO-2245-18TR, MIT, May 1975.

P. Carajilescov and N. Todreas, "Experimental and Analytical Study of Axial Turbulent Flows in an Interion Subchannel of a Bare Rod Bundle", COO-2245-19TR, MIT.

* B. Chen and N. Todreas, "Prediction of Coolant Temperature Field in a Breeder Reactor Including Interassembly Heat Transfer", COO-2245-20TR, MIT, May 1975.

* Revised - See Section B.2

B.1 Original Topical Reports (Continued)

F. Carre and N. Todreas, "Development of Input Data to ENERGY Code for Analysis of Reactor Fuel Bundles", COO-2245-21TR, MIT, May 1975.

H. Ninokata and N. E. Todreas, "Turbulent Momentum Exchange Coefficients for Reactor Fuel Bundle Analysis", COO-2245-22TR, MIT, June 1975.

R. Anoba and N. Todreas, "Coolant Mixing in LMFBR Rod Buncles and Outlet Plenum Mixing Transients, COO-2245-24TR, MIT, August 1975.

* B. Bosy, "Fabrication Details for Wire Wrapped Fuel Assembly Components", COO-2245-27TR, MIT, November 1975.

Ralph G. Bennett and Michael W. Golay, "Interferometric Investigation of Turbulently Fluctuating Temperature in an LMFBR Outlet Plenum Geometry", COO-2245-29TR, MIT, June 1976.

N. E. Todreas, "Thermal Analysis Methods for LMFBR Wire Wrapped Bundles", COO-2245-32TR, MIT, November 1976.

K. L. Basehore and N. E. Todreas, "Development of Stability Criteria and an Interassembly Conduction Model for the Thermal-Hydraulics Code SUPERENERGY", COO-2245-33TR, MIT, December 1976.

Robert Masterson and Neil E. Todreas, "Analysis of the Feasibility of Implementing an Implicit Temporal Differencing Scheme in the SUPERENERGY Code", COO-2245-35TR, MIT, February 1977.

S. Glazer, C. Chiu and N. Todreas, "Collection and Evaluation of Salt Mixing Data with the Real Time Data Acquisition System", COO-2245-36TR, MIT, April 1977.

B. Mikic, E. U. Khan and N. E. Todreas, "An Approximate Method for Predicting Temperature Distribution in Wire Wrapped Fuel Assemblies of an LMFBR", COO-2245-37TR, MIT, April 1977.

J. T. Hawley, C. Chiu and N. Todreas, "Development of a Technique for Subchannel Flow Rate Measurements in LMFBR Wire Wrapped Assemblies", to be issued as COO-2245-39TR 6/80. Never issued. Replaced by DOE/ET/37240-80TR.

* Revised - See Section B.2

B.1 Original Topical Reports (Continued)

* C. Chiu and N. Todreas, "WARD Blanket Assembly Pre-Test Predictions by SUPERENERGY", COO-2245-40TR, MIT, May 1977.

C. Chiu, N. Todreas, W. M. Rohsenow, "Flow Split Measurements in LMFBR Blanket Assemblies", COO-2245-41TR, MIT, April 1978.

C. Chiu, J. Hawley, W. M. Rohsenow and N. Todreas, "Pressure Drop Measurements in Wire Wrapped Blanket Assemblies", COO-2245-42TR, July 1977.

C. Chiu, W. M. Rohsenow and N. Todreas, "Mixing Experiments in LMFBR Wire Wrapped Blanket Assemblies", COO-2245-43TR, April 1978.

Yi Ben Chen and Michael W. Golay, "Coolant Mixing in the LMFBR Outlet Plenum", COO-2245-44TR, June 1977.

J. Kelly and N. Todreas, "Turbulent Interchange in Triangular Array Bare Rod Bundles", COO-2245-45TR, July 1977.

K. L. Basehore and N. E. Todreas, "Assessment of the Need to Incorporate a Variable Swirl Flow Model into the ENERGY Code", COO-2245-46TR, July 1977.

K. L. Basehore and N. Todreas, "Analysis of the Thermal-Hydraulic Behavior in the CRBR Secondary Control Assembly, Including Interassembly Heat Transfer Effects", COO-2245-47TR, July 1977.

J. G. Bartzis and N. E. Todreas, "Hydrodynamic Behavior of a Bare Rod Bundle", COO-2245-48TR, MIT, June 1977.

M. R. Fakori-Monazah and N. E. Todreas, "Measurement and Analysis of Flow Wall Shear Stress in an Interior Subchannel of Triangular Array Rods", COO-2245-49TR, MIT, August 1977.

* A. S. Hanson and N. E. Todreas, "Fluid Mixing Studies in an Hexagonal 61-Pin, Wire-Wrapped Rod Bundle", COO-2245-51TR, MIT, August 1977.

S. Glazer, N. Todreas, W. Rohsenow, and A. Sonin, "TRANSENERGY S - Computer Codes for Coolant Temperature Prediction in LMFBR Cores During Transient Events", COO-2245-52TR, MIT, February 1981.

C. Chiu, W. M. Rohsenow, and N. E. Todreas, "Mixing Experiments in an Alternating Wire Wrapped Assembly", COO-2245-54TR, MIT, December 1977.

* Revised - See Section B.2

B.1 Original Topical Reports (Continued)

* C. Chiu, W. M. Rohsenow and N. E. Todreas, "Turbulent Sweeping Flow Mixing Model for Wire Wrapped LMFBR Assemblies", COO-2245-55TR, MIT, April 1978.

* C. Chiu, W. M. Rohsenow and N. E. Todreas, "Flow Split Model for LMFBR Wire Wrapped Assemblies", COO-2245-56TR, MIT, April 1978.

K. Basehore and N. E. Todreas, "SUPERENERGY: Multiassembly Thermal-Hydraulic LMFBR Code", to be issued as Topical Report COO-2245-57TR, MIT, NED

C-N. Wong and L. Wolf, "A 3-D Slug Flow Heat Transfer Analysis of Coupled Coolant Cells in Finite LMFBR Bundles", COO-2245-58TR, MIT, February 1978.

Roohollah Karimi and L. Wolf, "Two Dimensional Structural Analysis of Reactor Fuel Element Claddings Due to Local Effects", COO-2245-59TR, MIT, April 1978.

Vincent Manno and Michael Golay, "Measurement of Heat and Momentum Eddy Diffusivities in Recirculating LMFBR Outlet Plenum Flows", COO-2245-61TR, MIT, June 1978.

* Hafeez Khan, Chong Chiu and Neil Todreas, "Laboratory Manual for Salt Mixing Test in Rod Bundles", COO-2245-62TR, MIT, October 1978.

J. Y. Kim and L. Wolf, "Fully-Developed Mixed Convection Heat Transfer and Pressure Drop in Characteristic Coolant Cells of Finite Hexagonal Bare Bundles", COO-2245-67TR, MIT, Dec. 1978.

M. K. Yeung and L. Wolf, "A Multicell Slug Flow Heat Transfer Analysis of Finite LMFBR Bundles", COO-2245-68TR, MIT, December 1978.

S. F. Wang, W. M. Rohsenow, N. E. Todreas, "Steady, Laminar, Fully-Developed Mixed Convection in Finite Rod Arrays", COO-2245-73TR, MIT, Feb. 1981.

P. D. Symolon, N. E. Todreas, "A Manual for Use with the Computer Code Superenergy-Data Reduction Version", COO-2245-74TR, MIT, February 1980.

K. J. Burns, N. E. Todreas, "Laboratory Manual for Static Pressure Drop Experiments in LMFBR Wire Wrapped Rod Bundles," DOE/ET/37240-77TR, July 1980.

K. J. Burns, N. E. Todreas, "A Comparison Between the SIMPLE and ENERGY Code Mixing Models," DOE/ET/37240-78TR, July 1980.

* Revised - See Section B.2

B.1 Original Topical Reports (Continued)

J. T. Hawley, C. Chiu, W. M. Rohsenow, N. E. Todreas, "Correlations for Subchannel and Bundle Friction Factors and Flowsplit Parameters for Laminar, Transition, and Turbulent Longitudinal Flows in Wire Wrap Spaced Hexagonal Arrays", DOE/ET/37240-79TR, Dec. 1980.

J. T. Hawley, C. Chiu, N. E. Todreas, "M.I.T. Extraction Method for Measuring Average Subchannel Axial Velocities in Reactor Assemblies", DOE/ET/37240-80TR, July 1980.

K. J. Burns, W. M. Rohsenow, N. E. Todreas, "Laminar/ Transition Sweeping Flow Mixing Model for Wire Wrapped LMFBR Assemblies", DOE/ET/37240-81TR, July 1980.

T.E. Greene, N. E. Todreas, "Criteria for Onset of Mixed Convection in Wire Wrap Spaced Hexagonal Arrays", Report DOE/ET/37240-82TR, to be issued.

D. R. Boyle and M. W. Golay, "Transient Effects in Turbulence Modelling", DOE/ET/37240-83TR, Feb. 1980.

P. D. Symolon and N. E. Todreas, "Fluid Mixing Studies in a Hexagonal 217 Pin Wire Wrapped Rod Bundle," DOE/ET/ 37240-84TR, Feb. 1981.

S. F. Wang, W. M. Rohsenow, and N. E. Todreas, "Flow Split, Pressure Drop, and Mixing Experiments in a 61 Pin Shaved-Wire Blanket Assembly, DOE/ET/37240-86TR, Feb. 1981.

S. F. Wang, N. E. Todreas, "Computer Model for M.I.T. Correlations for Friction Factors, Flow Split, and Mixing Parameters in LMFBR Wire-Wrapped Rod Assemblies, DOE/ET/ 37240-87TR, Feb. 1981.

S. F. Wang and N. E. Todreas, "Experimental Investigations of Laminar Mixed Convection in a Square Array of Bare Rods," Report No. DOE/ET/37240-88TR, Feb. 1981.

Y. N. Chan and N. E. Todreas, "A Simple LMFBR Axial Flow Friction Factor Correlation," DOE/ET/37240-92TR, Sept. 1981.

S-K. Cheng and N. E. Todreas, "Fluid Mixing Studies in a Hexagonal 37 Pin Wire-Wrapped Rod Bundle," DOE/ET/37240-96TR, Feb. 1982.

Reports Issued Under This Contract

B.2 Revised Topical Reports (Available from National Technical Information Service, U.S. Department of Commerce, Springfield, VA 22151)

S. F. Wang and N. E. Todreas, "Input Parameters to Codes Which Analyze LMFBR Wire-Wrapped Bundles," COO-2245-17TR, (Revision I), MIT, May, 1979.

** E. Khan, W. Rohsenow, A. Sonin, N. Todreas, "Manual for ENERGY Codes I, II, III Computer Programs", COO-2245-18TR, Revision I, MIT, July 1976.

** B. C. Chen and N. E. Todreas, "Prediction of Coolant Temperature Field in a Breeder Reactor Including Inter-assembly Heat Transfer," COO-2245-20TR, (Revision I), MIT, December, 1976.

H. Khan, "Fabrication Details for Wire-Wrapped Fuel Assembly Components," COO-2245-27TR, (Revision I), MIT, September, 1978.

** K. W. Chiu, "Fabrication Details for Wire-Wrapped Fuel Assembly Components," COO-2245-27TR, (Revision II), MIT, September, 1979.

C. Chiu, W. M. Rohsenow and N. E. Todreas, "Turbulent Sweeping Flow Mixing Model for Wire Wrapped LMFBR Assemblies", COO-2245-55TR, Rev. 1, MIT 1978.

** J. T. Hawley, Y. N. Chan and N. E. Todreas,"Input Parameters to Codes which Analyze LMFBR Wire Wrapped Bundles," COO-2245-17TR, (Revision II), December 1980.

** P. D. Symolon and N. E. Todreas, "Fluid Mixing Studies in a Hexagonal 61 Pin Wire Wrapped Rod Bundle," COO-2245-51TR, (Revision I), February 1981.

** Y. N. Chan and N. E. Todreas, "Turbulent Sweeping Flow Mixing Model for Wire Wrapped LMFBR Assemblies," COO-2245-55TR, (Revision II), December 1980.

** Y. N. Chan and N. E. Todreas, "Turbulent Flow Split Model and Supporting Experiments for Wire Wrapped Core Assemblies," COO-2245-56TR, (Revision I), December 1980.

** Y. N. Chan and N. E. Todreas, "Laboratory Manual for Salt Mixing Test in 37- and 217-Pin Bundles," COO-2245-62TR, (Revision I), August 1980.

** Latest Revision

Reports Issued Under This Contract

B.2 Revised Topical Reports (Continued) (Available from National Technical Information Service, U. S. Department of Commerce, Springfield, VA 22151)

** T. E. Greene and N. E. Todreas, "WARD Blanket Assembly Pre-Test Predictions by SUPERENERGY," COO-2245-40TR, Revision I, April 1981.

** Latest Revision

Reports Issued Under This Contract

C. Papers and Summaries

Y. B. Chen, K. L. Ip, and N. E. Todreas, "Velocity Measurements in Edge Channels of Wire-Wrapped LMFBR Fuel Assemblies," American Nuclear Society Transactions, Vol. 19, 1974, pp. 323-324.

P. Carajilescov and N. Todreas, "Experimental and Analytical Study of Axial Turbulent Flows in an Interior Subchannel of a Bare Rod Bundle," J. of Heat Transfer, Vol. 98, No. 2, May 1976, pp. 262-268, (Included as Appendix to Quarterly Progress Report, COO-2245-15).

E. Khan, W. Rohsenow, A. Sonin, and N. Todreas, "A Porous Body Model for Predicting Temperature Distribution in Wire-Wrapped Fuel Rod Assemblies," Nuclear Engineering and Design, 35 (1975), pp. 1-12.

E. Khan, W. Rohsenow, A. Sonin, and N. Todreas, "A Porous Body Model for Predicting Temperature Distribution in Wire-Wrapped Rod Assemblies Operating in Combined Forced and Free Convection," Nuclear Engineering and Design, 35 (1975), pp. 199-211.

R. G. Bennett and M. W. Golay, "Development of An Optical Method for Measurement of Temperature Fluctuation in Turbulent Flows," American Nuclear Society Transactions, Vol. 22, 1975, p. 581.

B. Chen and N. Todreas, "Prediction of the Coolant Temperature Field in a Breeder Reactor Including Interassembly Heat Transfer," Nuclear Engineering and Design, 35, (1975), pp. 423-440, (Included as Appendix to Quarterly Progress Report, COO-2245-23).

R. Bennett and M. W. Golay, "Interferometric Investigation of Turbulently Fluctuating Temperature in an LMFBR Outlet Plenum Geometry," Presented at the ASME Annual Winter Meeting, December, 1976, (Included as Appendix in Quarterly Progress Report, COO-2245-30).

B. B. Mikic, E. U. Khan, and N. E. Todreas, "An Approximate Method for Predicting Temperature Distribution in Wire-Wrapped Fuel Assemblies of a Liquid Metal Fast Breeder Reactor," Mech. Res. Comm., Vol. 3, (1976), pp. 353-360.

L. Wolf, R. Karimi, J. Y. Kim, C. N. Wong, and M. K. Yeung, "2-D Thermoelastic Analysis of LMFBR Fuel Rod Claddings," Paper C4/d, 4th International Conf. Structural Mechanics in Reactor Technology, San Francisco, August 1977.

Reports Issued Under This Contract

C. Papers and Summaries (Continued)

M. Yeung, and L. Wolf, "Effective Conduction Mixing Lengths for Subchannel Analysis of Finite Hexagonal LMFBR Bundles," Transactions of the American Nuclear Society, June 1977, Vol. 26, pp 463-464.

C. Chiu and N. Todreas, "Flow Split Measurements in an LMFBR Radial Blanket Assembly," Transactions of the American Nuclear Society, June 1977, Vol. 26, pp 455-456.

J. Y. Kim and L. Wolf, "Laminar Mixed Convection Heat Transfer in Finite Hexagonal Bundles," Transactions of the American Nuclear Society, (1977), Vol. 27, pp 384-385.

J. Kelly and N. Todreas, "Turbulent Interchange in Triangular Array Bare Rod Bundles," Paper NR-3, Presented at Sixth International Heat Transfer Conference, Toronto, August 1978.

C. Chiu, N. E. Todreas, and W. M. Rohsenow, "Turbulent Flow Split Experiment and Model for Wire-Wrapped Assemblies," Transactions of the American Nuclear Society, June, 1978, Vol. 28, TANSAO 28, (1978), pp 536-537, ISSN: 0003-018X.

C. Chiu, N. E. Todreas, and W. M. Rohsenow, "Pressure Drop Measurements in LMFBR Wire-Wrapped Blanket Bundles," Transactions of the American Nuclear Society, Vol. 30, pp 541-543, (1978).

C. Chiu, N. E. Todreas, and W. M. Rohsenow, "Turbulent Mixing Experiment and Model for Wire-Wrapped Assemblies," Trans. of the American Nuclear Society, Vol. 30, pp 547-548 (1978).

M. Fakory and N. Todreas, "Experimental Investigation of Flow Resistance and Wall Shear Stress in the Interior Subchannel of a Triangular Array of Parallel Rods," Jl. Fluids Eng., Vol. 101, pp 429-435 (Dec. 1979).

J. G. Bartzis and N. E. Todreas, "Turbulence Modeling of Axial Flow in a Bare Rod Bundle," Jl. Ht. Trans., Vol. 101, No. 4, pp 628-634 (Nov. 1979).

Reports Issued Under This Contract

C. Papers and Summaries (Continued)

C. Chiu, W. M. Rohsenow, and N. E. Todreas, "Prediction of Temperature Distribution in Wire-Wrapped Nuclear Fuel Rod Assemblies," Proceedings NATO Mtg, Vol. 1, pp 175-184, published by Hemisphere Pub. Co., Washington, DC (1978).

S. Glazer, T. Greene, N. Todreas, and L. Wolf, "Transient Thermal-Hydraulic Analysis in the Forced-Convection Regime (TRANSENERGY)," TANSOA, Vol. 32, Atlanta, 1979.

C. Chiu, W. M. Rohsenow, and N. E. Todreas, "Turbulent Flow Split Model and Supporting Experiments for Wire-Wrapped Core Assemblies," Nuclear Technology, Vol. 50, pp 40-52, August 1980.

J. T. Hawley, C. Chiu, W. M. Rohsenow and N. E. Todreas, "Subchannel and Bundle Friction Factors and Flow Split - Parameters for Laminar, Transition and Turbulent Longitudinal Flows in Wire Wrap Spaced Hexagonal Arrays," Proceedings ANS/ASME/NRC Int'l Topical Mtg. on Nuc. Reactor T/H, NUREG/CP-0014, 3, pp 1766-1788, Oct. 1980.

S. F. Wang, W. M. Rohsenow and N. E., "Subchannel Friction Factors for Bare Rod Arrays under Mixed Convection Conditions," Decay Heat Removal and Natural Convection in Fast Breeder Reactors, A. K. Agrawal and J. G. Guppy, Eds., Hemisphere Publishing Corp., NY pp 95-109, 1981.

Chiu, C., Morris, R., and N. Todreas, "Experimental Techniques for Liquid Metal Cooled Fast Breeder Reactor Fuel Assembly Thermal/Hydraulic Tests," Invited Paper for Special Issue of Nuclear Engineering and Design, Vol.62, No.1-3, 253-270, Dec.1980.

Bishop, A. and N. Todreas, "Hydraulic Characteristics of Wire-Wrapped Rod Bundles," Invited Paper for Special Issue of Nuclear Engineering and Design, Vol.62, No.1-3, 271-293, Dec.1980.

ABSTRACT

Flow-split, pressure-drop, and mixing experiments were performed on a 37-pin LMFBR rod bundle with a P/D = 1.154 and H/D = 13.4 to verify the Chiu-Hawley-Burns correlations and to supplement the existing data base. The isokinetic extraction method, pitot-static probe pressure-measurement method, and salt-tracer-injection method were used for these experiments.

The experimental results of the turbulent-flow-split parameters were predicted by the correlations within 3%. However, significant discrepancy between data and correlation existed in the transition flow regime (Re_b < 10,000). Flow-split parameters for Re_b < 3,000 were not attainable because of the restriction of the isokinetic extraction method. The friction factor results showed a smooth transition from the laminar-flow regime to turbulent-flow regime. They were slightly overpredicted by the correlations, especially in the laminar-flow regime.

The local swirl-flow ratio, C_{IL}, in the turbulent-flow regime was found to be about 0.28, which was within 10% of the correlation value 0.265. The predicted value of local effective enhanced eddy diffusivity, ε^*_{IL}, 0.154, however, was slightly higher than the experimental result, 0.12. Nevertheless, the experimental results were still within the ±35% accuracy of the correlations in the turbulent-flow regime. Some discrepancy in transition-flow regime was found between the experimental results and predictions, especially for ε^*_{IL}.

ACKNOWLEDGEMENTS

The authors would like to thank Yee-Ning Chan for his great help in constructing the new bundle. Thanks are also due to Joseph (Tiny) Caloggero of the Engineering Project Laboratory and Ray Johnson of the Mechanical Engineering Machine Shop for their assistance in modification of the experimental apparatus.

Sponsorship of this work through the Department of Energy is also acknowledged.

NOMENCLATURE

A_b	Bundle flow area (in^2)
A_1	Interior subchannel flow area (in^2)
A_2	Edge subchannel flow area (in^2)
A_3	Corner subchannel flow area (in^2)
C_1	Swirl flow ratio
C_{1L}	Local swirl flow ratio
C_i	Detected subchannel salt concentration
C_i^*	Dimensionless ratio of salt concentration
C_{ip}^*	Predicted dimensionless salt concentration by DRV code
D	Rod diameter (in)
D_F	Flat to flat distance (in)
D_g	Distance between rods and duct wall (in)
D_w	Wire diameter (in)
De_b	Bundle average equivalent hydraulic diameter (in)
De_1	Interior subchannel equivalent hydraulic diameter (in)
De_2	Edge subchannel equivalent hydraulic diameter (in)
f	Looseness factor
f_b	Bundle average friction factor
f_1	Interior subchannel friction factor
f_2	Edge subchannel friction factor
G	Bundle flow rate (GPM)
H	Wire lead length (in)
m_b	Bundle volumetric flow rate
m_L	Loop volumetric flow rate

m_1	Interior subchannel volumetric flow rate
m_2	Edge subchannel volumetric flow rate
m_j	salt solution injection flow rate
N_{RING}	Number of rings of rods in an assembly
N_R	Number of pins in one assembly
P	Rod pitch (in)
ΔP_b	Bundle average pressure drop (inch water)
ΔP_1	Interior subchannel pressure drop (inch water)
ΔP_2	Edge subchannel pressure drop (inch water)
Re_b	Bundle average Reynolds number
Re_1	Interior subchannel Reynolds number
Re_2	Edge subchannel Reynolds number
S	Defined as $(A_2/A_1)/N_R + (A_3/A_1)/N_R^2$
T_{ff}	Flat to flat tolerance (in)
V_b	Bundle average flow velocity (ft/hr)
V_1	Interior subchannel flow velocity (ft/hr)
V_2	Edge subchannel flow velocity (ft/hr)
V_T	Average transverse velocity in edge region
X_1	Interior flow split parameter
X_2	Edge flow split parameter
ε_1^*	Effective enhanced eddy diffusivity (ft^2/hr)
ε_{1L}^*	Local effective enhanced eddy diffusivity
ν	Kinematic viscosity of water (ft^2/hr)
ϕ_t	Parameter defined by $V_T/V_b \tan\theta$ at turbulent flow regime
θ	Wire-wrap angle

TABLE OF CONTENTS

CHAPTER 1

INTRODUCTION

Helical wire-wraps are widely used in LMFBR (Liquid Metal Fast Breeder Reactor) fuel assemblies to promote coolant mixing and maintain proper spacing between fuel pins. Multi-channel analysis codes have been developed to predict temperature fields in these wire-wrapped LMFBR cores for thermal design and performance evaluation. Specific interest has been focused on predicting the fuel assembly duct wall temperatures for bowing calculations and the maximum fuel pin cladding temperatures.

Two major semi-empirical approaches have been used to develop these codes. The first approach is embodied in the COBRA and THI-3D codes which solve the coupled continuity, momentum and energy equations. The second approach is embodied in the ENERGY and COTEC codes which utilize only the lumped subchannel energy equation, thereby avoiding the need for the momentum-continuity coupling by supplying additional input data [1]. To use the later method, the following information is required for those additional input data:

(a) the axially-averaged flow distribution (i.e., flow split parameters) within the bundle,

(b) bundle overall friction factor, and

(c) the effective coolant mixing flow between the interior subchannels and the sweeping velocity in

the edge subchannels (i.e., mixing parameters ε^*_{IL} and C_{IL}).

Experimental studies with wire-wrapped bundles using either tracers or heated pins have been conducted by many investigators [2]. Most of these experiments were designed to simulate either the fuel assembly with pitch to diameter ratio (P/D) near 1.25 or the blanket assembly with P/D near 1.07. Based on these data, Chiu, Hawley and Burns calibrated the empirical constants in their correlations which predict those input parameters required in the ENERGY code [3,4].

Because it is not used as a typical design, a bundle with P/D in the middle of the two extremes, say near 1.15, has not been investigated at M.I.T. before. To verify the Chiu, Hawley and Burns correlations and to fill the gap in the data base, a 37-pin bundle with P/D equal to 1.154 and H/D equal to 13.4 was fabricated and studied. Flow split, pressure drop and mixing experiments were performed to obtain flow split parameters, friction factors and mixing parameters. The results of flow split experiments were used in the other two experiments to reduce the friction factors and mixing parameters. Figure 1.1 shows the relations among these experiments.

Previous experiments of this geometry were performed [5,6] but their data were flawed due to the degraded dimensional control in the bundle housings which were salvaged from previous blanket geometry tests. In this attempt a new,

well-controlled housing is used. No new experimental methods were introduced except for some minor modifications which will be elaborated in the next section.

CHAPTER 2

TEST SECTION AND EXPERIMENTAL METHOD

2.1 Test Section

2.1.1 Test Section Design and Fabrication

The design and fabrication of this 37-pin bundle test section is essentially identical to the previous one [5], except for the housing, rod diameter and wire diameter. The dimensions of the previous aluminum and plexiglass housing were found to be non-uniform. Since it was too expensive to build a new housing, the new 37-pin assembly was designed to fit an extruded, hexagonal housing originally used for a 217-pin bundle. A non-standard rod diameter of 0.592 inch was selected and this called for modifications to the collars and clamps originally machined for the 0.5 inch diameter rod. The rods were machined in accordance with the procedure documented by B. Bosy [7]. The wire-wrapping device was also modified to wrap with an 8-inch lead length.

The hexagonal mounting device of the 217-pin assembly was inverted and was drilled to accommodate seven 1/4-inch rods. These seven rods were aligned horizontally to secure the 37 rods of the bundle vertically. The rods were assembled onto the hexagonal mounting device and then the whole assembly was inserted into the housing until the ends of the rods were flush with the housing exit plane. The hexagonal mounting

was then fastened securely to the housing with six screws. Figure 2.1 illustrates the relative positions of housing, hexagonal mounting device and rods and some design parameters.

Two hollow rods, one in the center position and the other adjacent to the wall, were installed in this bundle. These are the instrumentation rods used for inserting the injector to measure the pressure drop in the pressure drop experiment and to inject the saline solution in the mixing experiment. Two stainless steel plugs were fabricated to plug the exit end of these two hollow rods when they were not in use.

The average flat to flat distance of the housing was 4.336". With 0.592" rod diameter and 0.089" wire diameter, the tolerance was calculated to be 0.027". After the assembly was mounted in place, the distances between each adjacent pair of rods and between the edge rods and duct at the exit plane were measured. The average gaps between rods and between edge rod and duct were 0.0913" and 0.0964" respectively. The looseness factor, according to its definition [8], was

$$F \equiv (P-D-D_w) \times \sqrt{3} \times N_{RING}/T_{ff} = 0.447$$

where

$$T_{ff} \equiv D_F - (\sqrt{3}\, N_{RING}+1)(D+D_w)$$

$$N_{RING} \equiv \{[3 + (12N_R-3)^{1/2}]/6\} - 1$$

The design value of the wire lead length was 8". However, after the rod was wrapped with wire, a lead length of a little less than 8" was shown by the wire position at the exit plane. The correct value was calculated to be 7.935". This may be attributed to the precision of the wire wrapping device.

The bundle geometry and some important as-built geometrical parameters at the exit plane are shown in Figure 2.2, and some subchannel based geometrical parameters are tabulated in Table 2.1.

2.1.2 Test Loop

The test loop of this experiment was exactly the same as the one used before. Figure 2.3 shows this loop. For flow rates higher than 56 GPM, flowmeter M3 was used. Otherwise, flowmeters M1 and M2 were used.

Flowmeter M3 (40-300 GPM) was calibrated using the technique discussed in Appendix A of Reference 5. However, the calibrated values were found to be in error at low flow rates (from 40 to 70 GPM). The readings in M1 (0-14 GPM) and M2 (0-37 GPM) were accurate. Since the same pressure drop implies the same flow rate, the readings of M1 plus M3 can be used to calibrate M3 at low flow rates from 40 to 56 GPM with the help of pressure drop data. The new calibration curve of M3 is shown in Figure 2.4.

2.2 Flow Split Experiment

The flow extraction by the isokinetic condition measurement method of Reference 9 was used in the flow split experiment. No attempt was made to measure the corner subchannel flow rates because it was not practical to fabricate a small collector to collect the corner subchannel flows alone. The flow velocity of the corner subchannel was assumed to be the same as that of the edge subchannel.

The flat to flat measuring technique [5] was used in collecting interior subchannel flow to reduce experimental time. Therefore, instead of the entire 54, only the 18 interior subchannels which are numbered in Figure 2.5 were measured. Also shown in this figure are the three rings of measured interior subchannels and the wire position in two different types of interior subchannels. The effect of the wire was eliminated when the flow rates of all 6 subchannels in each ring were measured and averaged. Therefore, an average interior flow rate over one lead length was obtained by averaging 18 interior flow rates. A similar situation was afforded by the edge subchannels except that there is only one ring, and the wire positions were the same in the three subchannels of each face. For each run, i.e., at each bundle flow rate, these 36 subchannel flow rates were collected to provide a data set at a given flow condition.

The isokinetic method was not applicable at low bundle flow rates because the siphon head was not maintainable while

attempting to reach the isokinetic condition. For this bundle, this condition was observed at flow rates lower than 70 GPM. A short stainless steel rod was inserted into the sampling tube to decrease the collecting flow area so as to prevent the loss of siphon head. Even with this modification, the lowest flow rate at which the isokinetic condition was attainable was 32.5 GPM, which corresponds to Re_b = 3470 and is still in the transition flow regime.

The highest flow rate attainable was about 220 GPM. To extend the data to higher Reynolds numbers, steam was injected into the water tank to increase the water temperature and hence decrease its kinematic viscosity. However, only 10°C difference was obtained, and kinematic viscosity decreased only to about 0.8 of its initial value.

2.3 Pressure Drop Experiment

The pressure drop experiment was discussed in detail in Reference 10. Two collinear 30° holes with respect to rod vertical axis were drilled on each of the two instrumentation hollow rods: one is 8" below the exit end and the other is 32" below the exit end. Figure 2.6 shows an instrumentation rod, the 30° holes and the injector which was used as a pressure tap in the pressure drop experiment. The center instrumentation rod was aligned such that the 30° holes were directed into subchannel 1 to measure the interior subchannel pressure drop. For the edge one, the holes were directed

into subchannel 71 to measure edge subchannel pressure drop (c.f. Figures 2.2 and 2.5).

The 30° hole was selected by the trade-off between easy manufacture and less disturbance to the flow condition. Ideally, the hole should be zero degrees to prevent any horizontal velocity of the injection tracer. However, this was impossible to fabricate, and hence 30° was selected to make drilling possible.

The 8" and 32" depths were selected because the pressure drop across several integral numbers of lead lengths was desired. Pressure drop across these three lead lengths would not be affected by the disturbance of pressure field caused by wire present, and would reduce the percentage measuring error.

Originally, the pressure was measured by two differential pressure gauges with ranges of 0-50 inches of water and 0-150 inches of water respectively. It was found that in laminar flow, the pressure drop was so small ($\sim$ 0.1 inch of water) that it was not resolvable by the pressure gauge. To improve the resolution, a one meter long manometer was implemented to measure the static pressure at low and intermediate flow rates. When the flow rate was higher than 100 GPM, the pressure at the 32" depth was higher than 100 cm of water. Then the pressure had to be measured by a 0-150 inch pressure gauge.

The manometer was constructed simply by attaching a glass tube to a meter stick [6]. It was mounted such that the bottom end of the glass tube was a little lower than the water level in the upper plenum. A clear plastic tube connected this bottom end to the upper end of the injection tube. The hydrostatic head at the pressure tap drove the water to a level, and the reading was recorded as the static pressure.

Pressure at different flow rates were first measured at one position. Then the pressure tap was slid to the other position, and the pressure at the same flow rates were measured. The difference between these two readings is the static pressure drop across the distance between the two positions.

2.4 Mixing Experiments

The experimental equipment and procedure of this mixing experiment were virtually identical to those used in the previous mixing tests [11, 12]. A flow separator was not required in this 37-pin bundle because the subchannel flow area was large enough for the platinum tips of the probes to be inserted directly in the subchannel without electrically shorting them by inadvertant conduct with the rods. A probe support structure was designed and fabricated to hold the probes in precise position [5].

Figure 2.7 shows the subchannel numbering scheme which is the same as that used in the SUPERENERGY-DRV code [13].

Previous experiments used a slightly different scheme.

The data acquisition system [14] used was identical to that of the previous tests. However, the data storage function of that system was not working, and the data sets had to be recorded manually. The data sets were first photographed and then transcribed by hand with the help of a microfiche reader.

Only the 32" depth holes of the two injection rods shown in Figure 2.6 were used to inject saline water. The selection of this depth was based on past experience which indicated that a 3-5 lead length injection depth would give the best result for the mixing parameters [15]. The interior injection rod was designed to inject saline water into subchannel 1; and the edge injection rod, subchannel 71.

Since the calibration data were the base for transfering the probe resistances detected in the mixing step to the salt concentrations in each subchannel, the probe calibration step was the most important step in this experiment. An error in one calibration data set would cause an error in all the subsequent concentrations of the mixing result for that subchannel. Therefore, several data sets were taken at each calibration concentration to prevent any possible flawed data.

Following the recommendations of Reference 11, the calibration concentrations were selected to be 0, 2, 4, 8, 12, 16 and 20 grams of salt per 100 lbm of water, and the concentration of the saline injection water was set at 800 grams/100

lbm. It was later found that for this injection concentration, salt concentrations of less than 2.0 grams/100 lbm were detected in practically all the subchannels. This meant that only two calibration points, i.e., 0 and 2 grams/100 lbm, could be used for calibrating data. Since the calibration curve (probe resistance vs. salt concentration) is concave [14], this would give higher detected concentration than it should be, and hence make the mass balance ratio higher than 1. However, the relative dimensionless ratios of salt concentration were only slightly affected because all the probes were calibrated this way and boosted to a higher level by the same factor.

In the mixing step, the injection flow rate was calculated at each bundle flow rate by equating the axial component of the injection velocity with the bundle average axial velocity to minimize the disturbance to the flow. Background calibration correction data were taken for each flow rate before the salt tracer was injected. This calibration correction data not only eliminated the discrepancy caused by the flow effect, but also compensated the decreasing sensitivity of each probe with time due to degradation of the platinized probe surface. Mixing data were then taken after the injected flow rate was steady at preset value.

CHAPTER 3

EXPERIMENTAL RESULTS

The bundle average Reynolds number, Re_b, is given by

$$Re_b = \frac{V_b D_{eb}}{\nu}$$

Substituting the numerical value of De_b and conversion factor for flow rate, we get

$$Re_b = 4.07 \frac{G}{\nu}$$

where G is is GPM and ν is in ft^2/hr. The kinematic viscosity ν as a function of temperature is tabulated in Table 3.1 for water at 1 atm.

Both the flow split and pressure drop experiments were performed over a range of flow rates. In the pressure drop experiments, data were taken from very low flow rates ($\sim$ 2 GPM, $Re_b \sim 100$) to the highest flow rate allowed by the overflow capacity of the upper plenum ($\sim$ 230 GPM, $Re_b \sim 23{,}000$). However, as mentioned in Section 2, flow split experiments were not possible at low flow rates ($\lesssim$ 30 GPM, $Re_b \lesssim 3{,}000$). Therefore, laminar flow split data were not available for reducing laminar mixing data.

In the mixing experiments, data were taken for bundle flow rates from $\sim$ 2 GPM to $\sim$ 250 GPM, corresponding to $Re_b \sim$

200 to 30,000 for the interior injection position. The difference in Re_b for the same bundle flow rate (e.g., 2 GPM) between this experiment and the pressure drop experiment was caused by differences in the water temperature on the dates that they were performed. For the edge injection position, the data were taken from $Re_b \sim 400$ to $Re_b \sim 26{,}000$. Higher flow rates were attainable in the mixing experiments because the probe supporter placed at the bundle exit plane reduced the flow impulse, thereby increasing the effective overflow capacity of the existing upper plenum.

All the experimental results will be compared with the Chiu, Hawley and Burns correlations which are the basis of the WIWRAP code [4]. Table 3.2 lists all the predicted parameters calculated by the WIWRAP code as functions of Re_b for this bundle.

3.1 Flow Split Experimental Results

Let m_1 and m_2 be the average volumetric flow rate of eighteen interior and eighteen edge subchannels, respectively. Under the assumption that $x_3 = x_2$, the collected bundle flow rate is

$$m_b = 54m_1 + 18m_2 + 6\left(\frac{A_3}{A_2} m_2\right)$$

$$= 54m_1 + 20m_2$$

since $A_3 = 0.0420$ in^2 and $A_2 = 0.1273$ in^2.

The average velocities of bundle, interior and edge subchannels are

$$V_b = \frac{m_b}{A_b} \quad , \quad V_1 = \frac{m_1}{A_1} \quad , \quad V_2 = \frac{m_2}{A_2}$$

The flow split parameters were then obtained by their definitions:

$$x_1 \equiv \frac{V_1}{V_b} \quad , \quad x_2 \equiv \frac{V_2}{V_b}$$

To check the validity of the isokinetic technique, the total collected flow rate m_b was compared with the calibrated flow rate m_L, and their difference was expressed as the mass balance error:

$$\text{mass balance error} = \frac{m_b - m_L}{m_L}$$

Table 3.3 shows the experimental results of sixteen runs of flow split experiments. The flow split parameters versus bundle Reynolds number are illustrated in Figures 3.1 and 3.2. Figure 3.3 shows a typical collected normalized flow split map for eighteen interior and eighteen edge subchannels at Re_b = 10480. The normalized flow split maps for all sixteen runs are presented in Appendix A. Note that in all these figures the flow split value in each subchannel was the average velocity in each subchannel divided by bundle average velocity, where subchannel average velocity was calculated by the

collected subchannel flow rate divided by its actual (i.e., with or without wire) flow area.

The error associated with the experimental results of flow split parameters by using this isokinetic extraction method was estimated to be ±5% in the turbulent flow regime [16]. For the transition flow regime (say, $Re_b < 6,000$), the isokinetic condition is difficult to achieve, so that the uncertainty in data would increase. The error would conservatively be estimated to be doubled, i.e., ±10% for $Re_b < 6,000$. These errors were illustrated in Figures 3.1 and 3.2 by the error bars associated with the two data points: one in the turbulent flow regime, the other in the transition/laminar flow regime.

3.2 Pressure Drop Experimental Results

The purpose of this experiment was to find the bundle average and subchannel friction factors. Table 3.4 shows the pressure drop experimental data, where the bundle average pressure drop ΔP_b was simply determined from a force balance which averages the pressure drop data for interior (ΔP_1) and edge (ΔP_2) subchannel as follows:

$$\Delta P_b = \frac{N_1 A_1 \Delta P_1 + N_2 A_2 \Delta P_2}{N_1 A_1 + N_2 A_2} \qquad (3.1)$$

$$= 0.591\ \Delta P_1 + 0.409\ \Delta P_2$$

The relationship between the pressure drop data and the friction factors are

$$\Delta P_i = f_i \frac{L}{De_i} \frac{\rho V_i^2}{2g_c} \tag{3.2}$$

where L is the distance across which the pressure drops were measured. It is three lead lengths, i.e., 24" in this experiment.

Substituting L, De_i, and some conversion factors into Equation (3.2), we get the following formulae:

$$f_b = 18.45 \frac{\Delta P_b}{G^2}$$

$$f_1 = 17.01 \frac{\Delta P_1}{(x_1 G)^2}$$

$$f_2 = 21.58 \frac{\Delta P_2}{(x_2 G)^2} \tag{3.3}$$

where ΔP_i is in inches of water, G is in GPM, and x_i are the experimental flow split results.

To investigate the subchannel friction factor as a function of subchannel Reynolds number, a knowledge of the subchannel Reynolds numbers is required. They are calculated simply from

$$Re_i = Re_b \frac{De_i}{De_b} x_i$$

i.e.,

$$Re_1 = 0.92\ Re_b x_1$$

$$Re_2 = 1.17\ Re_b x_2 \qquad (3.4)$$

As previously mentioned, the flow split parameters were not available for $Re_b \leq 3{,}500$; hence, the subchannel friction factors and Reynolds numbers are not calculable for this range unless the flow split parameters are estimated. We simply assume that the flow split parameters are constant for $Re_b \leq 3{,}500$. Another extreme assumption, i.e., extrapolating the data curve to get the unattainable flow split parameters, however, is worthwhile investigating. Appendix B presents the comparison between these two assumptions.

Table 3.5 tabulates the calculated results of Re_i and f_i. Figures 3.4, 3.5 and 3.6 illustrate f_b, f_1 and f_2 versus Re_b, Re_1 and Re_2, respectively.

The error associated with this pressure drop experiment was discussed in detail in Reference 6. According to this reference, the errors involved in friction factors are about ±60% at $Re_b = 200$, 30% at $Re_b = 500$ and 20% for $Re_b \geq 6{,}000$, as illustrated by the error bars in Figures 3.4, 3.5 and 3.6.

3.3 Mixing Experimental Results

3.3.1 Data Reduction Code

An intermediate data reduction subroutine, MIXDATA, was added into the SUPERENERGY-DRV code (hereafter referred to as DRV) to convert probe resistances to dimensionless salt concentrations. The original version of DRV (DRV1) was used rather than DRV2, because no improvement was found by using DRV2 [17].

The DRV calibrates the mixing parameters ε_1^* and C_1 by finding the values of ε_1^* and C_1 that generate a distribution which most closely match the salt concentration distribution obtained from the mixing experiment. The prediction distribution which yields a "best fit" to the experimental distribution is determined by the mean square indicator (MSI), defined as

$$MSI = \sqrt{\sum_i (C_i^* - C_{ip}^*)^2}$$

where

C_i^* = experimental dimensionless salt concentration

C_{ip}^* = prediction dimensionless salt concentration by DRV code

i = number of subchannels, 78 in this experiment

The values of ε_1^* and C_1 which correspond to a minimum value of MSI are the reduced results.

DRV was also modified to search for the best fit mixing parameters automatically. This revised DRV requires an initial guess of ε_1^* or C_1, while the old version requires the maximum and minimum bounds of these parameters. This revised code is listed in Appendix C.

3.3.2 Experimental Results

i) Effective Enhanced Eddy Diffusivity

The interior injection results were reduced to get the effective enhanced eddy diffusivity ε_1^*. Since in this case very little salt reached the edge region of the bundle, the results of ε_1^* reduced from DRV were relatively insensitive to the value of C_1 input to DRV. For this bundle, Chiu-Burns' mixing parameter correlations predict C_1 to be 0.29 for $Re_b > 3{,}000$, 0.20 for $Re_b = 1{,}000$ and 0.1 for $Re_b = 200$. To reduce ε_1^*, C_1 was fixed at 0.3 for $Re_b > 3{,}200$, 0.2 for $3{,}200 \geq Re > 1{,}500$ and 0.1 for $1{,}500 \geq Re_b$.

The flow split parameters must be input to DRV to calculate the dimensionless salt concentration and the mass balance ratio which is defined by the total detected salt divided by injected salt, i.e.,

$$\text{mass balance ratio} = \sum_i m_i C_i / m_j C_j$$

Also, in reducing mixing parameters, flow split parameters are required to give different velocities in interior and edge subchannels. Note that the flow split values have no effect on determining the local value of ε^*_{1L}, and have only slight effect on determining C_{1L} (see Appendix E for discussion of this effect). However, ε^*_1 and C_1 will be affected by these parameters, since they are calculated from $\varepsilon^*_{1L} \cdot x_1$ and $C_{1L} \cdot x_2$, respectively. The experimental results of Figures 3.1 and 3.2 with the assumption that the flow splits are constant for $Re_b < 3,500$ were used to calculate the mixing parameters ε^*_1 and C_1.

Table 3.6 illustrates the results of 16 runs for interior injection experiments. Figures 3.7 and 3.8 show ε^*_1 and ε^*_{1L} as functions of Re_b, respectively. The Chiu-Burns correlation for ε^*_{1L} is plotted in Figure 3.8 for comparison. Figure 3.9 shows a typical experimental dimensionless salt concentration map (left side), and the dimensionless salt concentration map predicted by DRV (right side) for an interior injection case. The detailed experimental and predicted dimensionless salt concentration maps for all 16 runs are included in Appendix D.

ii) Swirl Flow Ratio

The edge injection results were reduced to get the swirl flow ratio, C_1. About half of the salt tracer diffused into the interior region in this case, and this must be simulated by inputing the correct ε^*_1 into the DRV to reduce C_1. However,

ε_1^* has already been determined in a previous paragraph without the precise knowledge of C_1.

Table 3.7 illustrates the results of 14 runs for edge injection experiments. Figures 3.10 and 3.11 show C_1 and C_{1L} as functions of Re_b, respectively. The Chiu-Burns correlation for C_{1L} is also present in Figure 3.11 for comparison. Figure 3.12 shows the same kind of maps for edge injection as does Figure 3.9. The detailed maps of all 14 runs are also included in Appendix D.

iii) Error Analysis

The error associated with this experiment is discussed in detail and evaluated in Appendix E. The results are shown in Table 3.8. These errors are also illustrated by the error bars in Figures 3.7, 3.8, 3.10 and 3.11.

CHAPTER 4

DISCUSSION AND COMPARISON OF RESULTS

4.1 Flow Split Parameters

As tabulated in Table 3.2, all the mass balance errors are less than 5% except the one at the lowest flow rate. This was expected because at that flow rate, the isokinetic condition was very difficult to achieve, hence the larger percentage error.

Mass balance error is not only caused by the error inherent in the isokinetic technique, but also by the error in recording the indicated flow rate and by the accuracy of the calibration curve. All the mass balance errors except that for the highest flow rate are negative, indicating that either the calibration curve of flow meter is not accurate or that there is a systematic error in the measuring technique. However, all these factors lead only to a mass error of 5% or less. This accuracy in mass balances serves to establish confidence in the isokinetic procedure.

Figures 3.1 and 3.2 show that the transition flow split behavior starts from Re_b = 12,000. This is consistent with data from Chiu's 61-pin bundle with P/D = 1.067 and H/D = 8 [8]. Also, the trends of this transition phenomenon are quite similar in these two bundles. Thomas Chiu's 37-pin data [5] were considered to be flawed because the bundle dimensional symmetry was poor and the transition phenomenon

was not shown. Symolon's 217-pin bundle data [17] (P/D = 1.25, H/D = 52) also showed this transition phenomenon, but considerable scatter existed.

Figures 3.1 and 3.2 show excellent agreement of data with the Chiu-Hawley correlations in the turbulent flow regime. Flow split experiments of Symolon's 217-pin bundle also confirmed the validity of the correlations at the turbulent flow regime. Note that the correlations for turbulent flow split were calibrated before Symolon's experiment and the present work were done. However, significant discrepancy between the experimental results and predictions was found in the transition/laminar flow regime for all these bundles. The correlations for the transition/laminar flow regime need to be revised and/or recalibrated.

Figure 3.2 as well as the results of Chiu's 61-pin bundle (H/D = 8) and Symolon's 217-pin bundle show that x_2 decreases before it saturates. However, some bundle data show a different trend: x_2 increases before it saturates, e.g., Chiu's 61-pin with P/D = 1.067, H/D = 4 [8] and Wang's shaved-wire 61-pin with P/D = 1.067, H/D = 8 [18]. Besides, some investigators' data show that x_2 is less than x_1, e.g., Lorenz's isokinetic sampling results [19] and some unpublished Japanese data. These might be caused by experimental error, which would introduce these opposite results since x_1 and x_2 were quite close to 1.0.

4.2 Friction Factors

Equations (3.1) and (3.3) show that the bundle friction factor is determined only by experimental subchannel pressure drop data. On the other hand, the subchannel friction factors were determined by both subchannel pressure drop and flow split data. Note that the flow split behavior and hence the subchannel friction factors are determinable only from experimental flow split data.

A transition regime of bundle friction factor was observed to start from $Re_b \simeq 400$ in Figure 3.4 as well as all the other wire wrapped bundle data. We can arbitrarily define $Re_b < 400$ as the laminar flow regime and high Re_b (say 10,000) as the turbulent flow regime for this friction factor's behavior.

In the laminar flow regime, f_b was observed to behave as C_L/Re_b. The constant C_L for this bundle was calculated to be 95, as shown in Figure 3.4. C_L was 90 and 160 for Chiu's H/D = 8 and 4 bundles, respectively [19]; 70 for Symonlon's 217-pin [17], and 85 for T. Chiu's 37-pin (P/D = 1.15, H/D = 21.0) [5].

As for the turbulent flow regime, the data for $Re_b >$ 10,000 show $f_b = 0.20/Re_b^{0.18}$ or $0.40/Re_b^{0.25}$, depending on which relation was used. The second one was a better fit. Since there is error associated with the data, it is difficult to ascertain which relation is more accurate. However, Hawley correlated the world data into $f_b = C_T/Re_b^{0.18}$ in his

correlation [20]. If $f_b = C_T/Re_b^{0.25}$, then the following C_T values apply: 0.48 and 0.90 for Chiu's H/D = 8 and 4 bundles, respectively; 0.29 for Symolon's 217-pin, and 0.31 for T. Chiu's 37-pin.

Figure 3.4 shows that Chiu-Hawley's friction factor correlations slightly overpredict f_b, especially in the laminar flow regime.

4.3 Mixing Parameters

As shown in Tables 3.5 and 3.6, all the mass balance ratios except run 22 are higher than 1. The average value is about 1.4. This high mass balance ratio was expected because of the calibration procedure discussed in Section 2.3.

For interior injection, for all runs except Re_b of 430 and 200, the peak salt concentration occured at subchannel 2 instead of the injection subchannel 1 (refer to Appendix D). This phenomenon, namely that the maximum concentration did not occur at the injection subchannel at the bundle exit plane, had been observed before and was the motivation for the development of PRV-2. This behavior is believed to be caused by wire located about 1/4 lead length downstream of the injection hole, which caused the local sweeping flow to be a maximum at the injection position. Large amounts of the salt solution were diverted into subchannel 2 right after they had been injected. However, at very low flow rates (Re_b = 220, 430), this diversion effect decreased and the peak concentration remained in subchannel 1.

Uncertainty in determining ε_1^* would be caused by this maldistribution. To investigate this effect, subchannel 2 was used as the injection subchannel to reduce ε_1^*. The deviation was found to be about 10%, and was included as a component in the data reduction error, as discussed in Appendix E. The disturbance of a 30° injection direction also caused some uncertainty, especially in determining the swirl flow ratio.

Figures 3.7, 3.8, 3.9 and 3.10 show a clear trend of mixing parameters as functions of Re_b. As Re_b increases, these parameters increase to a saturated value. This kind of trend was also observed in Chiu's two 61-pin bundle (P/D = 1.067, H/D = 8, 4) [12] and Symolon's 217-pin bundle [17] results. The previous 37-pin bundle (P/D = 1.15, H/D = 21) data performed by Burns [6] was suspicious because the trend at the transition region was opposite. However, its turbulent (saturated) value of ε_1^* ($\sim$ 0.10) was almost the same as the present work ($\sim$ 0.11), while the swirl flow ratio C_1 ($\sim$ 0.20) was lower than the present work ($\sim$ 0.28).

The Chiu-Burns' correlations for mixing parameters in the turbulent flow regime predict the local swirl flow ratio C_{1L} accurately, but they overpredict the local effective enhanced eddy diffusivity ε_{1L}^*. Nevertheless, the data were still within the ±35% accuracy of the prediction curve. However, the transition/laminar mixing correlations were found to be flawed, since they could not accurately fit the

trend as shown in Figures 3.8 and 3.10. Other bundle results showed the same conclusion [12]; hence, the correlations may need to be revised.

It is interesting to compare ϕ_t, defined as the average transverse velocity in the edge region, V_T, divided by $V_b \tan\theta$, which is the transverse velocity component if the flow direction is the same as the wire direction, in the turbulent flow regime for different tested bundles. Note that ϕ_t can also be interpreted as $C_1/\tan\theta$. Table 4.1 shows this parameter from available data sets. The trend is clearly shown in this table: for high H/D, ϕ_t is larger than 1; for low H/D, ϕ_t is less than 1. The present work has a H/D = 13.4, about the median of the range of H/D's and, as expected, its $\phi_t \simeq 1.0$.

Finally, we compare this work's results with the other investigators' results of ε^*_{1L} and C_{1L} in the turbulent flow regime. To reduce the wire-wrapped angle effect, these parameters are multiplied by $\sqrt{\pi^2 P^2 + H^2} \;/\; P \quad (= \pi/\sin\theta)$ which, as we investigate from Chiu's correlation, is the only major factor introduced by different lead length [27]. Figures 4.1 and 4.2 illustrate these modified parameters as functions of P/D obtained by many investigators as well as Chiu's correlation. Table 4.2 lists the geometric parameters and types of experiment used by these investigators. Note that no data was available with P/D near 1.15 for the ε^*_{1L} parameters before our work. As shown, the C_{1L} parameters were well

predicted, while the ε^*_{1L} parameters scattered around the prediction curve. Figure 4.1 also shows that the turbulent ε^*_{1L} correlation is almost the best fitted curve; hence, no improvement is required in the present stage.

REFERENCES

1. Khan, E., Rohsenow, W., Sonin, A., and Todreas, N., "Manual for ENERGY Codes I, II, III Computer Programs," COO-2245-18TR, Revision I, M.I.T. (July 1976).

2. Bishop, A.A. and Todreas, N.E., "Hydraulic Characteristics of Wire-Wrapped Rod Bundle," Nucl. Eng. and Des., 62, 271-293 (1980).

3. Hawley, J.T., Chan, Y.N., and Todreas, N.E., "Input Parameters to Codes which Analyze LMFBR Wire-Wrapped Bundles," COO-2245-17TR, Revision II, M.I.T. (May 1979).

4. Wang, S.F. and Todreas, N.E., "Computer Model for M.I.T. Correlations for Friction Factors, Flow Splits, and Mixing Parameters in LMFBR Wire-Wrapped Rod Assemblies," COO-2245-87TR, M.I.T. (February 1981).

5. Chiu, T., "Fluid Mixing Studies in a Hexagonal 37-Pin Wire Wrapped Rod Bundle," S.M. Thesis, Dept. Nuclear Engineering, M.I.T. (September 1979).

6. Burns, K., "Thermal Hydraulic Studies of a 37-Pin LMFBR Wire Wrapped Rod Bundle," S.M. Thesis, Dept. Nuclear Engineering, M.I.T. (July 1980).

7. Chiu, K.W., "Fabrication Details for Wire-Wrapped Fuel Assembly Components," COO-2245-27TR, Revision II, M.I.T. (September 1979).

8. Chiu, C. and Todreas, N.E., "Flow Split Measurements in LMFBR Blanket Assemblies," COO-2245-41TR, M.I.T. (April 1978).

9. Hawley, J.T., Chiu, C., and Todreas, N.E., "M.I.T. Extraction Method for Measuring Average Subchannel Axial Velocities in Reactor Assemblies," DOE/ET/37240-80TR, M.I.T. (July 1980).

10. Burns, K.J. and Todreas, N.E., "Laboratory Manual for Static Pressure Drop Experiment in LMFBR Wire Wrapped Rod Bundles," DOE/ET/37240-77TR, M.I.T. (July 1980).

11. Chan, Y.N. and Todreas, N.E., "Laboratory Manual for Salt Mixing Test in 37- and 217-Pin Bundles," COO-2245-62TR, Revision I, M.I.T. (August 1980).

12. Chiu, C. and Todreas, N.E., "Mixing Experiments in LMFBR Wire Wrapped Blanket Assemblies," COO-2245-43TR, M.I.T. (April 1978).

13. Symolon, P.D. and Todreas, N.E., "A Manual for Use with the Computer Code SUPERENERGY -- Data Reduction Version," COO-2245-74TR, M.I.T. (February 1980).

14. Glazer, S., Chiu, C., and Todreas, N.E., "Collection and Evaluation of Salt Mixing Data with the Real Time Data Acquisition System," COO-2245-36TR, M.I.T. (April 1977).

15. Paul Symolon, personal communication.

16. Hawley, J.T., Chiu, C., and Todreas, N., "M.I.T. Extraction Method for Measuring Average Subchannel Axial Velocities in Reactor Assemblies," DOE/ET/37240-80TR, M.I.T. (July 1980).

17. Symolon, P.D. and Todreas, N.E., "Fluid Mixing Studies in a Hexagonal 217-pin Wire Wrapped Rod Bundle," DOE/ET/37240-84TR, M.I.T. (February 1981).

18. Wang, S.F., Rohsenow, W.M., and Todreas, N.E., "Flow Split, Pressure Drop, and Mixing Experiments in a 61-Pin Shaved-Wire Blanket Assembly," DOE/ET/37240-86TR, M.I.T. (February 1981).

19. Lorenz, J.J. and Ginsberg, T., "Coolant Mixing and Subchannel Velocities in a LMFBR Fuel Assembly," Nucl. Eng. and Des., 40, 315-316 (1977).

20. Hawley, J.T., Chiu, C., Rohsenow, W.M., and Todreas, N.E., "Correlations for Subchannel and Bundle Friction Factors and Flow Split Parameters for Laminar, Transition and Turbulent Longitudinal Flows in Wire Wrap Spaced Hexagonal Arrays," DOE/ET/37240-79TR (December 1980).

21. Hanson, A.S., Symolon, P.D., and Todreas, N.E., "Fluid Mixing Studies in a Hexagonal 61-Pin Wire Wrapped Rod Bundle," COO-2245-51TR, Revision I, M.I.T. (February 1981).

22. Chan, Y.N. and Todreas, N.E., "Turbulent Sweeping Flow Mixing Model for Wire Wrapped LMFBR Assemblies," COO-2245-55TR, Revision II (December 1980).

23. Okamoto, Y., Akuno, N., Emon, K., and Tamids, M., "Hydraulic Tests on FBR Fuel Sub-Assemblies," JAPFNR-24 (1971).

24. Hines, D.P., Boyd, L.R., and Marian, V.R., "In-Core-Boiling by Over Temperature Detector Development," General Electric NEDC-13650 (April 1971).

25. Baumann, W. and Hoffman, H., "Coolant Cross-Mixing of Sodium Flowing in Line Through Multi-Rod Bundles with Different Space Arrangements," Int. Seminar on Heat Transfer in Liquid Metals, Trogir, 1971.

26. Fontana, M., MacPherson, R.E., Gnadt, P.A., Wantland, J.L., and Parsly, L.F., ORNL-TM-4113, T191.

27. Collingham, R.E., Thorne, W.L., and McCormack, J.D., "217-Pin Wire Wrapped Bundle Coolant Mixing Test," HEDL-TME 71-146 (November 1971).

28. Chen, Y.B., Ip, K., and Todreas, N.E., "Velocity Measurement in Edge Subchannels of Wire Wrapped LMFBR Fuel Assemblies," ANS Transactions, 19, 323-324 (1974).

29. Skok, J., "Mixing of the Fluid Due to Helicoidal Wires of Fuel Pins in a Triangular Array," Progress in Heat and Mass Transfer, 7, (1973).

30. Pedersen, D.R., Pierce, R.D., Wilson, R.E., and Roop, C.J. , "Crossflow Mixing in a 91-Element Bundle," ANL/RAS 74-2 (February 1974).

31. Lafay, J., Menant, B., and Barroil, J., "Influence of Helical Wire Wrap Spacer System in a Water 19-Rod Bundle," ASME paper, 75-HT-22 (1975).

FIGURES

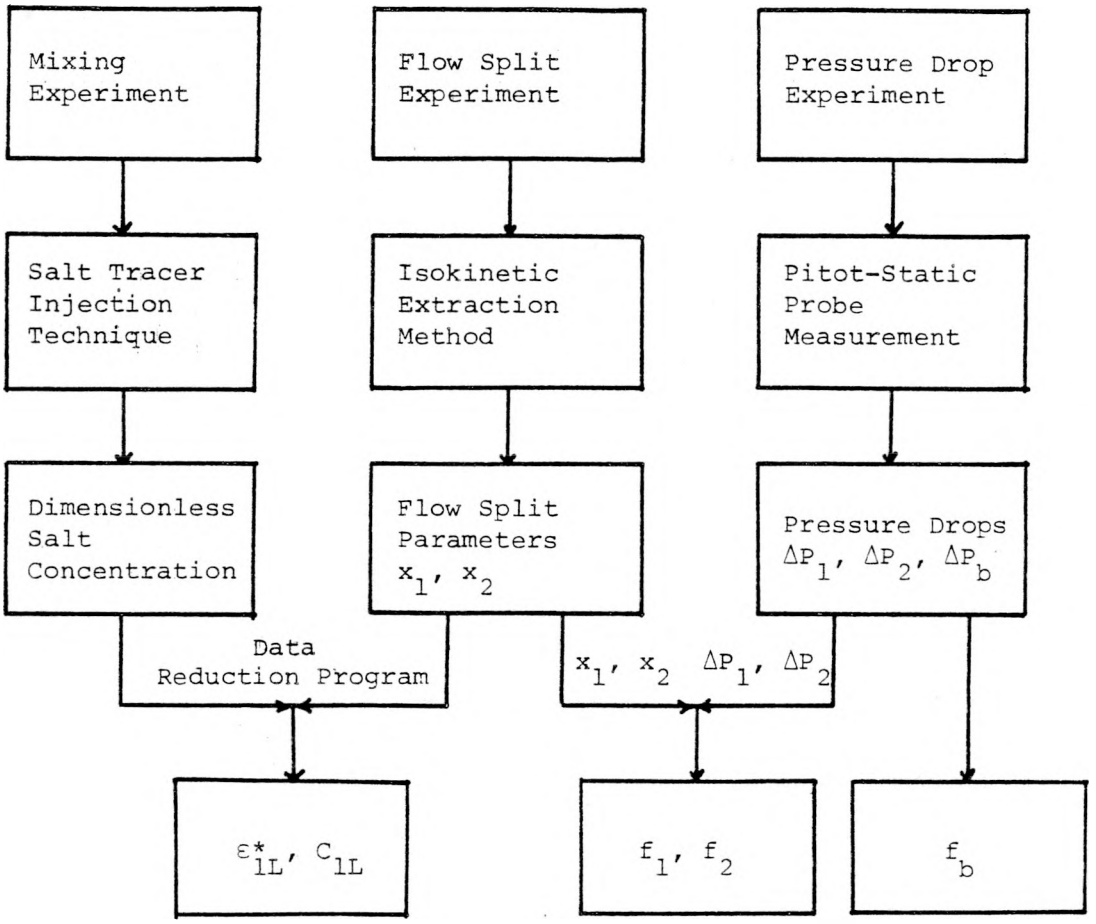

Figure 1.1 Relations Among Flow Split Experiment, Mixing Experiment and Pressure Drop Experiment

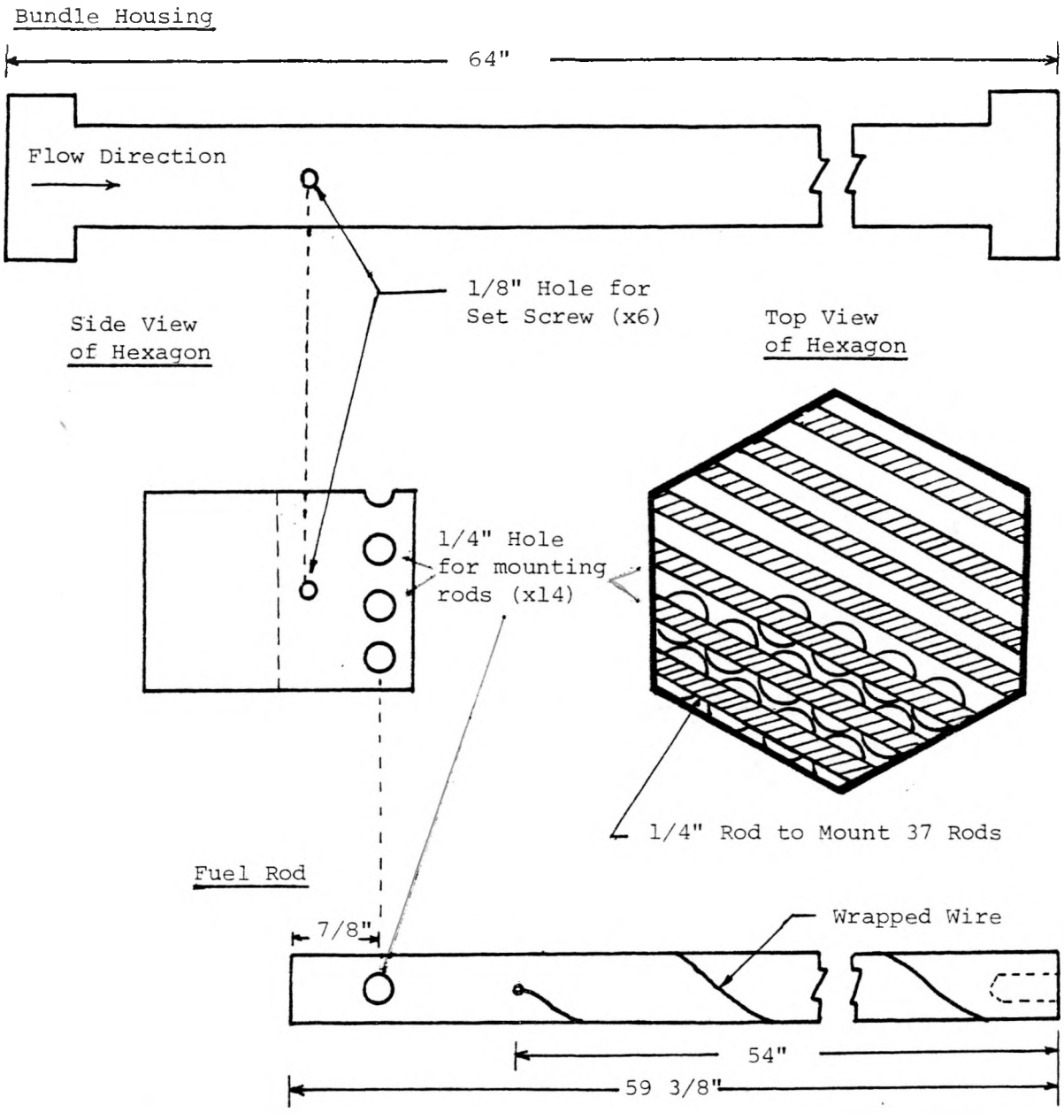

Figure 2.1 37-Pin Bundle Design Configuration

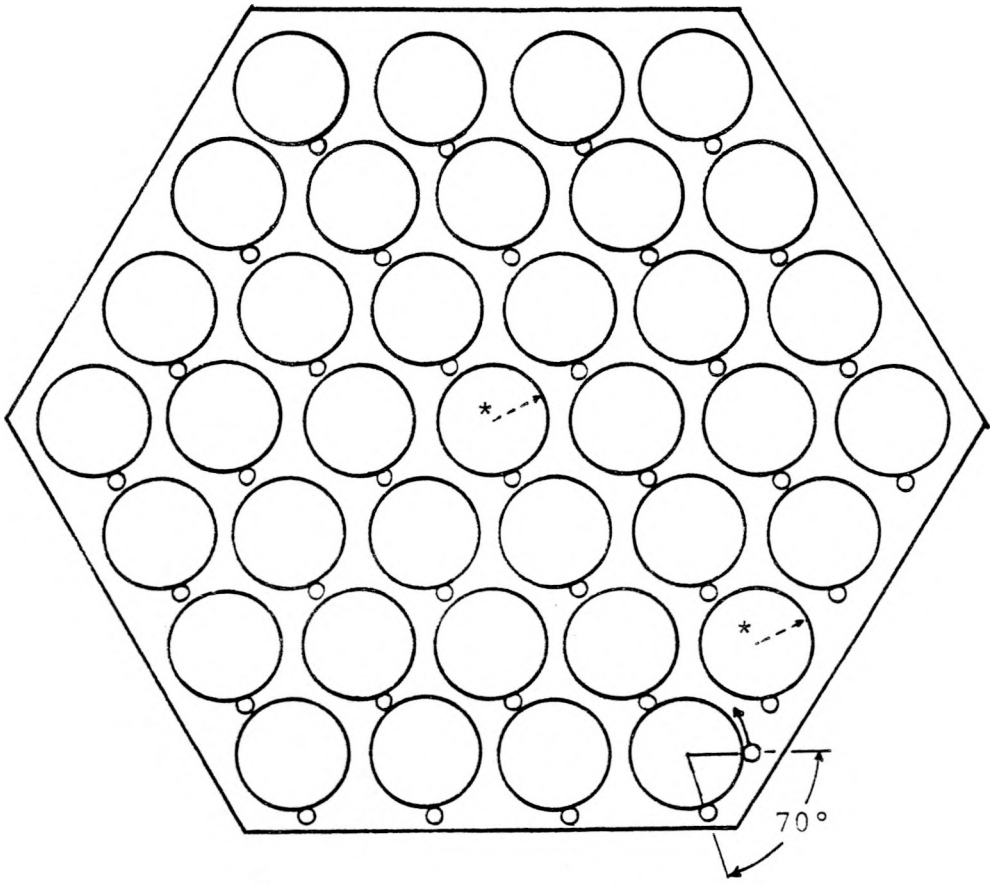

37-pin P/D = 1.154 H/D = 13.4 Design Parameters	
D = 0.592"	P = 0.683"
D_w = 0.089"	H = 7.935"
D_F = 4.336"	F = 0.447
D_g = 0.097"	θ = 16.8°
T_{ff} = 0.027"	S = 0.7675

Figure 2.2 As Built Geometry at Exit Plane

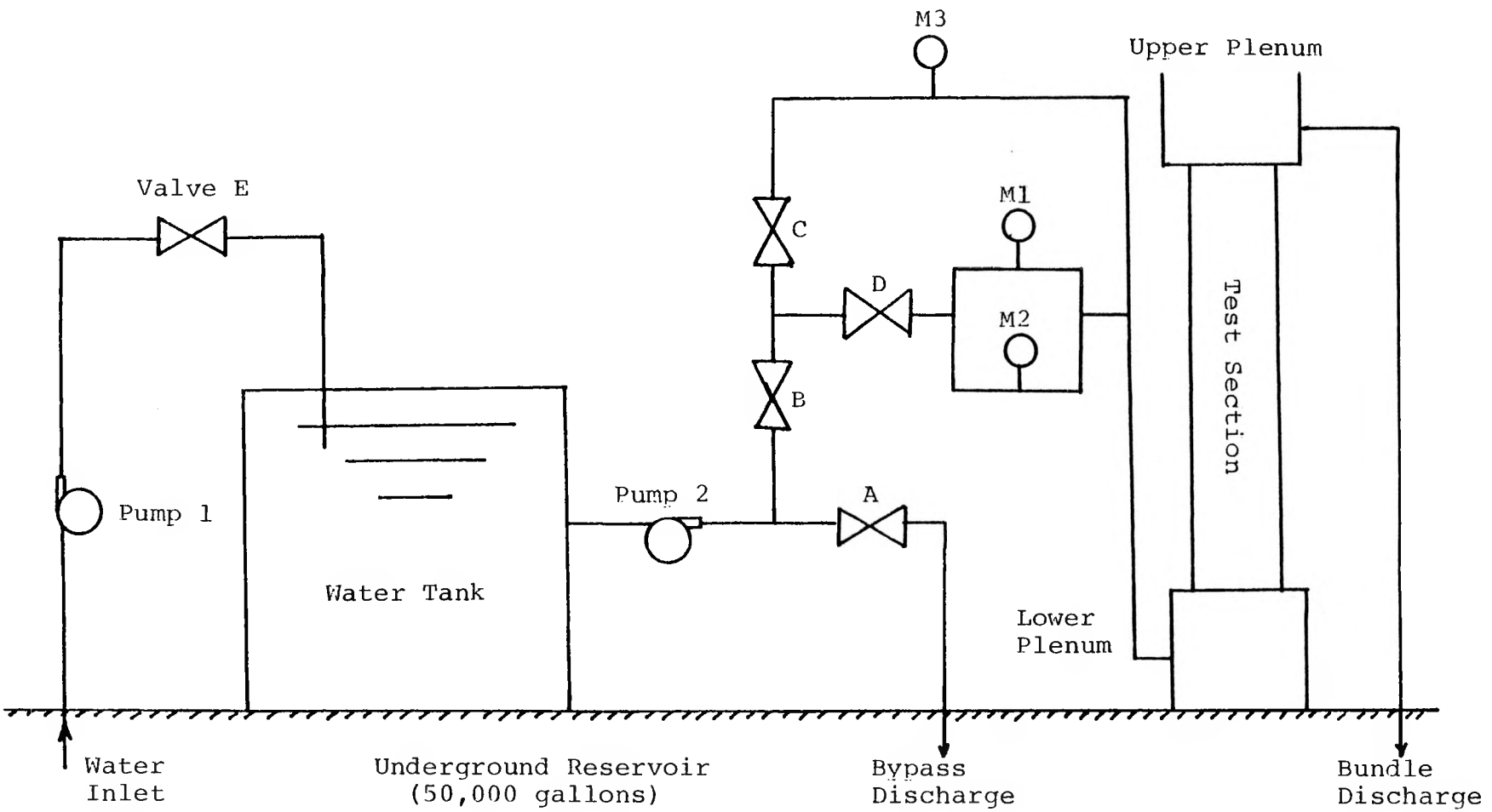

Figure 2.3 Layout of the Test Loop

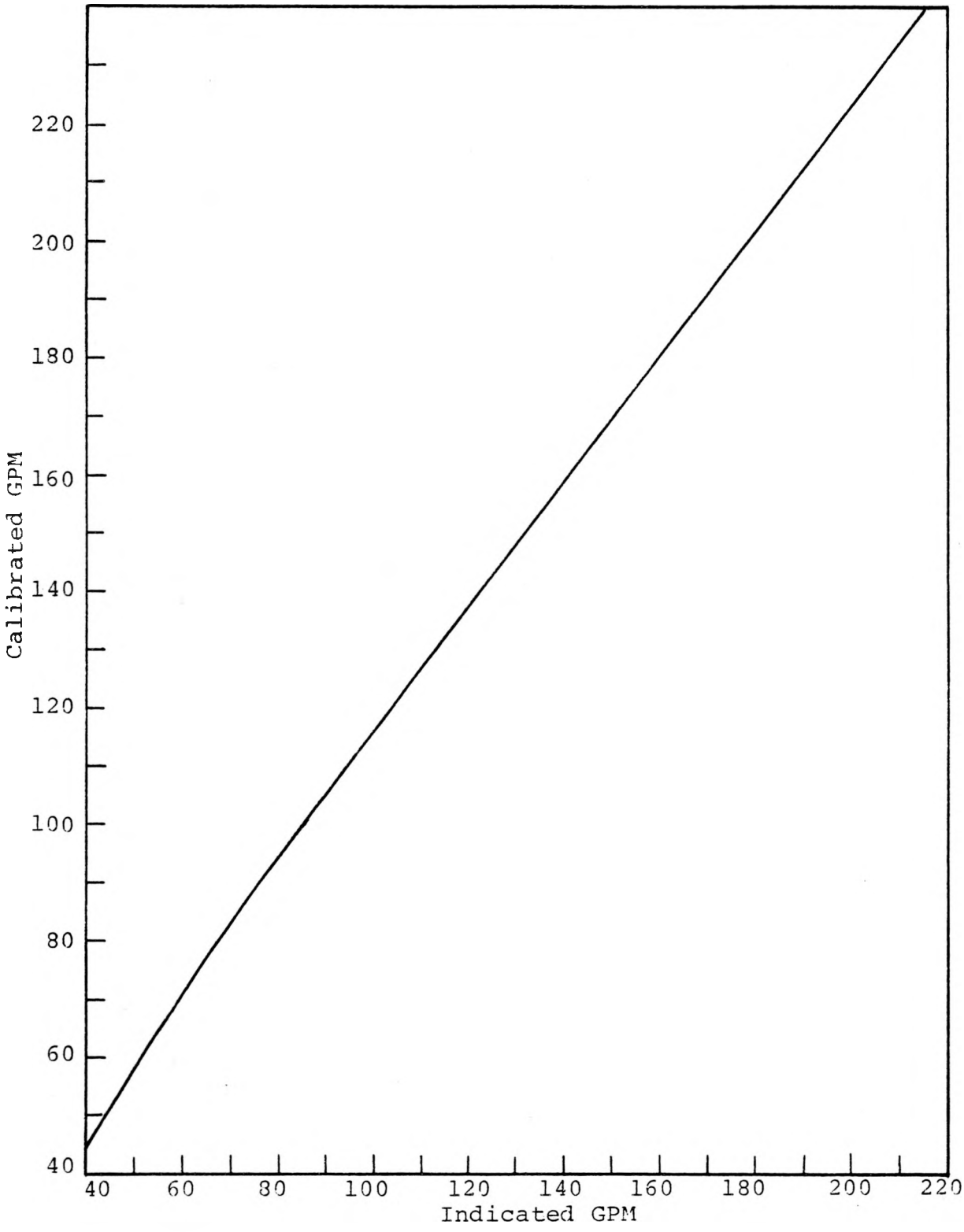

Figure 2.4 Calibration Curve for Rotometer M3

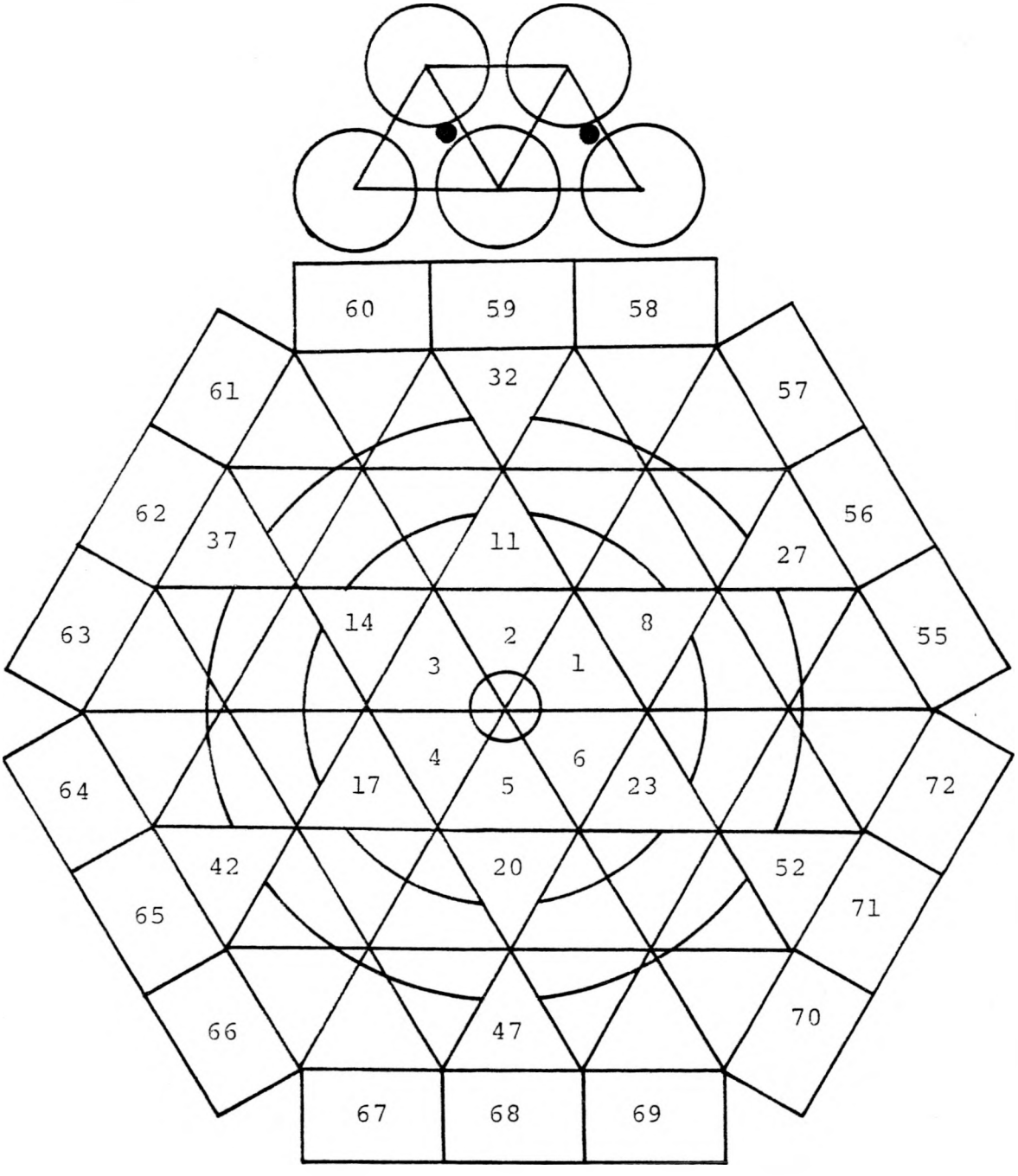

Figure 2.5 Flat to Flat Measurement Scheme and Wire Positions in Two Different Types of Interior Subchannel

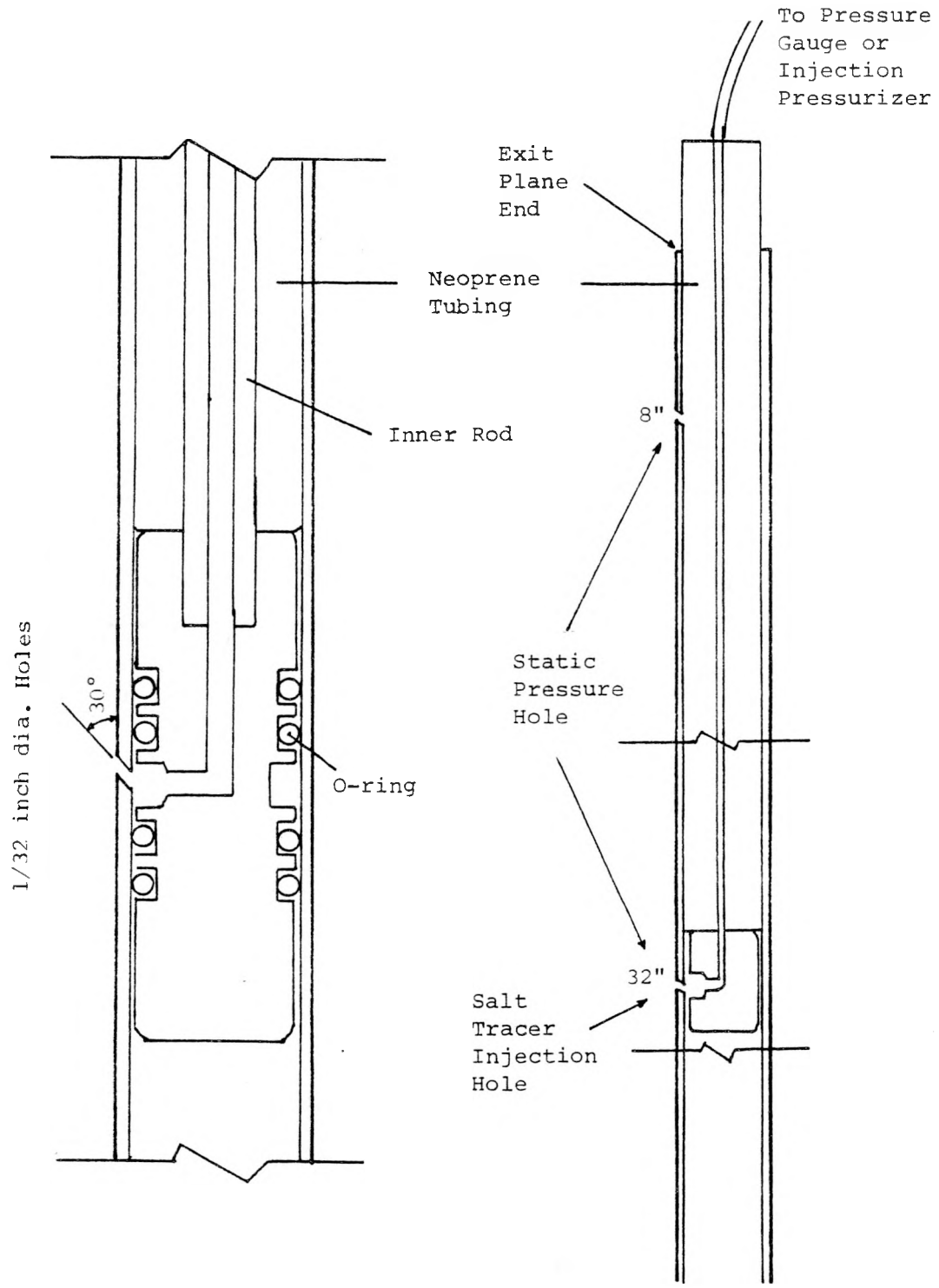

Figure 2.6 Design Configuration of Instrumentation Rod and Injector

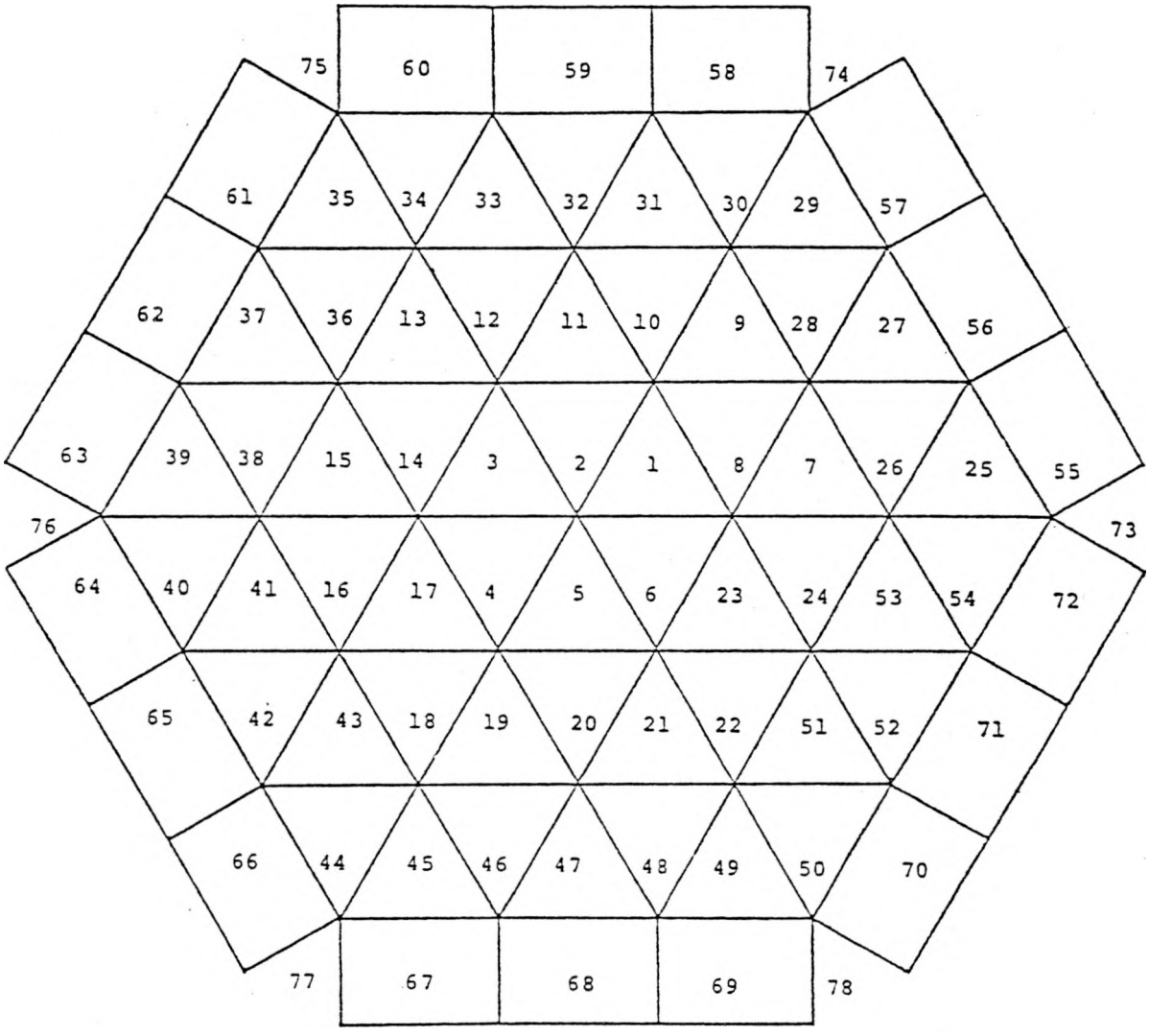

Figure 2.7 Subchannel Numbering Scheme

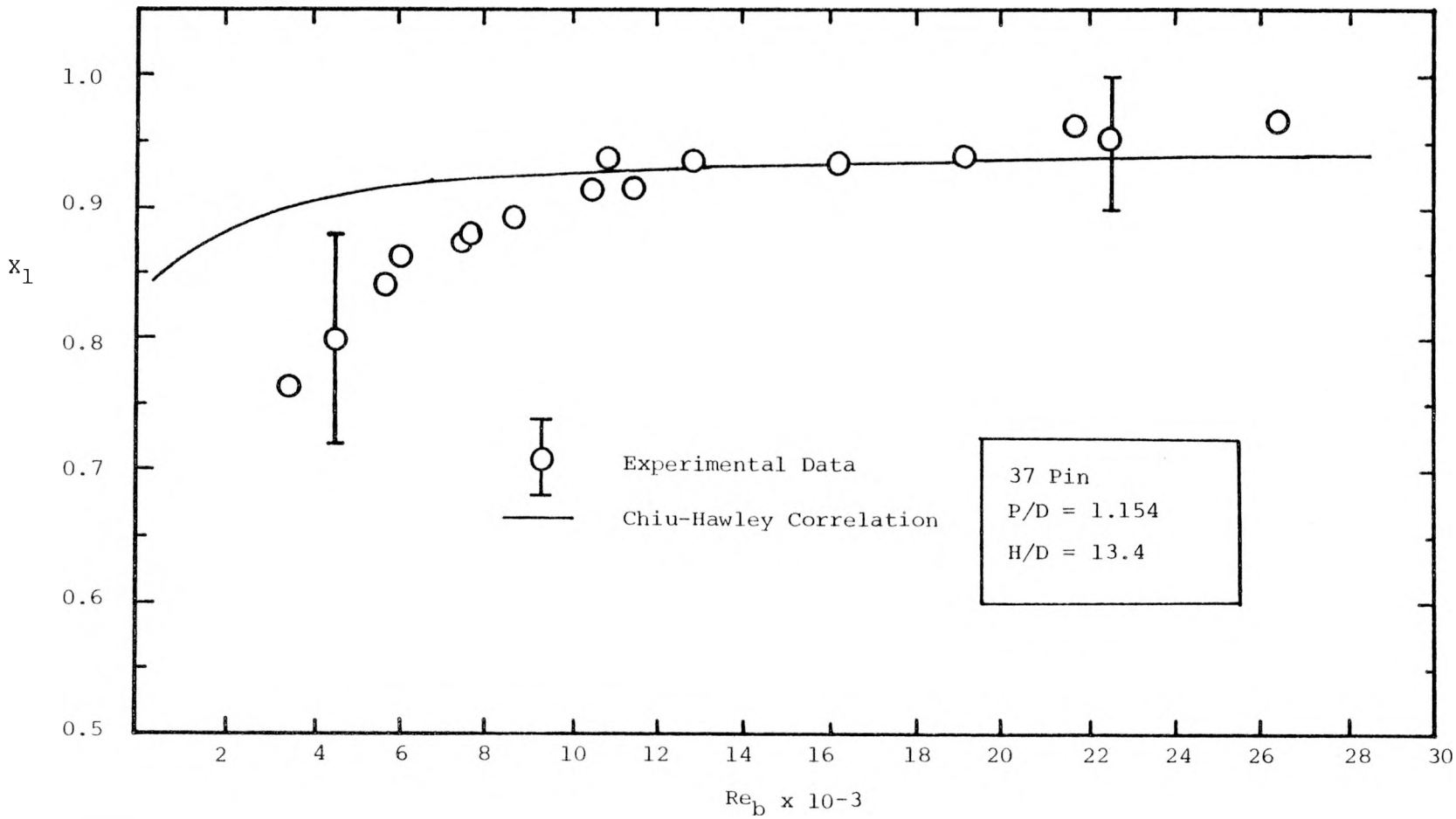

Figure 3.1 Interior Subchannel Flow Split Parameter X_1 versus Re_b

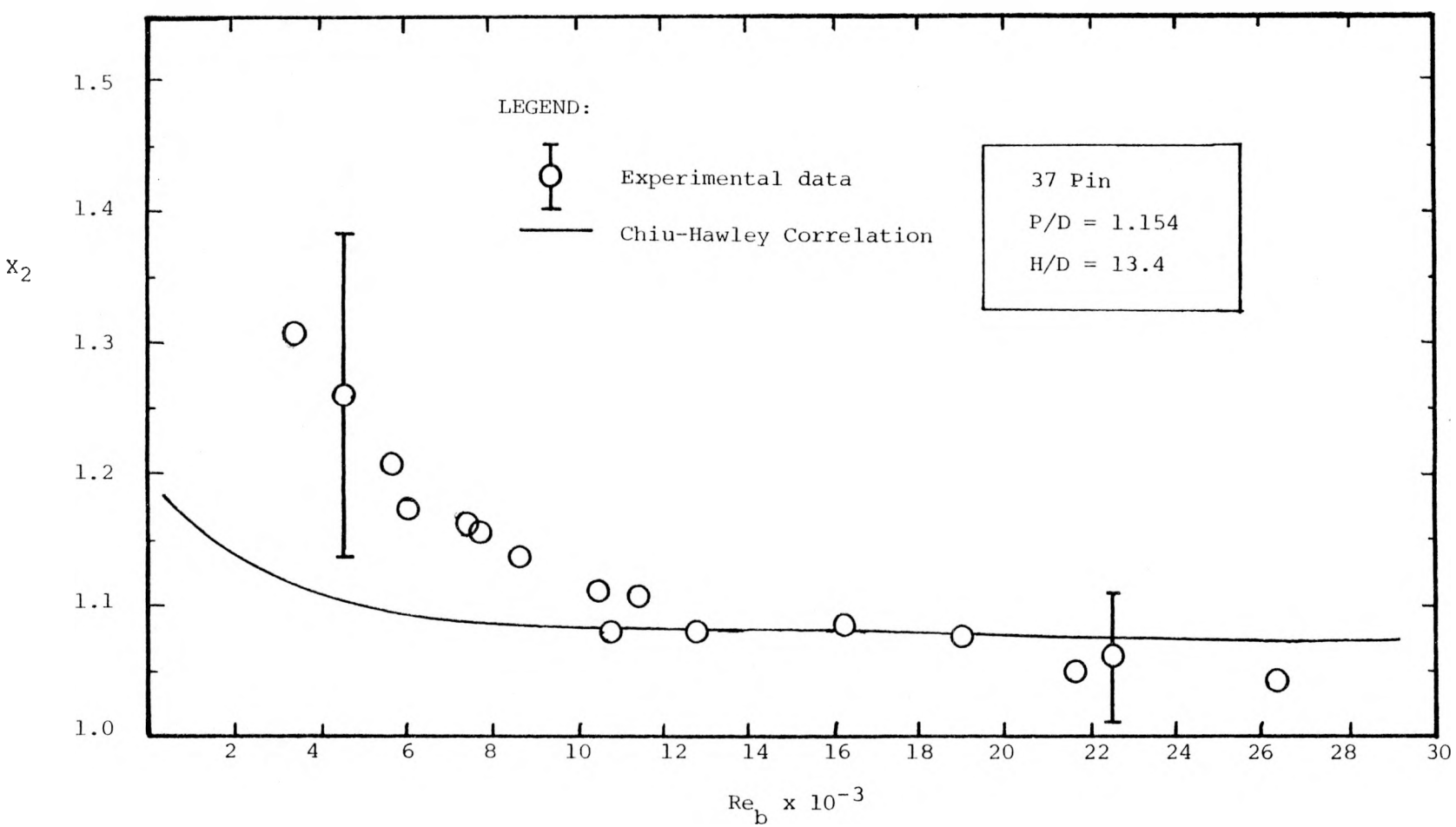

Figure 3.2 Edge Subchannel Flow Split Parameter X_2 versus Re_b

37-Pin P/D = 1.154 H/D = 13.4

M_L = 100 GPM
Re_b = 10480
X_1 = 0.915
X_2 = 1.110
Mass Balance Error = -3.7%

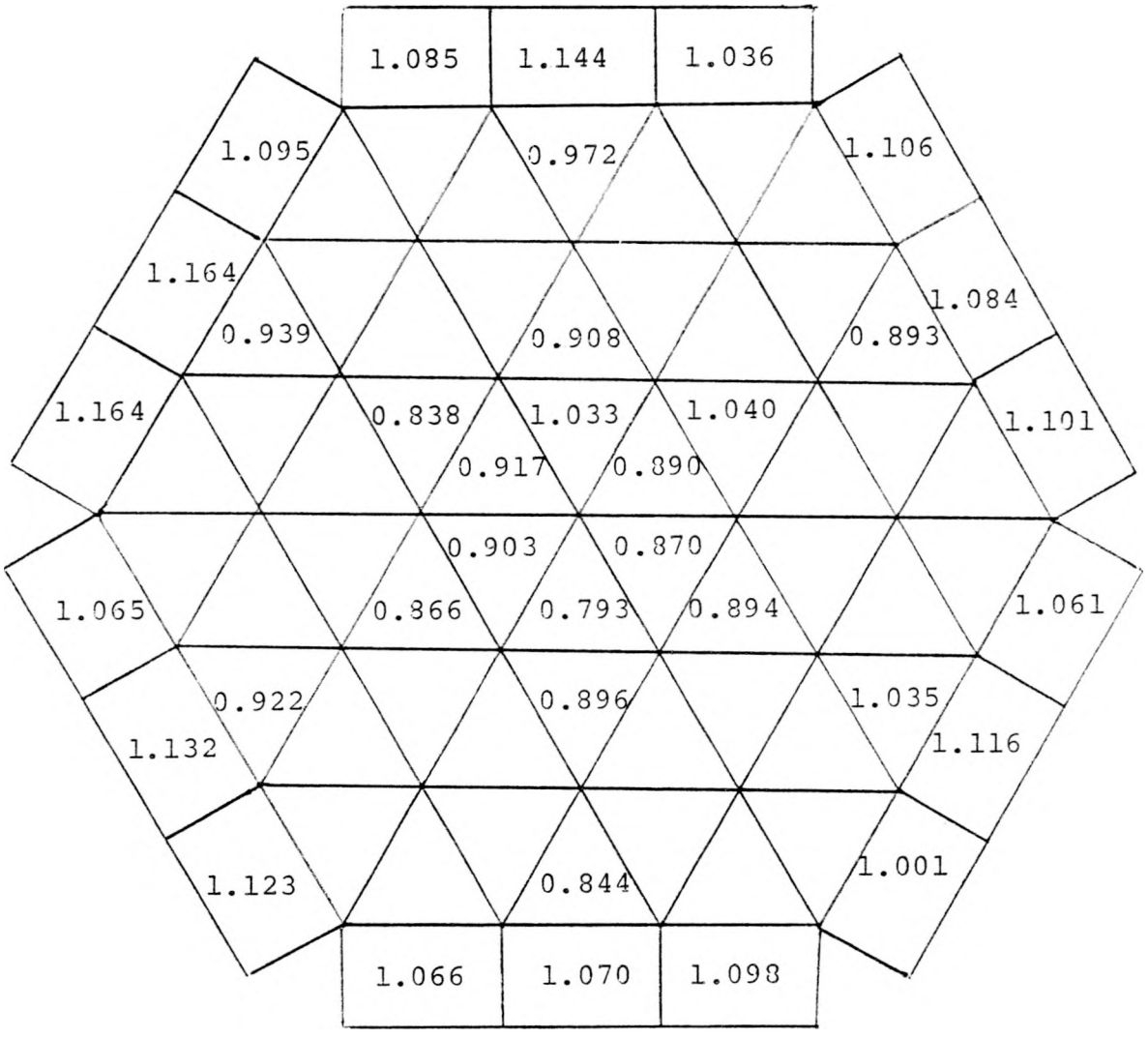

Figure 3.3 Normalized Subchannel Flow Split Map at Re_b = 10480

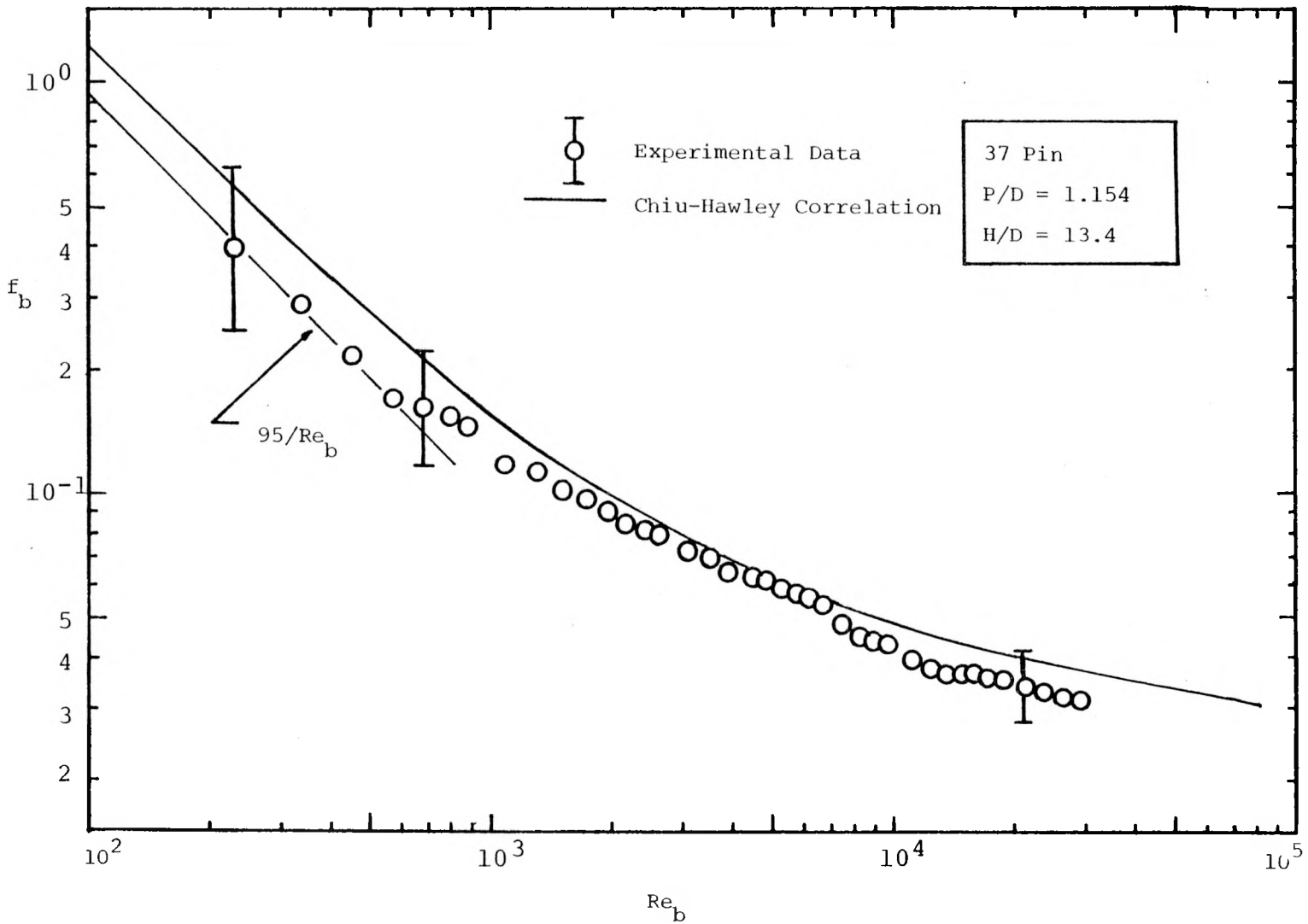

Figure 3.4 Bundle Average Friction Factor versus Re_b

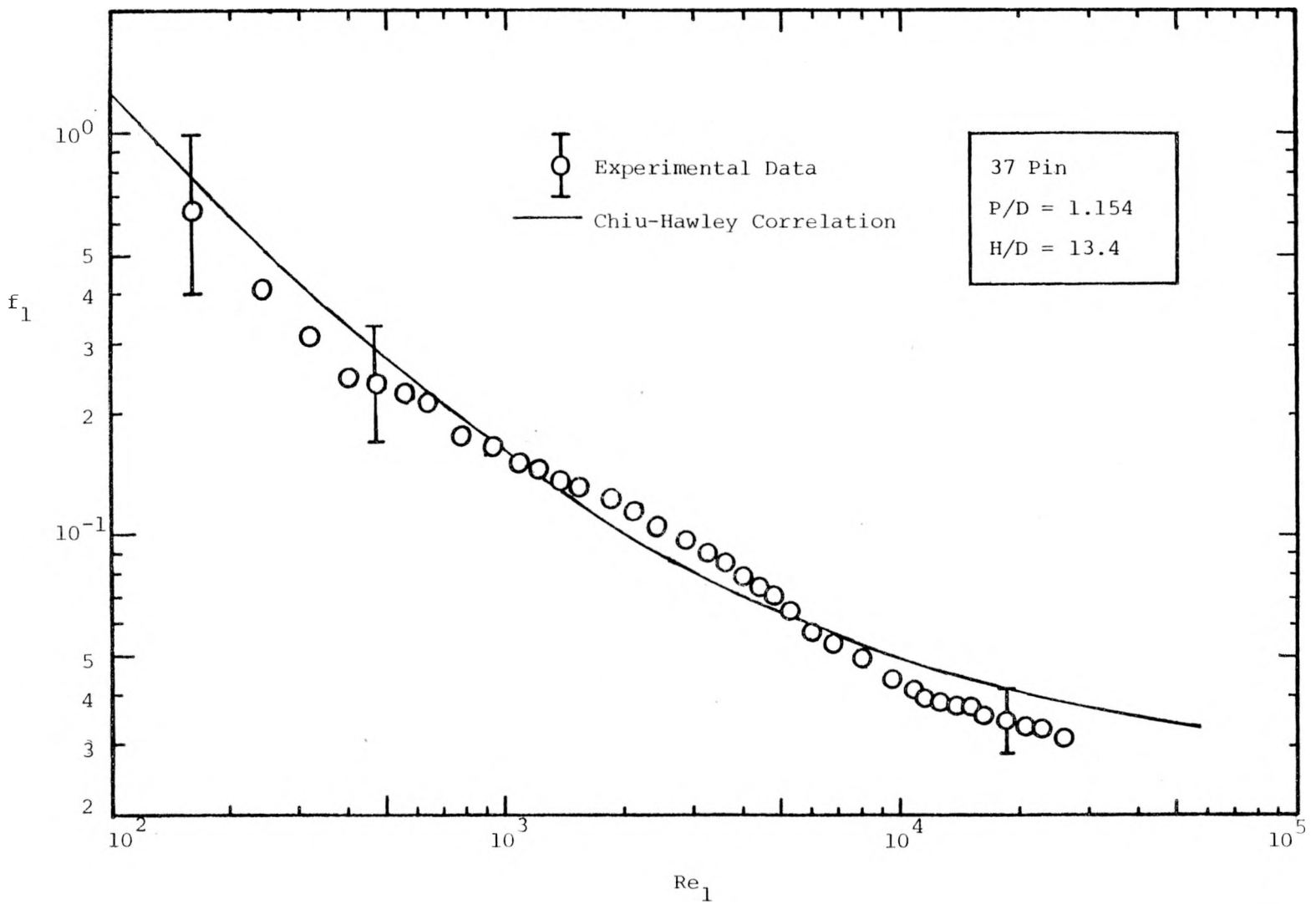

Figure 3.5 Interior Subchannel Friction Factor versus Interior Subchannel Reynolds Number

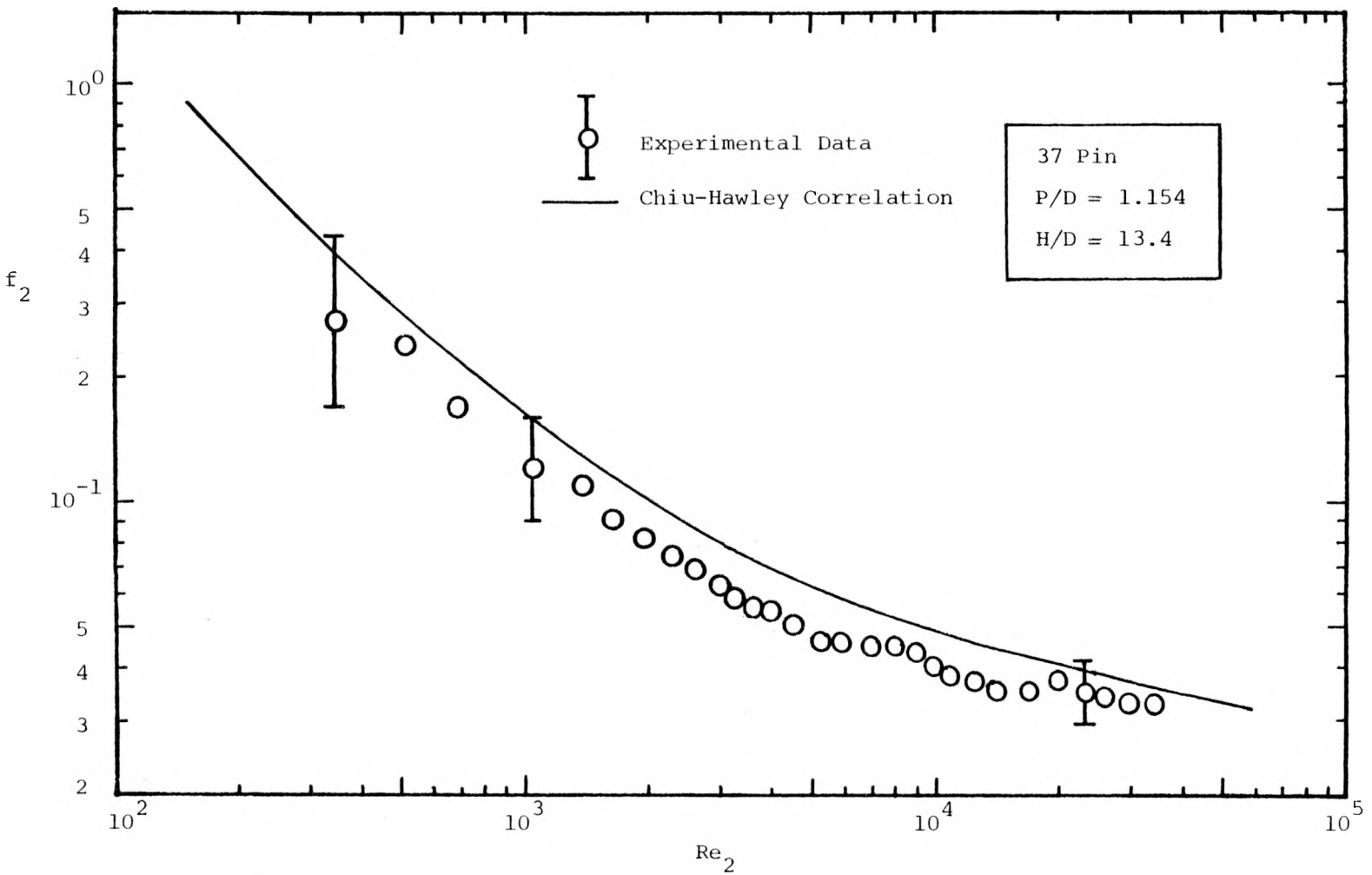

Figure 3.6 Edge Subchannel Friction Factor versus Edge Subchannel Reynolds Number

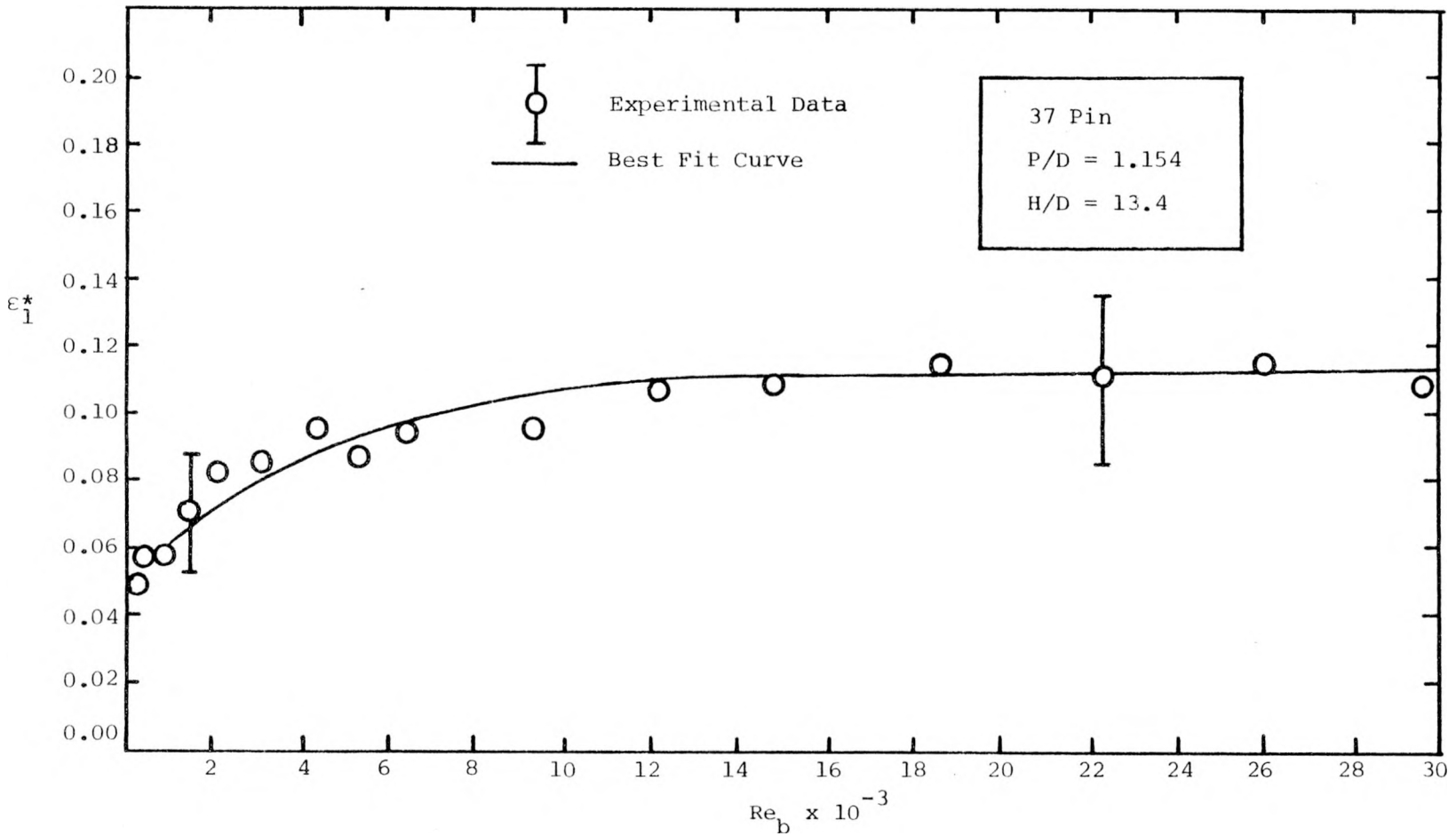

Figure 3.7 Effective Enhanced Eddy Diffusivity ε_1^* versus Re_b

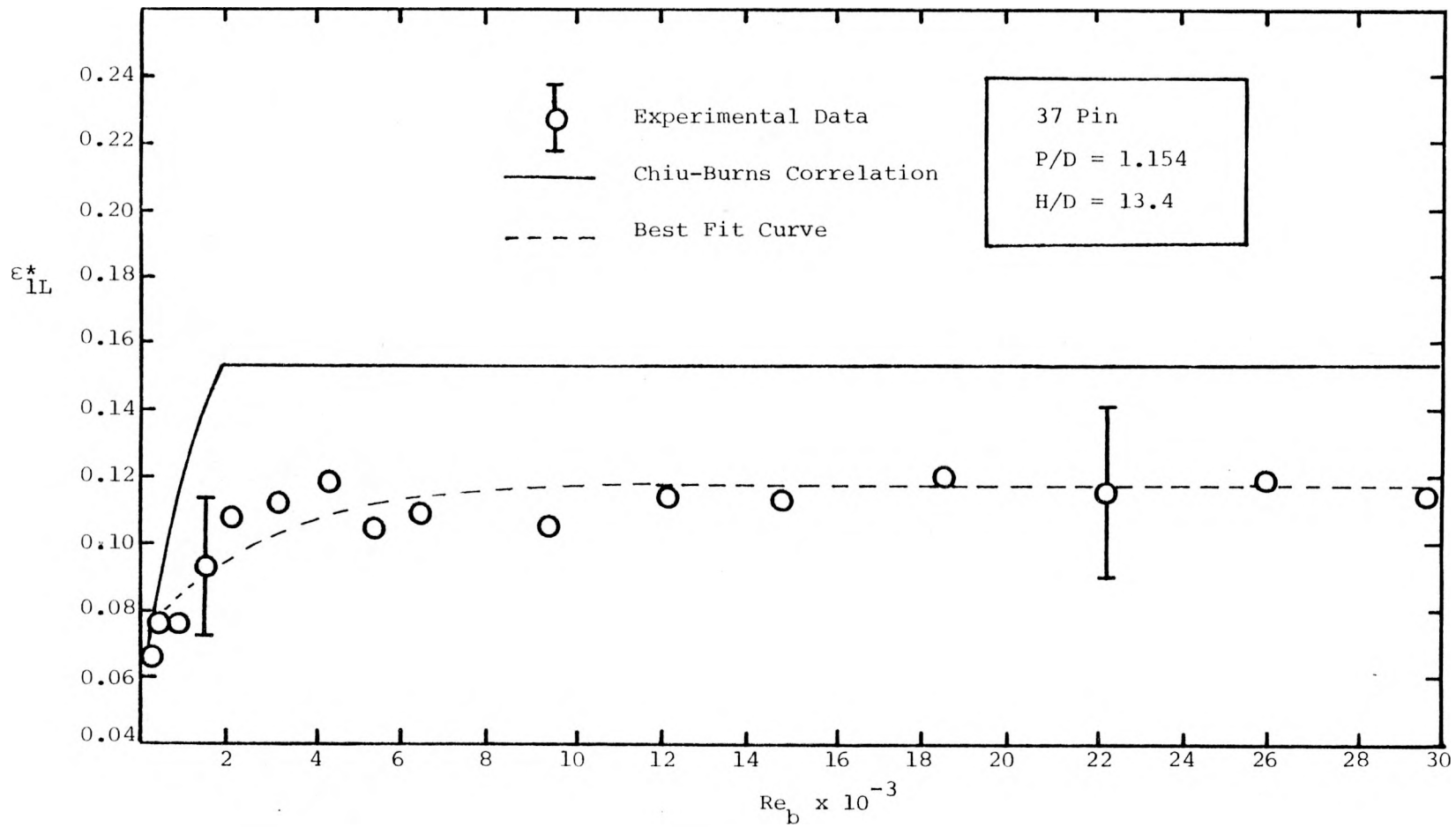

Figure 3.8 Local Effective Enhanced Eddy Diffusivity ε^*_{1L} versus Re_b

37 pin p/d= 1.154 h/d= 13.40
inj. subchannel = 1
inj. depth (in) = 32.0
bundle reynolds no.= 22100
mass balance ratio = 1.423
dimensionless ratios of salt concentration*100.0:

0.3 0.5 0.8 0.6 0.4
0.1 0.8 2.8 1.4 0.2
0.5 1.3 2.3 1.7
0.3 1.3 3.8 4.2 1.0 0.0
1.0 3.1 4.4 4.0 1.5
0.1 1.3 4.2 5.5 3.7 1.3 0.3
0.4 1.6 3.6 (3.9) 2.8 0.7
0.2 0.0
0.5 2.7 4.1 3.2 0.9 0.1
0.0 0.1 2.1 4.0 2.2 0.9 0.0
0.6 1.3 0.9 0.7 0.0
0.0 0.3 1.5 1.2 0.5 0.1
0.0 0.2 0.3 0.2
0.1 0.1 0.4 0.0 0.0
0.1 0.1 0.1 0.0 0.0

sup/drv results at minimum mean square indicator
effective eddy diffusivity E*1 = 0.111
swirl velocity ratio C1 = 0.300
min. mean square indicator = 6.44
dimensionless ratios of salt concentration*100.0:

0.4 0.4 0.5 0.5 0.5
0.3 0.6 1.0 1.0 0.5
0.5 1.2 1.6 1.2
0.3 0.8 2.1 2.8 2.0 0.5
0.5 1.6 3.2 3.2 1.5
0.2 0.6 2.1 4.1 4.1 2.0 0.4
0.3 1.2 3.2 (4.6) 3.2 1.1
0.2 0.3
0.2 1.0 2.8 4.1 2.8 1.0
0.1 0.5 1.6 3.2 3.2 1.6 0.3
0.3 1.0 2.1 2.1 1.0
0.1 0.5 1.2 1.6 1.2 0.3
0.2 0.6 0.8 0.5
0.1 0.2 0.4 0.4 0.2
0.1 0.1 0.1 0.1 0.1

Figure 3.9 Typical Experimental and Predicted Dimensionless Salt Concentration for Interior Injection at Re_b = 22,100

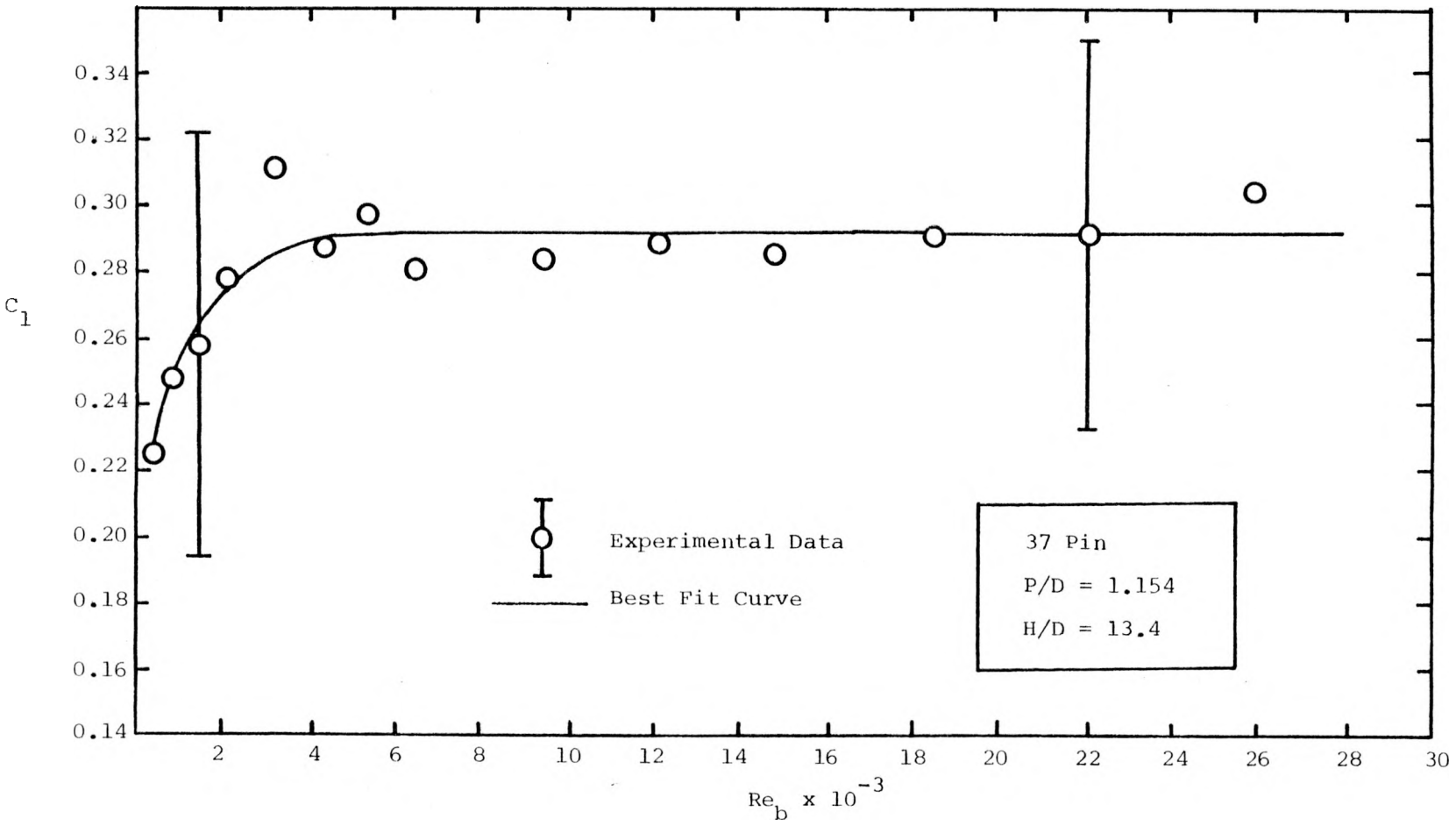

Figure 3.10 Swirl Flow Ratio C_1 versus Re_b

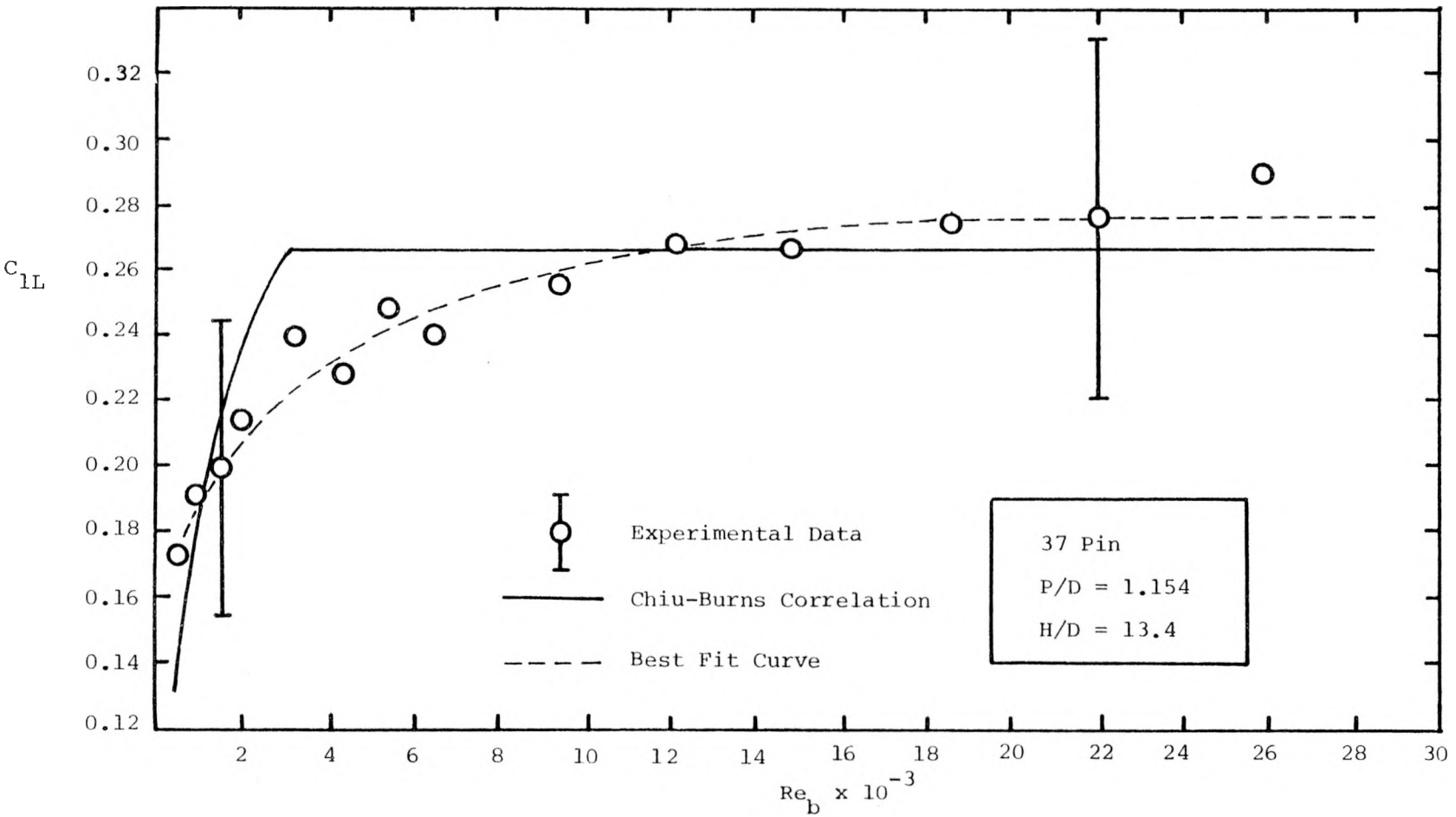

Figure 3.11 Local Swirl Flow Ratio C_{1L} versus Re_b

37 pin p/d= 1.154 h/d= 13.40
inj. subchannel = 71
inj. depth (in) = 32.0
bundle reynolds no.= 22100
mass balance ratio = 1.222
dimensionless ratios of salt concentration*100.0:

7.6 7.8 6.8 7.4 8.0
3.6 1.1 1.5 6.2 6.2
1.7 1.3 0.9 5.8
1.6 1.0 0.2 3.2 7.4 4.4
0.0 0.5 0.8 3.0 6.6
0.5 0.0 0.2 0.2 3.3 5.8 3.6
0.0 0.4 0.0 0.9 3.0 5.8
0.5 3.0
0.0 0.0 0.6 1.9 3.4 6.0
0.0 0.0 0.0 0.3 1.7 7.5 2.5
0.0 0.4 1.3 4.3 4.1
0.0 0.0 0.0 1.7 4.5 (1.4)
0.0 0.9 1.8 5.0
0.0 0.0 0.7 1.9 0.6
0.0 0.0 0.0 0.0 0.3

sup/drv results at minimum mean square indicator
effective eddy diffusivity E*1 = 0.110
swirl velocity ratio C1 = 0.291
min. mean square indicator = 9.29
dimensionless ratios of salt concentration*100.0:

5.3 5.8 7.2 8.2 8.1
3.7 2.5 3.6 5.6 7.7
1.8 1.8 3.2 6.1
2.4 0.7 0.7 1.8 4.9 6.5
0.8 0.3 0.8 2.7 6.1
1.4 0.3 0.1 0.6 2.3 5.6 4.8
0.4 0.1 0.2 1.1 3.8 6.0
1.1 3.1
0.2 0.1 0.2 1.2 3.5 5.0
0.6 0.1 0.1 0.6 2.2 4.3 2.6
0.1 0.1 0.6 1.9 3.1
0.3 0.0 0.2 1.0 2.3 (1.3)
0.0 0.2 0.7 1.4
0.1 0.1 0.3 0.8 0.6
0.1 0.1 0.1 0.2 0.2

Figure 3.12 Typical Experimental and Predicted Dimensionless Salt Concentration for Interior Injection at Re_b = 22,100

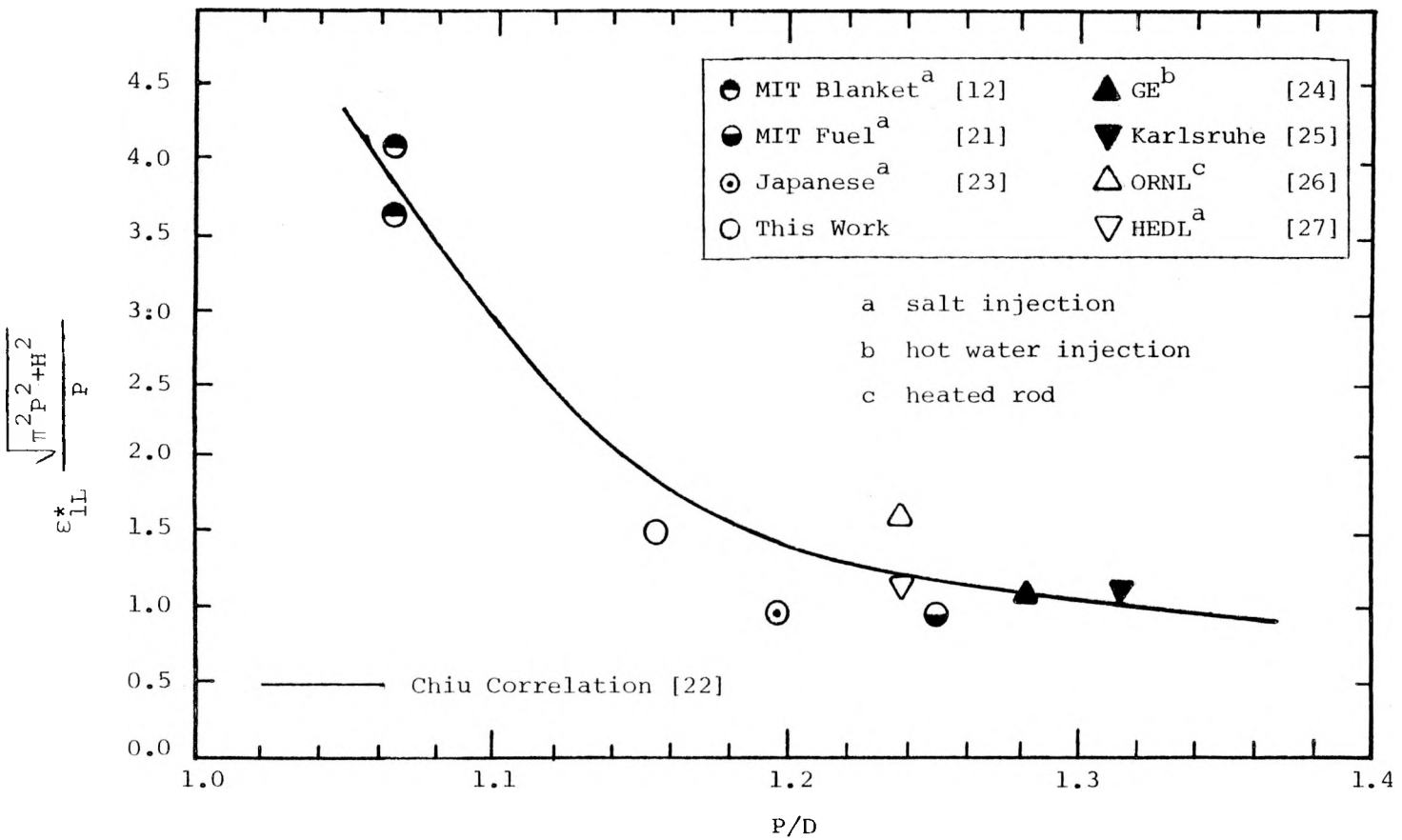

Figure 4.1 Experimental Data and Chiu Correlation for ε^*_{1L} in the Turbulent Flow Regime

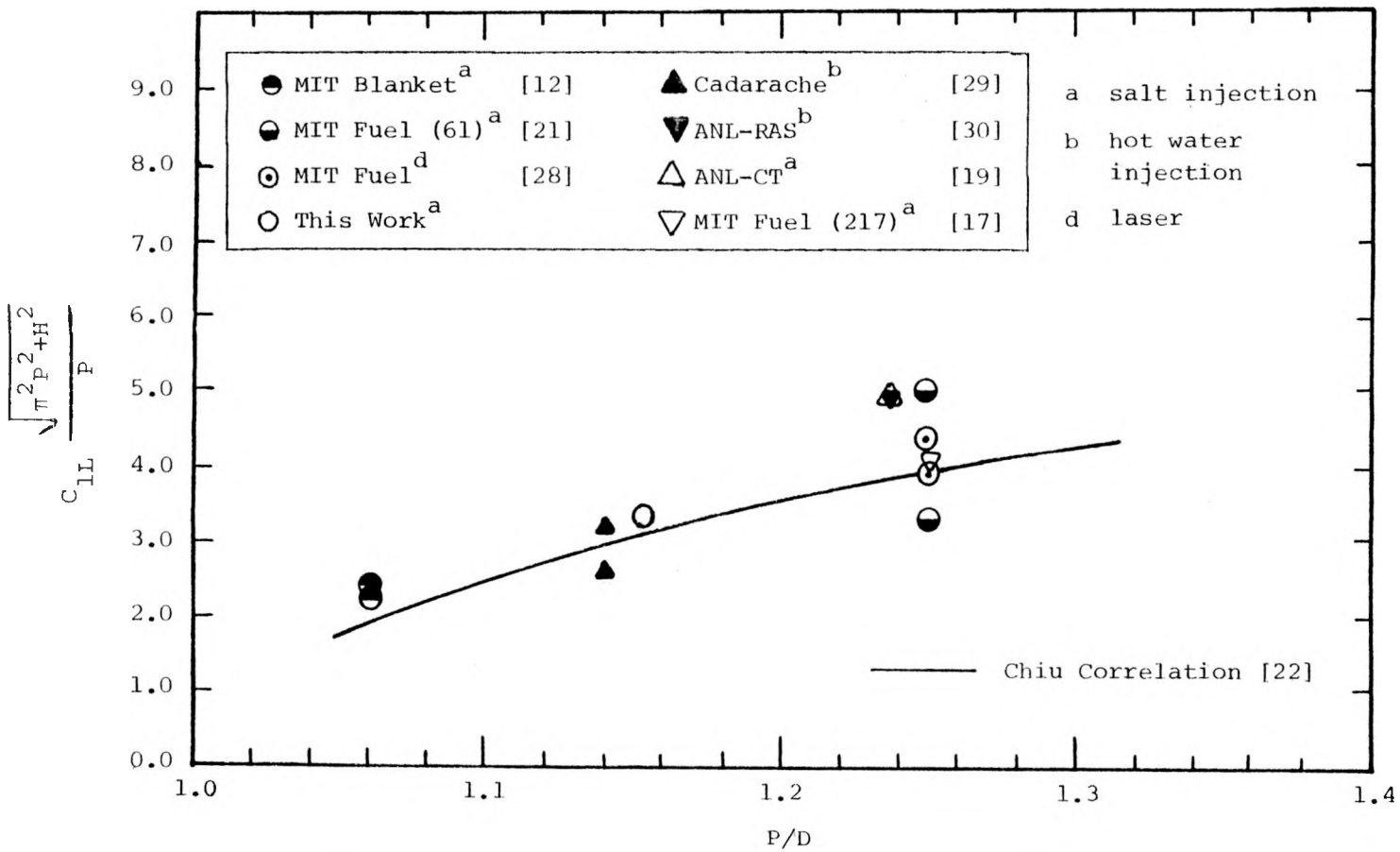

Figure 4.2 Experimental Data and Chiu Correlation for C_{1L} in the Turbulent Flow Regime

TABLES

Table 2.1

Subchannel Geometric Parameters

	Subchannel Numbers	Flow Area (in^2)	Equiv. Dia. (in)
Bundle average		5.856	0.248
Interior Subchannel Average	54	0.0613	0.228
With wire inside		0.0597	
Without wire inside		0.0630	
Edge Subchannel Average	18	0.1273	0.290
With wire inside		0.1257	
Without wire inside		0.1289	
Corner Subchannel	6	0.0420	0.207

Table 3.1

ν: Kinematic Viscosity of Water*

Temperature		ν ft^2/hr
°F	°C	
40	4.4	0.05993
45	7.2	0.05501
50	10.0	0.05073
55	12.8	0.04694
60	15.6	0.04363
65	18.3	0.04064
70	21.1	0.03802
75	23.9	0.03563
80	26.7	0.03350
85	29.4	0.03139
90	32.2	0.02978

*Source: F.M. White, "Viscous Fluid Flow," McGraw-Hill, New York (1974)

Table 3.2

Predicted Parameters by Chiu, Hawley and Burns' Correlations for This Bundle

Re_b	X_1	X_2	f_1	f_2	f_b	ε^*_{1L}	C_{1L}
200	0.840	1.208	0.799	0.490	0.612	0.0693	0.107
400	0.840	1.189	0.400	0.275	0.332	0.0884	0.136
700	0.858	1.175	0.256	0.173	0.204	0.108	0.165
1,000	0.865	1.163	0.189	0.132	0.153	0.122	0.187
2,000	0.884	1.135	0.112	0.0860	0.0948	0.154	0.239
3,000	0.897	1.119	0.0867	0.0706	0.0757	0.154	0.265
4,000	0.906	1.109	0.0742	0.0628	0.0660	0.154	0.265
5,000	0.912	1.102	0.0667	0.0579	0.0602	0.154	0.265
6,000	0.917	1.098	0.0616	0.0545	0.0562	0.154	0.265
7,000	0.920	1.094	0.0579	0.0520	0.0532	0.154	0.265
8,000	0.923	1.091	0.0551	0.0500	0.0510	0.154	0.265
10,000	0.927	1.087	0.0510	0.0471	0.0476	0.154	0.265
12,000	0.930	1.085	0.0482	0.0450	0.0453	0.154	0.265
15,000	0.933	1.082	0.0452	0.0427	0.0427	0.154	0.265
18,000	0.935	1.080	0.0431	0.0410	0.0409	0.154	0.265
21,000	0.937	1.079	0.0414	0.0396	0.0394	0.154	0.265
>100,000	0.944	1.073	--*	--	--	0.154	0.265

*This is Re_b dependent value.

Table 3.3

Flow Split Experimental Results

Run #	Flow Rate GPM	Re_b	X_1	X_2	Mass Balance Error
1	32.5	3,470	0.763	1.307	-12%
2	42.8	4,570	0.800	1.259	-5.0%
3	52.4	5,600	0.841	1.206	-3.5%
4	56	5,950	0.864	1.175	-1.6%
5	70	7,440	0.875	1.161	-2.2%
6	70	7,630	0.879	1.155	-1.4%
7	81	8,620	0.894	1.136	-2.8%
8	100	10,480	0.915	1.110	-3.7%
9	105	11,380	0.916	1.109	-3.5%
10	121	10,740	0.939	1.079	-3.6%
11	142	12,840	0.936	1.082	-4.4%
12	173	16,170	0.934	1.085	-2.8%
13	197	18,960	0.939	1.078	-3.4%
14	200	21,600	0.962	1.048	-2.2%
15	220	22,510	0.953	1.060	-2.0%
16	215*	26,300	0.967	1.042	+0.9%

*Steam injected into tank to heat the water, hence Reynolds number increased.

Table 3.4

Experimental Results of Pressure Drop Experiment

Bundle flow rate (GPM)	ΔP_1 (interior) cm of water	ΔP_1 (interior) in of water	ΔP_2 (edge) cm of water	ΔP_2 (edge) in of water	ΔP_b in of water
1.93	0.2	0.079	0.2	0.079	0.079
2.90	0.3	0.118	0.4	0.158	0.134
3.86	0.4	0.158	0.5	0.197	0.174
4.83	0.5	0.197	0.6	0.236	0.213
5.79	0.7	0.276	0.8	0.315	0.292
6.76	0.9	0.354	1.1	0.433	0.386
7.72	1.1	0.433	1.3	0.512	0.465
7.40	1.0	0.394	1.2	0.472	0.426
9.25	1.3	0.512	1.5	0.591	0.544
11.1	1.8	0.709	2.0	0.787	0.741
13.0	2.2	0.866	2.5	0.984	0.914
14.8	2.8	1.102	3.0	1.181	1.134
16.7	3.3	1.299	3.5	1.378	1.331
18.5	3.9	1.535	4.0	1.575	1.551
20.4	4.6	1.811	4.6	1.811	1.811
22.2	5.2	2.047	5.4	2.126	2.079
25.9	6.6	2.598	6.7	2.638	2.614
29.6	8.2	3.228	8.2	3.228	3.228
33.3	9.8	3.858	9.8	3.858	3.858
37.0	11.7	4.606	11.8	4.646	4.622
40.8	13.7	5.394	13.9	5.472	5.426
44.6	15.9	6.260	15.7	6.181	6.228
48.4	18.1	7.126	17.9	7.047	7.094
52.2	20.6	8.110	20.1	7.913	8.029
56.0	22.8	8.976	22.5	8.858	8.928
50.0	19.5	7.68	18.5	7.28	7.52
56.0	22.8	8.98	22.2	8.74	8.88
63.0	25.8	10.16	25.2	9.92	10.06
70.0	30.5	12.00	28.6	11.26	11.70
76.0	34.2	13.46	32.9	12.95	13.25
81.0	39.5	15.55	36.1	14.21	15.00
95.0	49.5	19.49	45.2	17.80	18.80
105.0	58.1	22.87	54.1	21.30	22.23
115.0	67.4	26.54	63.7	25.08	25.94
126.0	--	31.4	--	30.1	30.9
137.0	--	35.8	--	35.2	35.6
147.0	--	42.9	--	41.1	42.2
160.0	--	48.4	--	46.5	47.6
170.0	--	53.9	--	52.7	53.4
180.0	--	59.4	--	56.8	58.3
190.0	--	65.0	--	63.5	64.4
201.0	--	72.0	--	70.0	71.2
212.0	--	78.0	--	77.0	77.6
223.0	--	86.0	--	84.0	85.2
233.0	--	93.0	--	91.0	92.2
244.0	--	101.0	--	101.0	101.0
254.0	--	108.0	--	111.0	109.0

Table 3.5

Results of f_b, f_1 and f_2

Re_b	f_b	X_1	Re_1	f_1	X_2	Re_2	f_2
226	0.3913	0.76	158	0.6246	1.30	344	0.2704
340	0.2940	0.76	238	0.4132	1.30	517	0.2395
452	0.2155	0.76	317	0.3123	1.30	687	0.1689
565	0.1685	0.76	395	0.2487	1.30	859	0.1292
678	0.1607	0.76	474	0.2424	1.30	1,040	0.1200
791	0.1558	0.76	554	0.2281	1.30	1,200	0.1210
904	0.1440	0.76	633	0.2139	1.30	1,370	0.1097
866	0.1435	0.76	607	0.2119	1.30	1,310	0.1101
1,080	0.1173	0.76	757	0.1762	1.30	1,640	8.82 -2
1,300	0.1110	0.76	910	0.1694	1.30	1,970	8.15 -2
1,520	9.98 -2*	0.76	1,064	0.1503	1.30	2,310	7.44 -2
1,730	9.52 -2	0.76	1,210	0.1482	1.30	2,630	6.88 -2
1,960	8.80 -2	0.76	1,370	0.1371	1.30	2,980	6.31 -2
2,170	8.36 -2	0.76	1,520	0.1321	1.30	3,300	5.87 -2
2,390	8.02 -2	0.76	1,670	0.1282	1.30	3,630	5.56 -2
2,600	7.79 -2	0.76	1,820	0.1233	1.30	3,950	5.51 -2
3,030	7.18 -2	0.76	2,120	0.1141	1.30	4,610	5.02 -2
3,470	6.80 -2	0.76	2,430	0.1085	1.30	5,280	4.70 -2
3,900	6.42 -2	0.79	2,840	9.48 -2	1.28	5,840	4.58 -2
4,330	6.23 -2	0.80	3,190	8.94 -2	1.26	6,380	4.58 -2
4,780	6.02 -2	0.81	3,570	8.40 -2	1.25	6,970	4.52 -2
5,220	5.78 -2	0.83	3,990	7.77 -2	1.22	7,460	4.52 -2
5,670	5.58 -2	0.84	4,390	7.33 -2	1.21	8,020	4.47 -2
6,110	5.44 -2	0.85	4,790	7.01 -2	1.20	8,570	4.42 -2
6,560	5.25 -2	0.87	5,260	6.43 -2	1.17	8,970	4.50 -2
7,380	4.70 -2	0.88	5,980	5.62 -2	1.16	10,000	4.01 -2
8,190	4.41 -2	0.89	6,720	5.26 -2	1.14	10,900	3.82 -2
8,900	4.25 -2	0.90	7,380	4.89 -2	1.13	11,800	3.79 -2
9,480	4.22 -2	0.91	7,940	4.87 -2	1.12	12,500	3.73 -2
11,100	3.84 -2	0.92	9,410	4.33 -2	1.10	14,300	3.53 -2
12,300	3.72 -2	0.93	10,500	4.08 -2	1.09	15,700	3.51 -2
13,500	3.61 -2	0.94	11,700	3.86 -2	1.08	17,000	3.52 -2
14,400	3.59 -2	0.95	12,600	3.73 -2	1.07	18,100	3.56 -2
15,800	3.60 -2	0.95	13,800	3.70 -2	1.07	19,800	3.64 -2
17,200	3.60 -2	0.95	15,100	3.74 -2	1.06	21,300	3.65 -2
18,700	3.43 -2	0.96	16,600	3.49 -2	1.06	23,200	3.50 -2
19,900	3.41 -2	0.96	17,600	3.44 -2	1.05	24,400	3.57 -2
21,100	3.32 -2	0.96	18,700	3.39 -2	1.05	25,900	3.43 -2
22,200	3.39 -2	0.96	19,600	3.33 -2	1.05	27,300	3.44 -2
23,500	3.25 -2	0.96	20,800	3.29 -2	1.05	28,900	3.39 -2
24,800	3.19 -2	0.96	21,900	3.21 -2	1.05	30,400	3.36 -2
26,100	3.16 -2	0.96	23,100	3.20 -2	1.05	32,000	3.31 -2
27,300	3.13 -2	0.96	24,100	3.16 -2	1.05	33,500	3.29 -2
28,600	3.13 -2	0.96	25,300	3.13 -2	1.05	33,510	3.32 -2
29,700	3.12 -2	0.96	26,200	3.09 -2	1.05	36,500	3.37 -2

* $\underline{-2} \equiv \times 10^{-2}$

Table 3.6

Experimental Results of ε_1^* and ε_{1L}^*

Run	Re_b	X_1	X_2	Mass Balance Ratio	Input C_1	Minimum Mean Square Indicator	ε_1^*	ε_{1L}^*
1	220	0.76	1.30	1.70	0.10	11.92	0.049	0.065
2	430	0.76	1.30	1.81	0.10	8.19	0.058	0.076
3	860	0.76	1.30	1.35	0.10	5.64	0.058	0.076
4	1,500	0.76	1.30	1.39	0.10	5.63	0.071	0.093
5	2,200	0.76	1.30	1.15	0.20	5.23	0.082	0.108
6	3,200	0.76	1.30	1.36	0.20	5.54	0.085	0.112
7	4,300	0.80	1.26	1.13	0.30	5.27	0.095	0.119
8	5,400	0.84	1.20	1.31	0.30	5.88	0.087	0.104
9	6,500	0.86	1.17	1.44	0.30	5.93	0.094	0.109
10	9,400	0.91	1.11	1.58	0.30	5.89	0.095	0.104
11	12,200	0.94	1.08	1.57	0.30	6.13	0.107	0.114
12	14,800	0.95	1.07	1.67	0.30	5.71	0.109	0.115
13	18,600	0.96	1.06	1.58	0.30	6.39	0.115	0.120
14	22,100	0.96	1.05	1.42	0.30	6.44	0.111	0.116
15	26,000	0.96	1.05	1.42	0.30	6.28	0.114	0.119
16	29,600	0.96	1.05	1.43	0.30	6.44	0.108	0.113

Table 3.7

Experimental Results of C_1 and C_{1L}

Run	Re_b	X_1	X_2	Mass Balance Ratio	Input ε_1^*	Minimum Mean Square Indicator	C_1	C_{1L}
17	430	0.76	1.30	2.01	0.06	18.69	0.225	0.173
18	860	0.76	1.30	1.53	0.06	13.36	0.248	0.191
19	1,500	0.76	1.30	1.05	0.07	13.51	0.258	0.199
20	2,200	0.76	1.30	1.27	0.08	11.51	0.278	0.214
21	3,200	0.76	1.30	1.34	0.09	11.38	0.311	0.239
22	4,300	0.80	1.26	0.94	0.10	12.66	0.287	0.228
23	5,400	0.84	1.20	1.38	0.10	10.57	0.297	0.248
24	6,500	0.86	1.17	1.11	0.10	9.31	0.281	0.240
25	9,400	0.91	1.11	1.20	0.10	9.41	0.284	0.256
26	12,200	0.94	1.08	1.20	0.10	9.41	0.289	0.268
27	14,800	0.95	1.07	1.62	0.11	9.43	0.285	0.267
28	18,600	0.96	1.06	1.40	0.11	8.96	0.291	0.275
29	22,100	0.96	1.05	1.50	0.11	9.22	0.291	0.277
30	26,000	0.96	1.05	1.22	0.11	9.29	0.305	0.290

Table 3.8

Error Associated with Experimental Results of Mixing Parameters

	ε^*_{1L}	C_{1L}	ε^*_1	C_1
$Re_b < 6{,}000$	23%	23%	25%	25%
$Re_b \geq 6{,}000$	23%	21%	24%	22%

Table 4.1

ϕ_t from Different Bundle Results

Source	H/D	P/D	N_R	$\phi_t \equiv \frac{V_T}{V_b \tan\theta}$
MIT Blanket[a] [12]	4	1.067	61	0.41
MIT Blanket[a] [12]	8	1.067	61	0.86
MIT[a] *	13.4	1.154	37	1.07
Grenoble[c] [31]	19	1.19	19	1.30
MIT Fuel[b] [28]	24	1.25	61	1.26
MIT Fuel[b] [28]	48	1.25	61	1.59
ANL[a] [19]	48	1.24	91	1.2
MIT Fuel[a] [17]	52	1.25	217	1.45

* Our work

a Salt injection

b LDA

c Flow visualization (bubbles)

Table 4.2

Geometric Parameters and Type of Experiment for Mixing Data

Investigator		P/D	H/D	N_R	Type of Experiment
MIT Fuel (Chiu)	[12]	1.067	6, 4	61	Salt injection
Cadarache (Skok)	[29]	1.14	14, 21, 29	7	Hot water injection
MIT (Cheng)	*	1.154	13.4	37	Salt injection
Japanese (Okamoto)	[23]	1.20	43	91	Salt injection
HEDL (Collingham)	[27]	1.24	52	217	Salt injection
ANL-RAS (Pedersen)	[30]	1.24	48	91	Hot water injection
ANL-CT (Lorentz)	[19]	1.24	48	91	Salt injection
ORNL (Fontana)	[26]	1.24	52	19	Heated Rod
MIT Fuel (Chen)	[28]	1.25	24, 48	61	Laser
MIT Fuel (Hanson)	[21]	1.25	24, 48	61	Salt injection
MIT Fuel (Symolon)	[17]	1.25	52	217	Salt injection
GE (Hines)	[24]	1.28	24	127	Hot water injection
Karlsruhe (Baumann)	[25]	1.315	17, 33, 50	61	Heated rod

* Our work

APPENDIX A

NORMALIZED FLOW SPLIT MAP RESULTS OF FLOW SPLIT EXPERIMENT

RUN 1

M_L = 32.5 GPM

Re_b = 3,470

X_1 = 0.763

X_2 = 1.307

Mass Balance Error = -12%

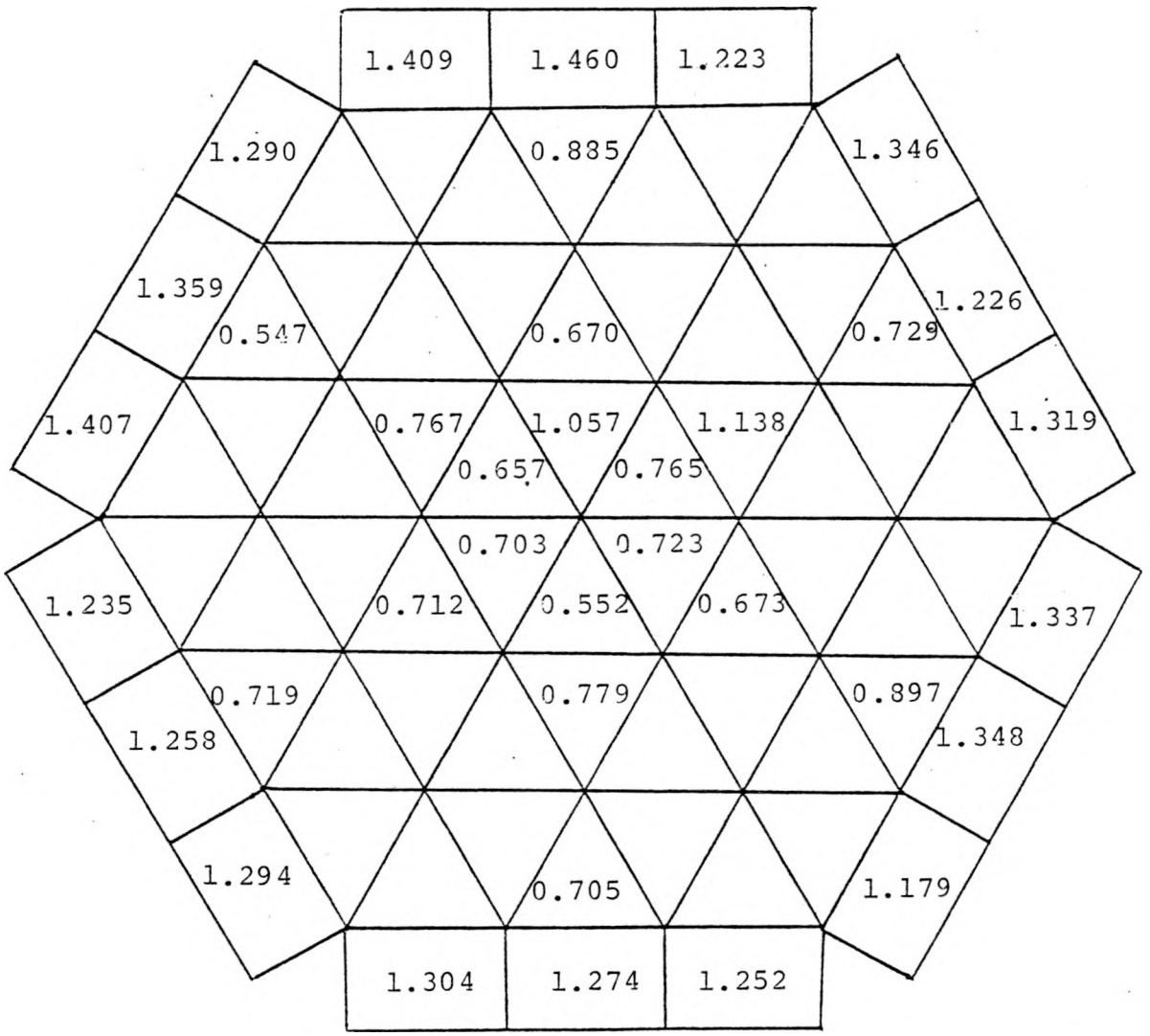

RUN 2

M_L = 42.8 GPM

Re_b = 4,570

X_1 = 0.800

X_2 = 1.259

Mass Balance Error = -5.0%

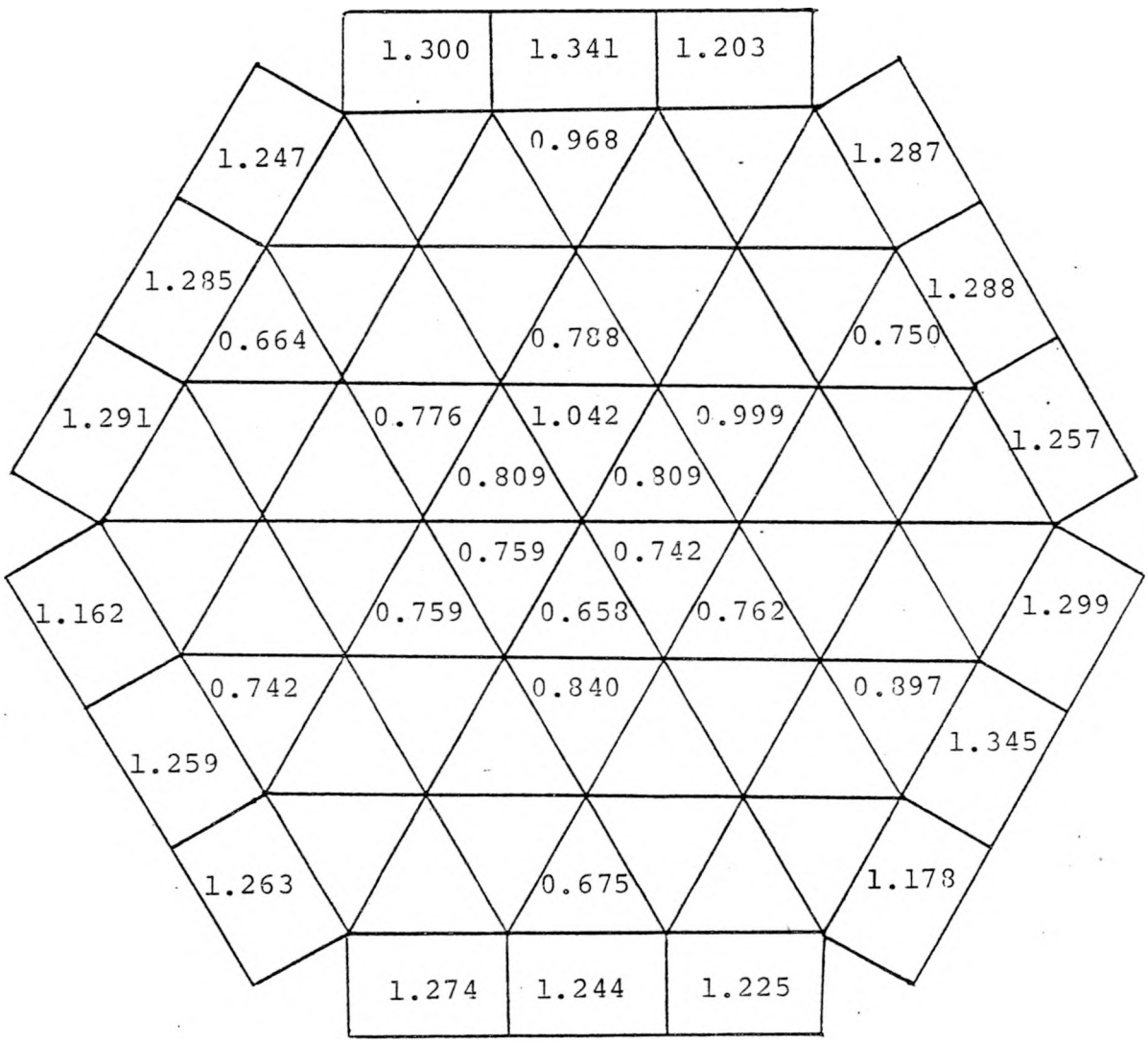

RUN 3

M_L = 52.4 GPM

Re_b = 5,600

X_1 = 0.841

X_2 = 1.206

Mass Balance Error = -3.5%

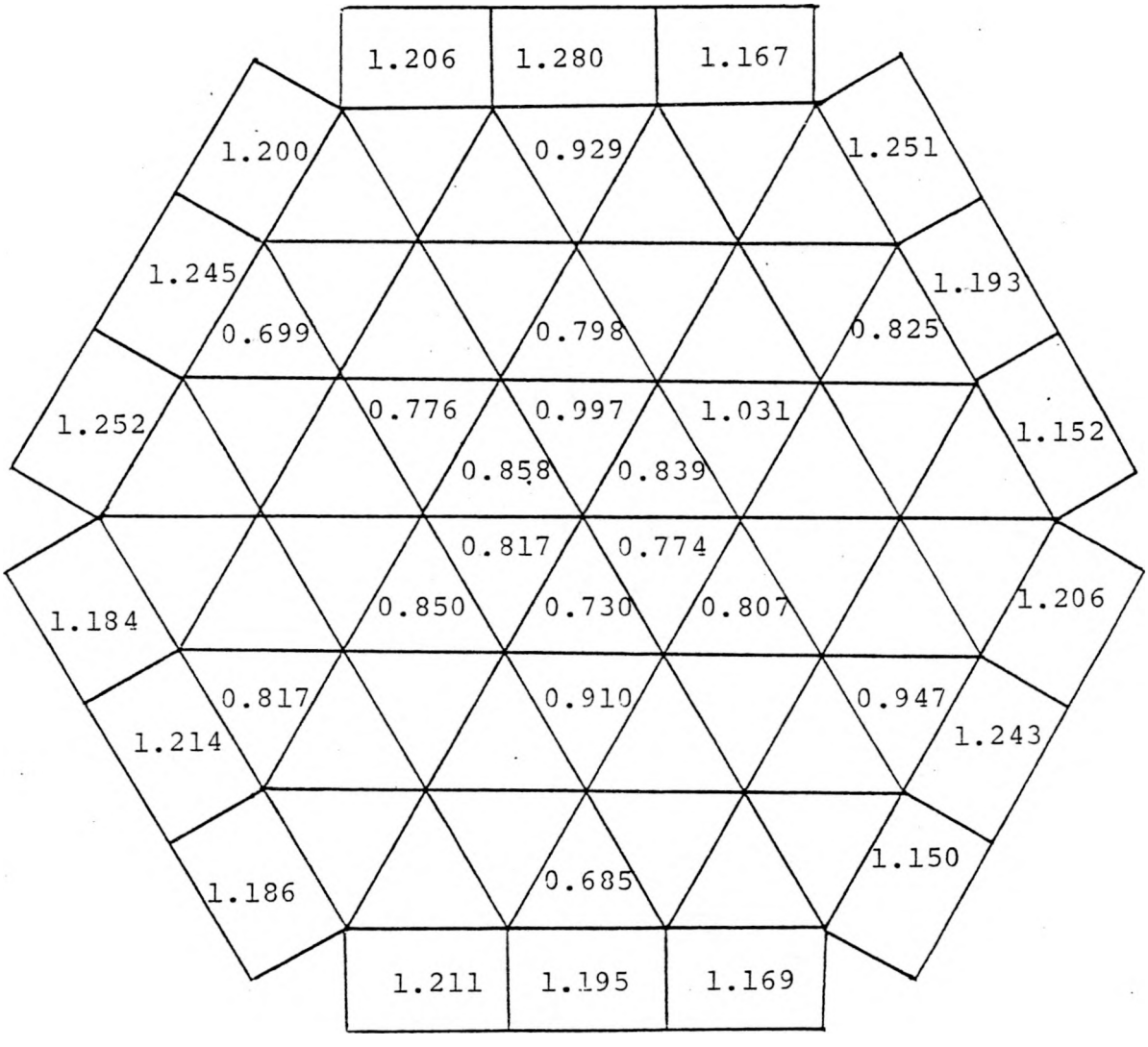

RUN 4

M_L = 56 GPM

Re_b = 5,950

X_1 = 0.864

X_2 = 1.175

Mass Balance Error = -1.6%

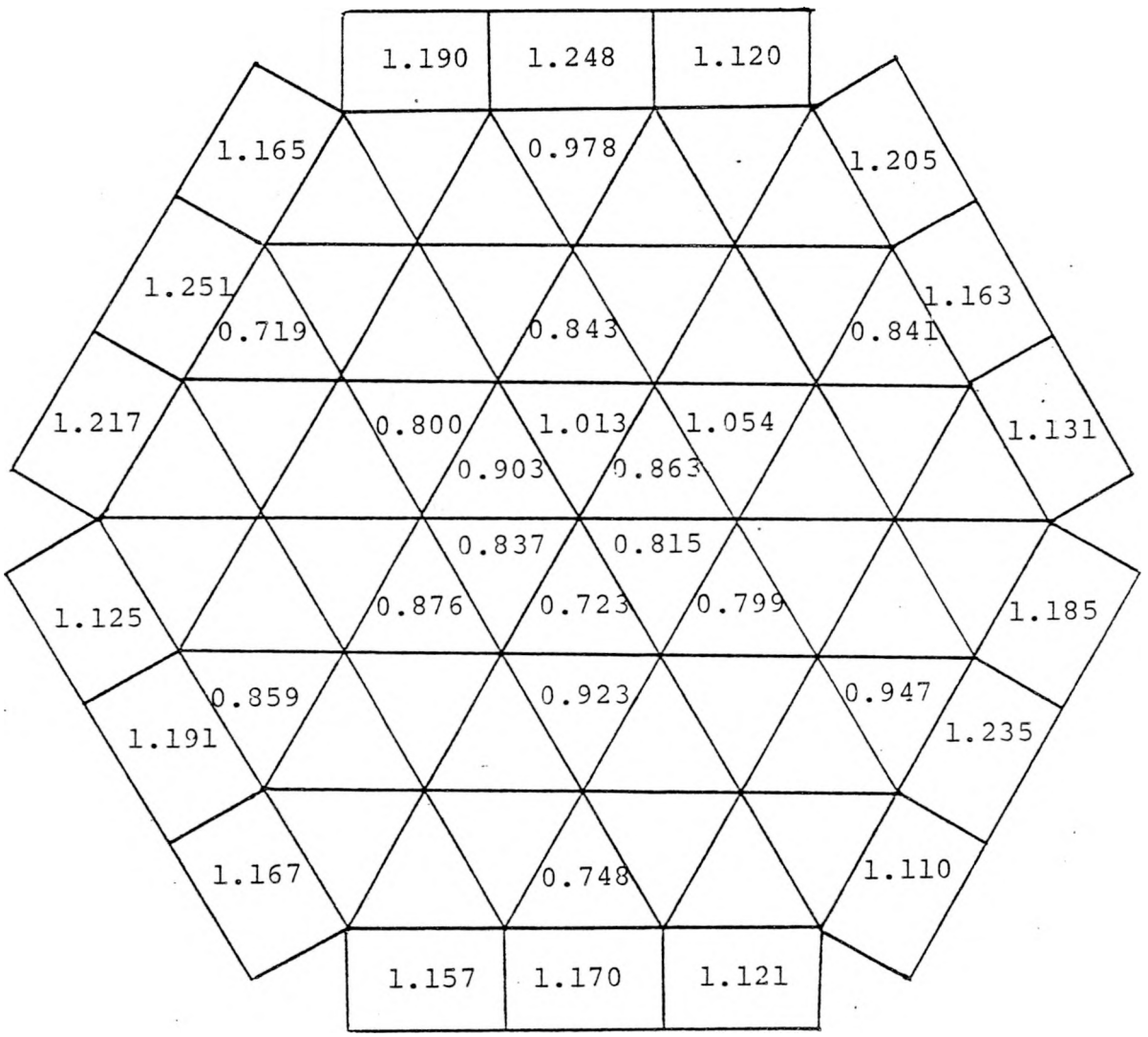

RUN 5

M_L = 70 GPM

Re_b = 7,440

X_1 = 0.875

X_2 = 1.161

Mass Balance Error = -2.2%

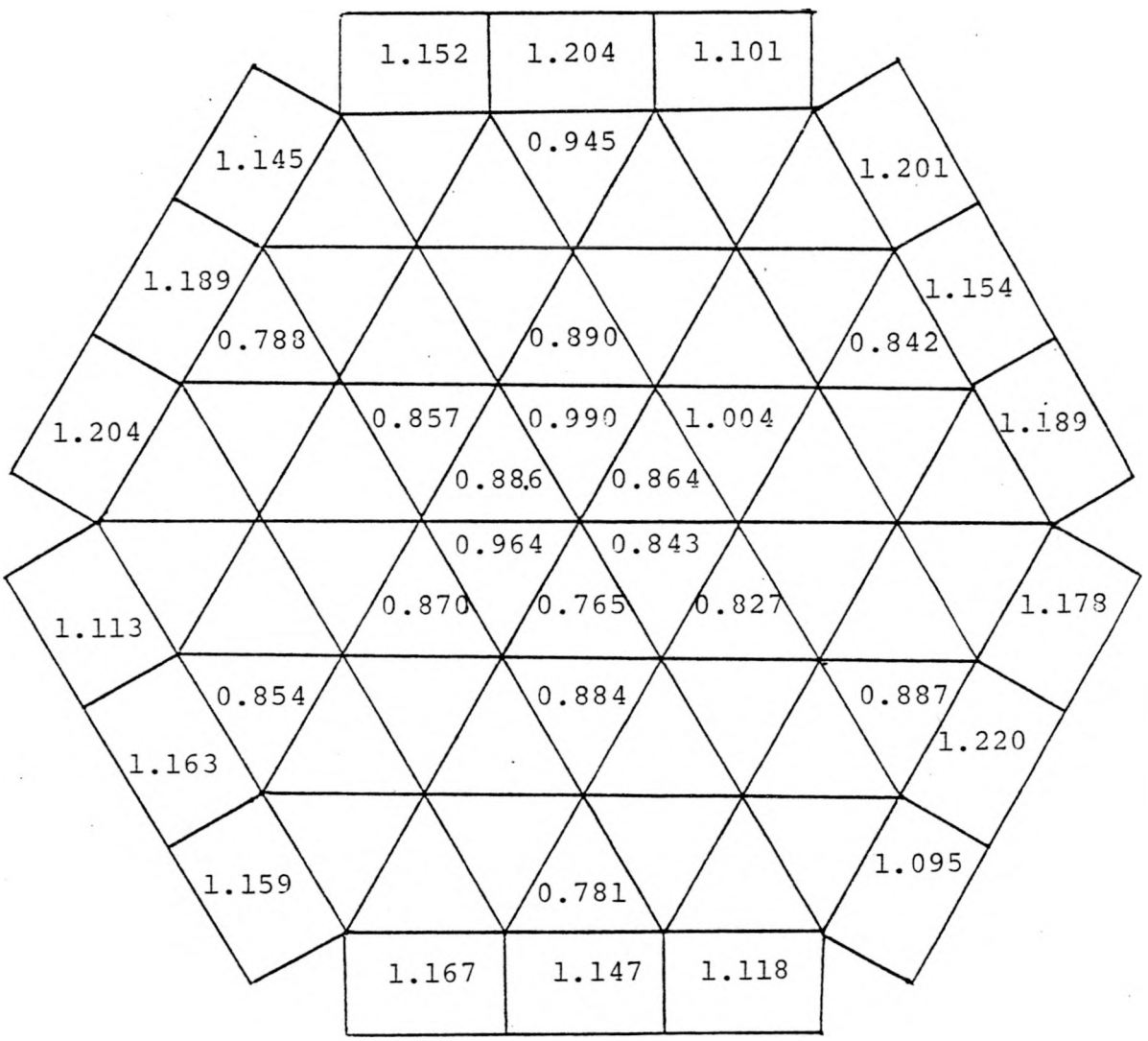

RUN 6

M_L = 70 GPM

Re_b = 7,630

X_1 = 0.879

X_2 = 1.155

Mass Balance Error = -1.4%

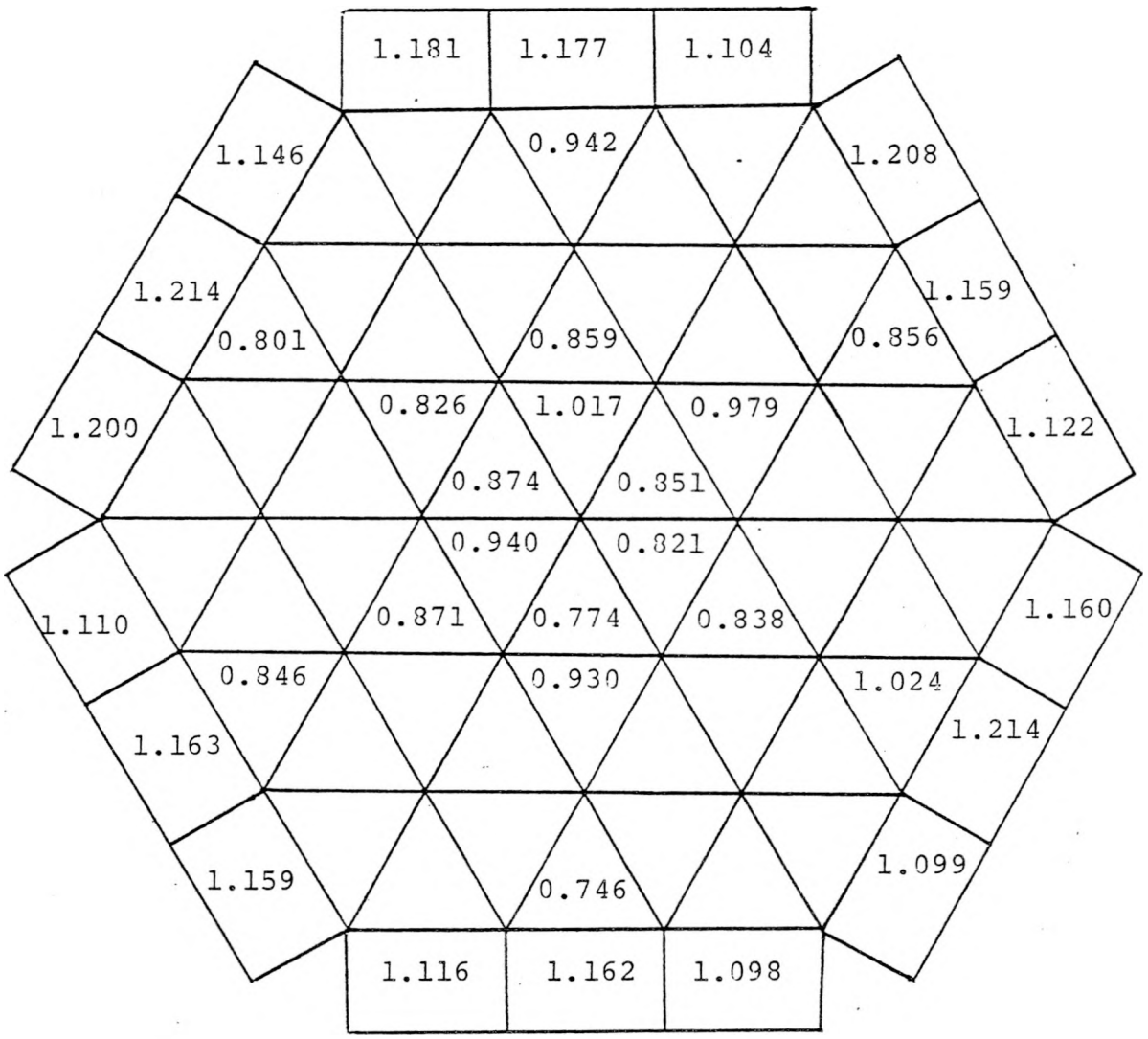

RUN 7

M_L = 81 GPM

Re_b = 8,620

X_1 = 0.894

X_2 = 1.136

Mass Balance Error = -2.8%

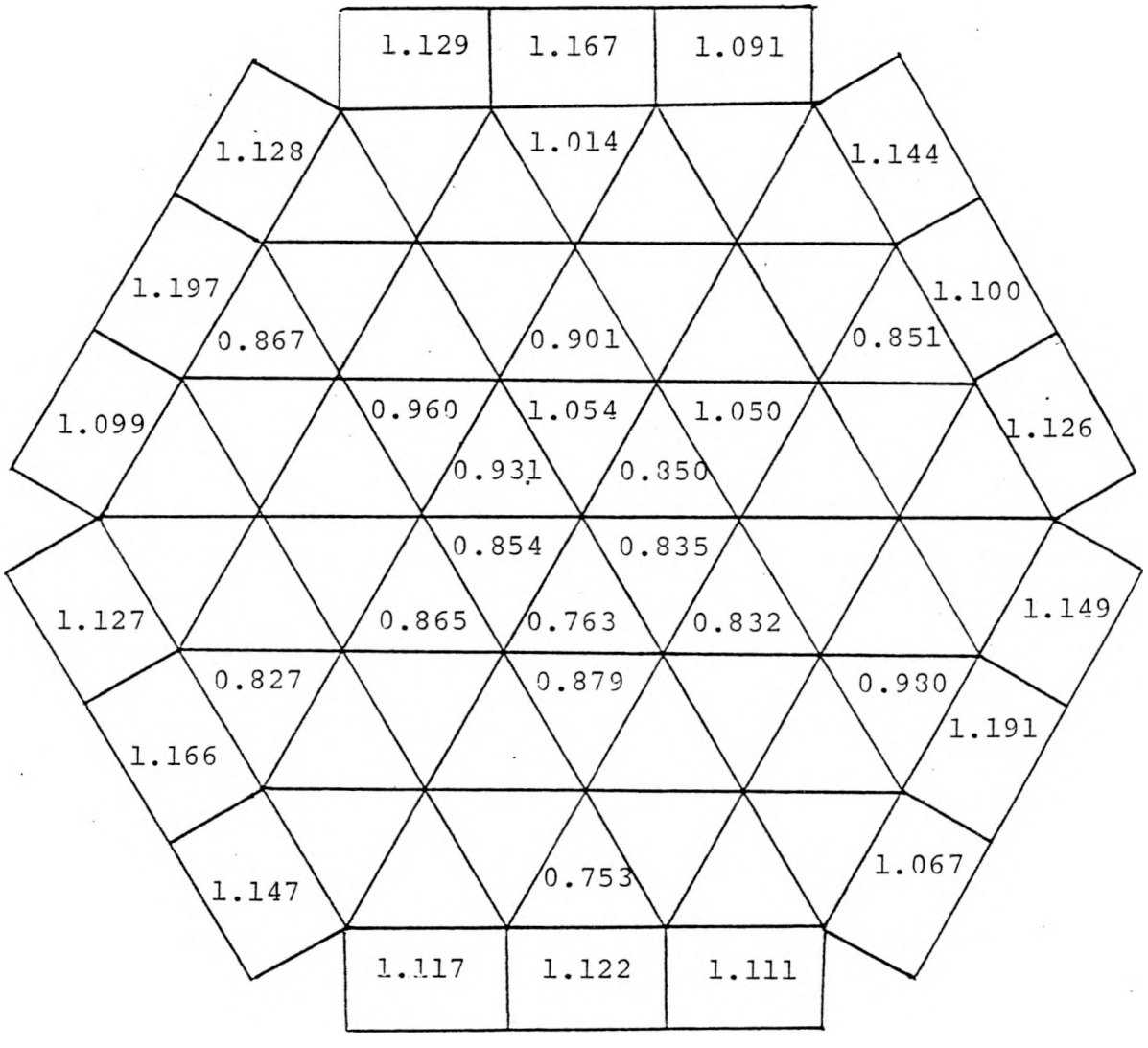

RUN 8

M_L = 100 GPM

Re_b = 10,480

X_1 = 0.915

X_2 = 1.110

Mass Balance Error = -3.7%

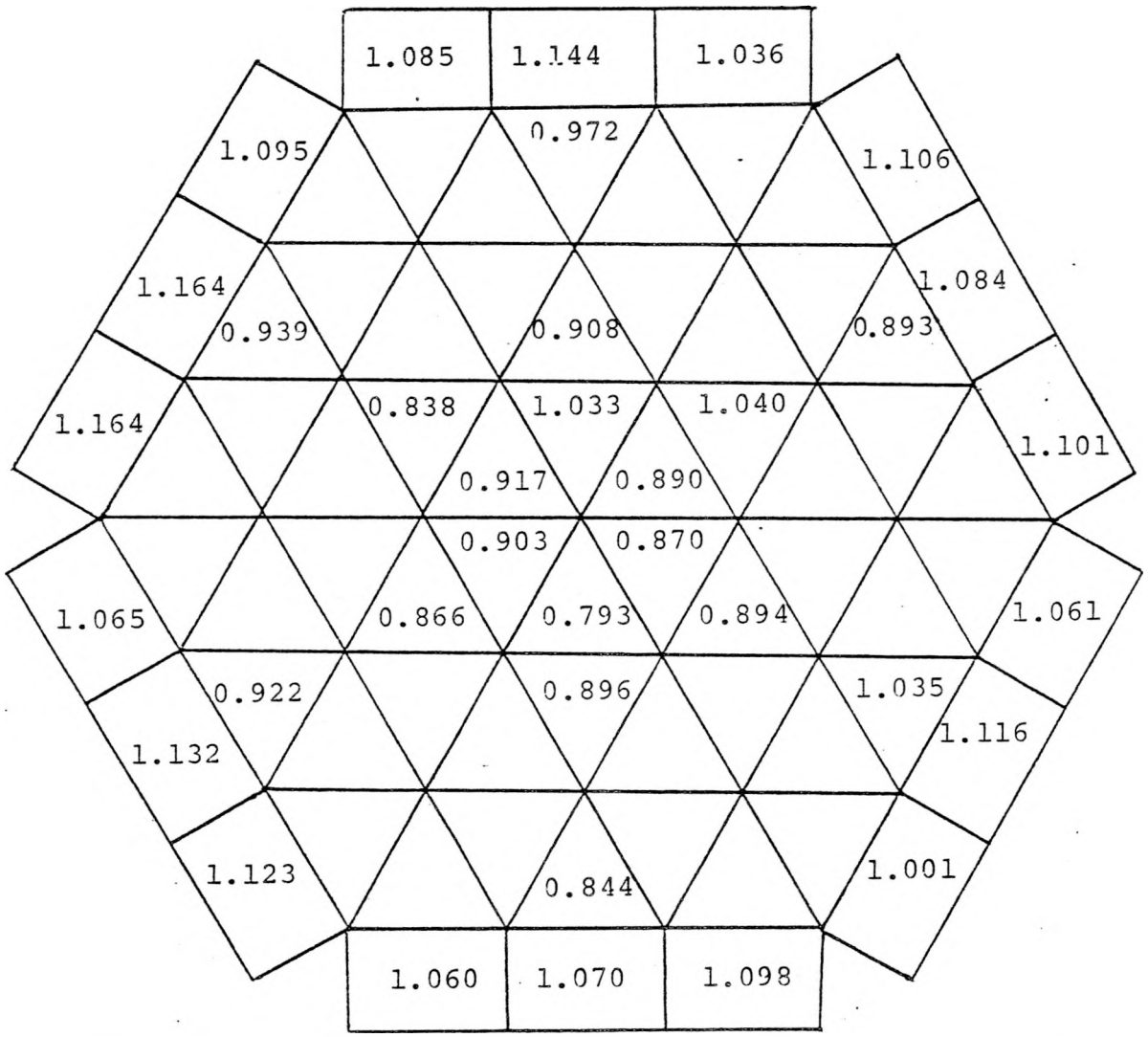

RUN 9

M_L = 105 GPM

Re_b = 11,380

X_1 = 0.916

X_2 = 1.109

Mass Balance Error = -3.5%

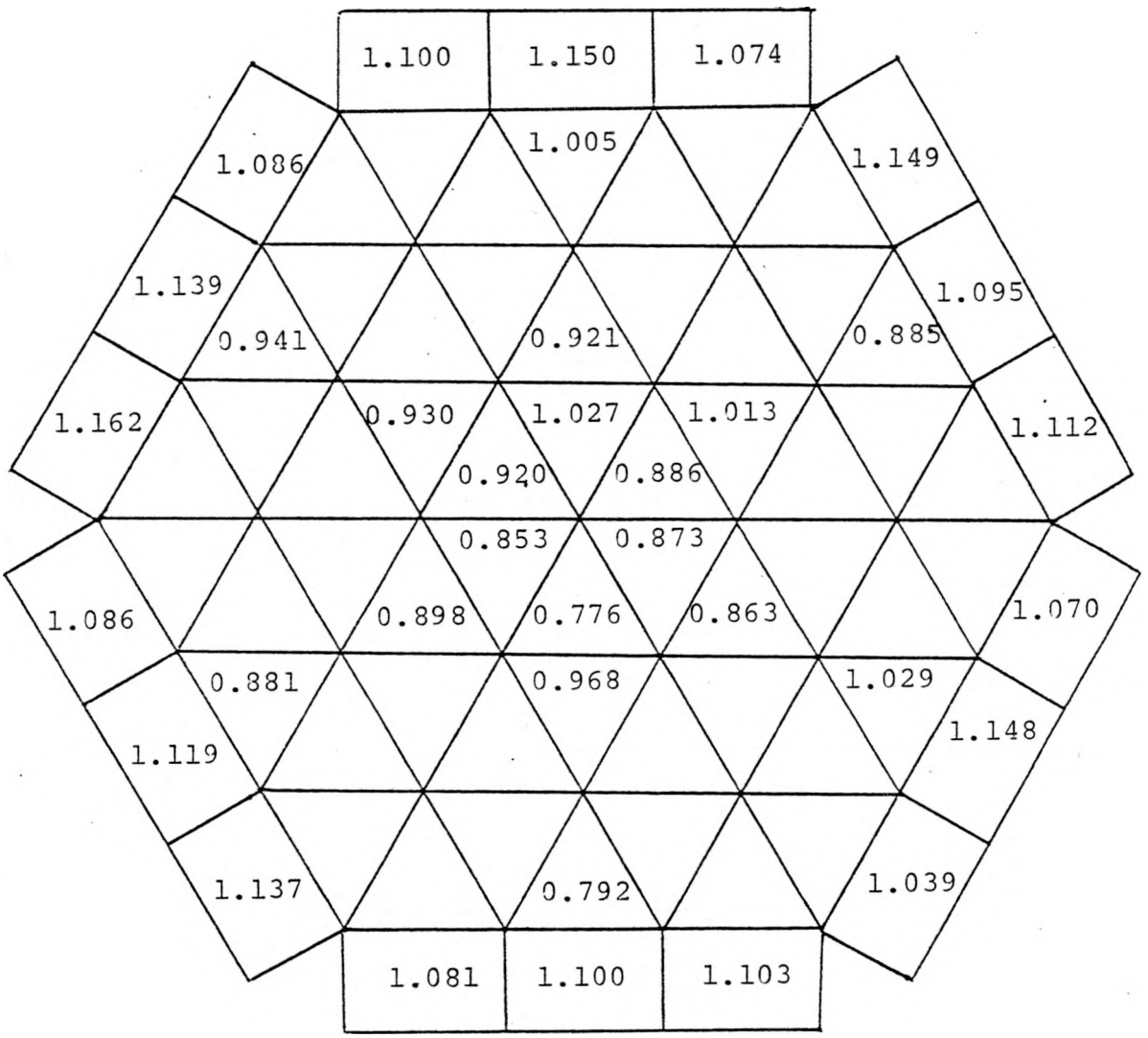

RUN 10

M_L = 121 GPM

Re_b = 10,740

X_1 = 0.949

X_2 = 1.079

Mass Balance Error = -3.6%

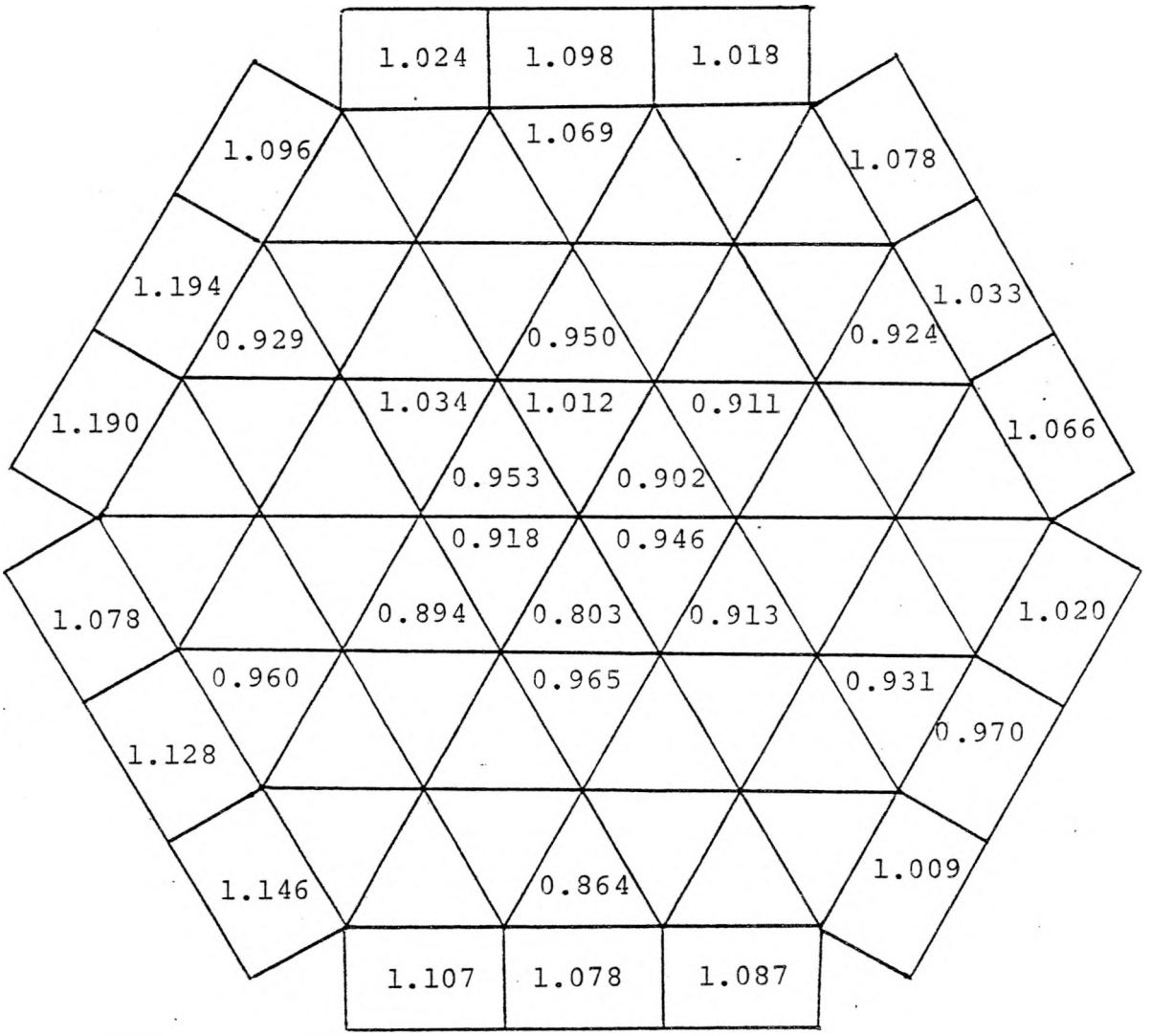

RUN 11

M_L = 142 GPM

Re_b = 12,840

X_1 = 0.936

X_2 = 1.082

Mass Balance Error = -4.4%

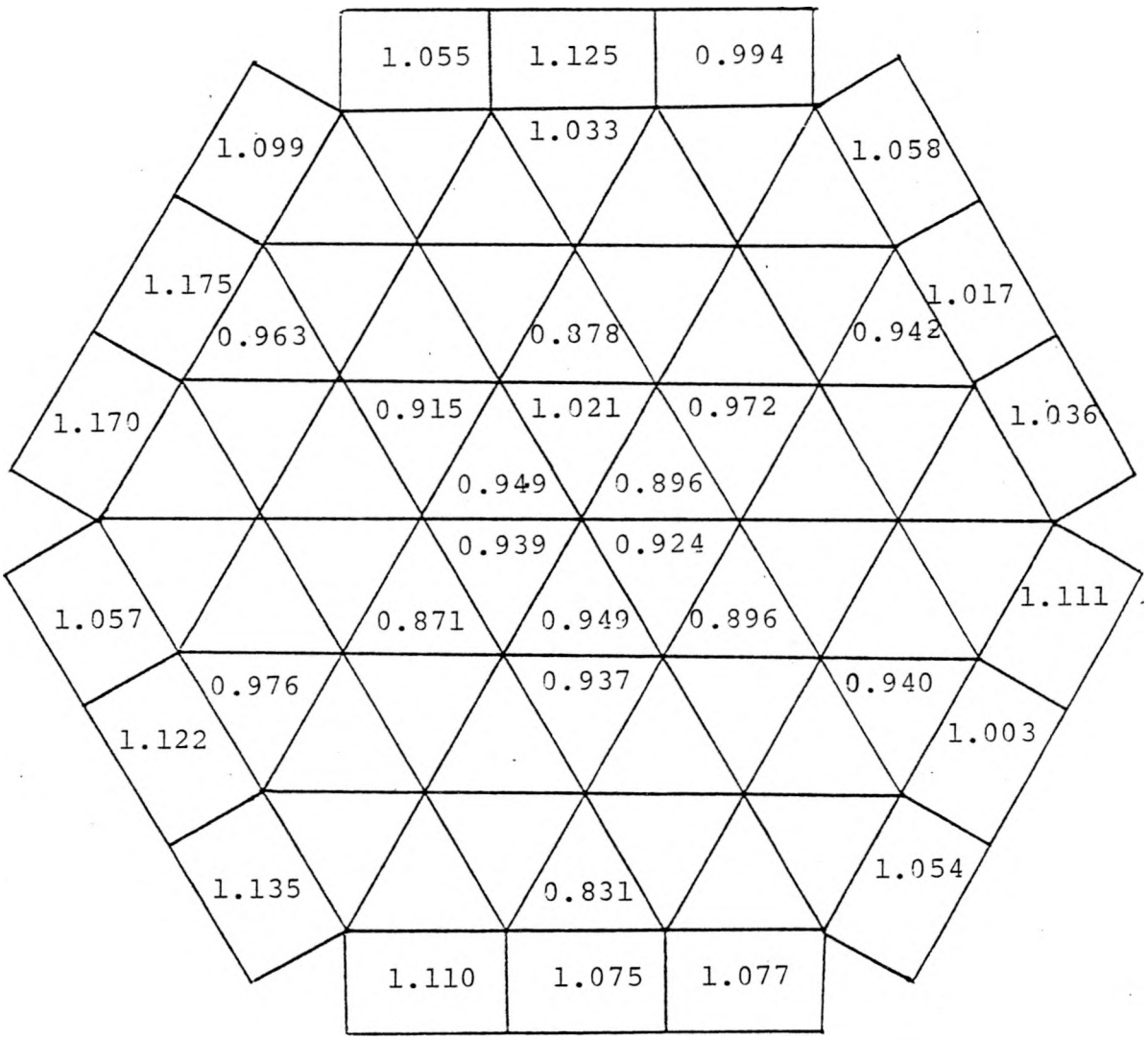

RUN 12

M_L = 173 GRM

Re_b = 16,170

X_1 = 0.934

X_2 = 1.085

Mass Balance Error = -2.8%

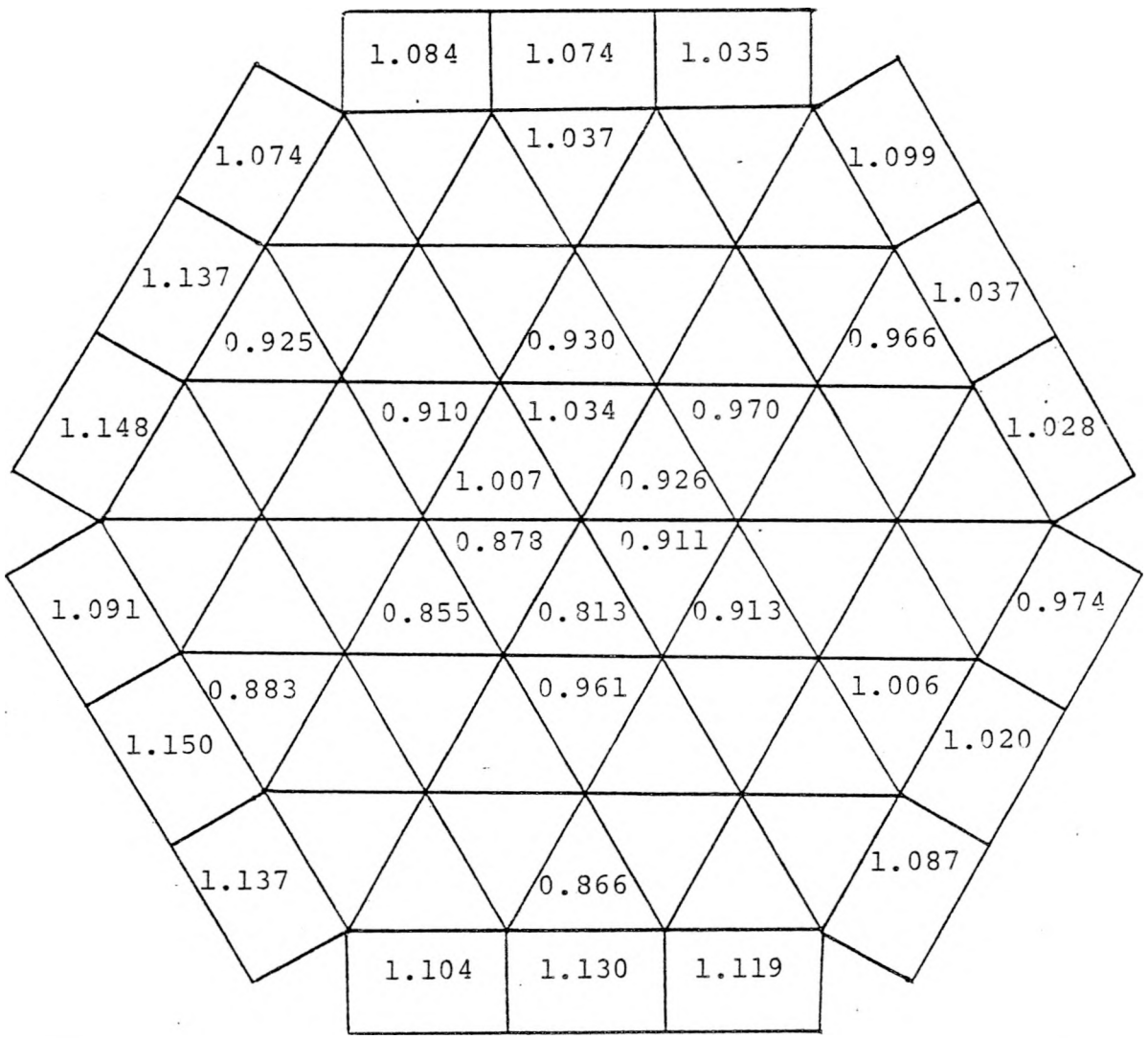

RUN 13

M_L = 197 GPM

Re_b = 18,960

X_1 = 0.939

X_2 = 1.078

Mass Balance Error = -3.4%

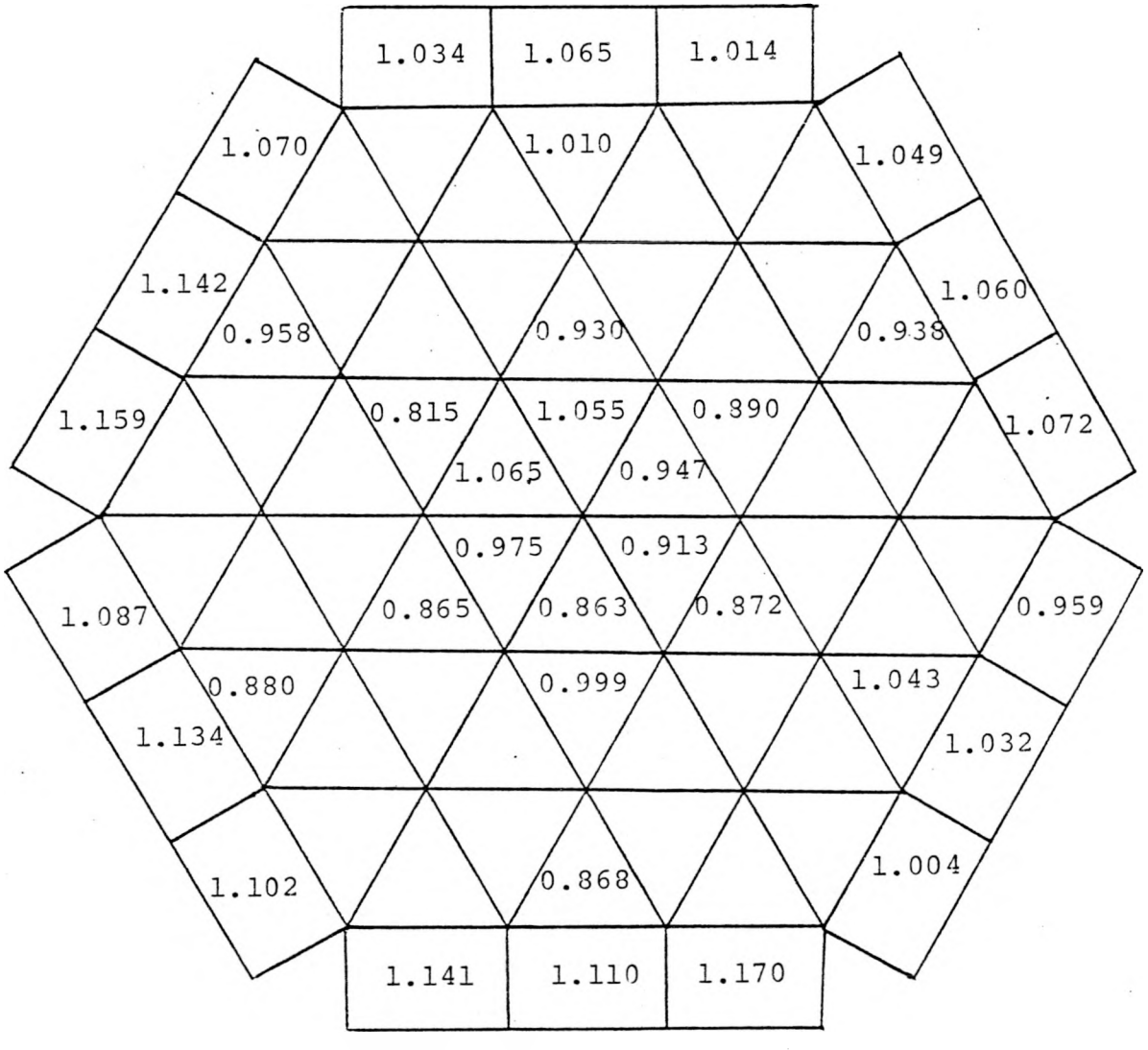

RUN 14

M_L = 224 GPM

Re_b = 21,600

X_1 = 0.962

X_2 = 1.048

Mass Balance Error = -2.2%

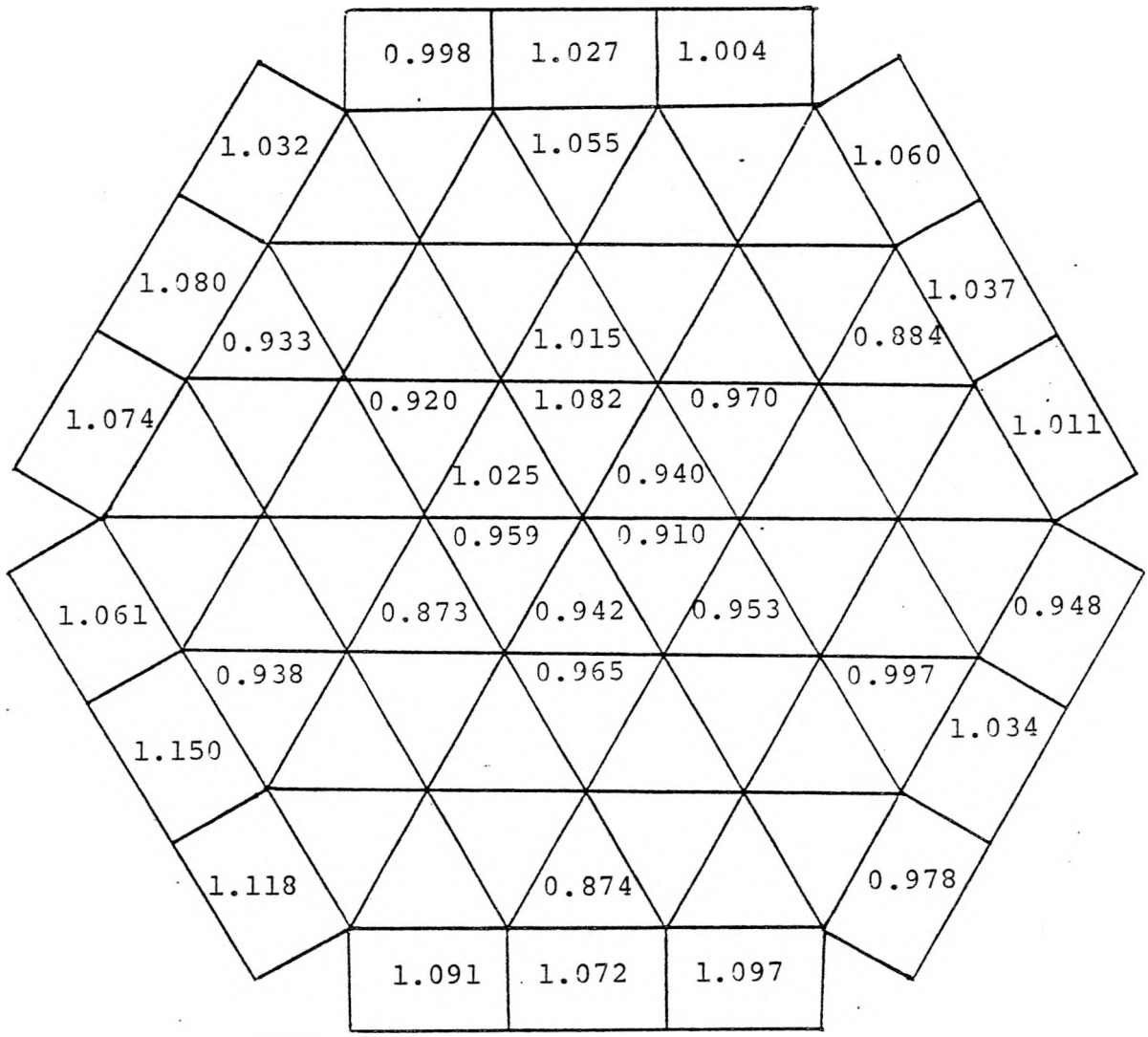

RUN 15

M_L = 220 GPM

Re_b = 22,510

X_1 = 0.953

X_2 = 1.060

Mass Balance Error = -2.0%

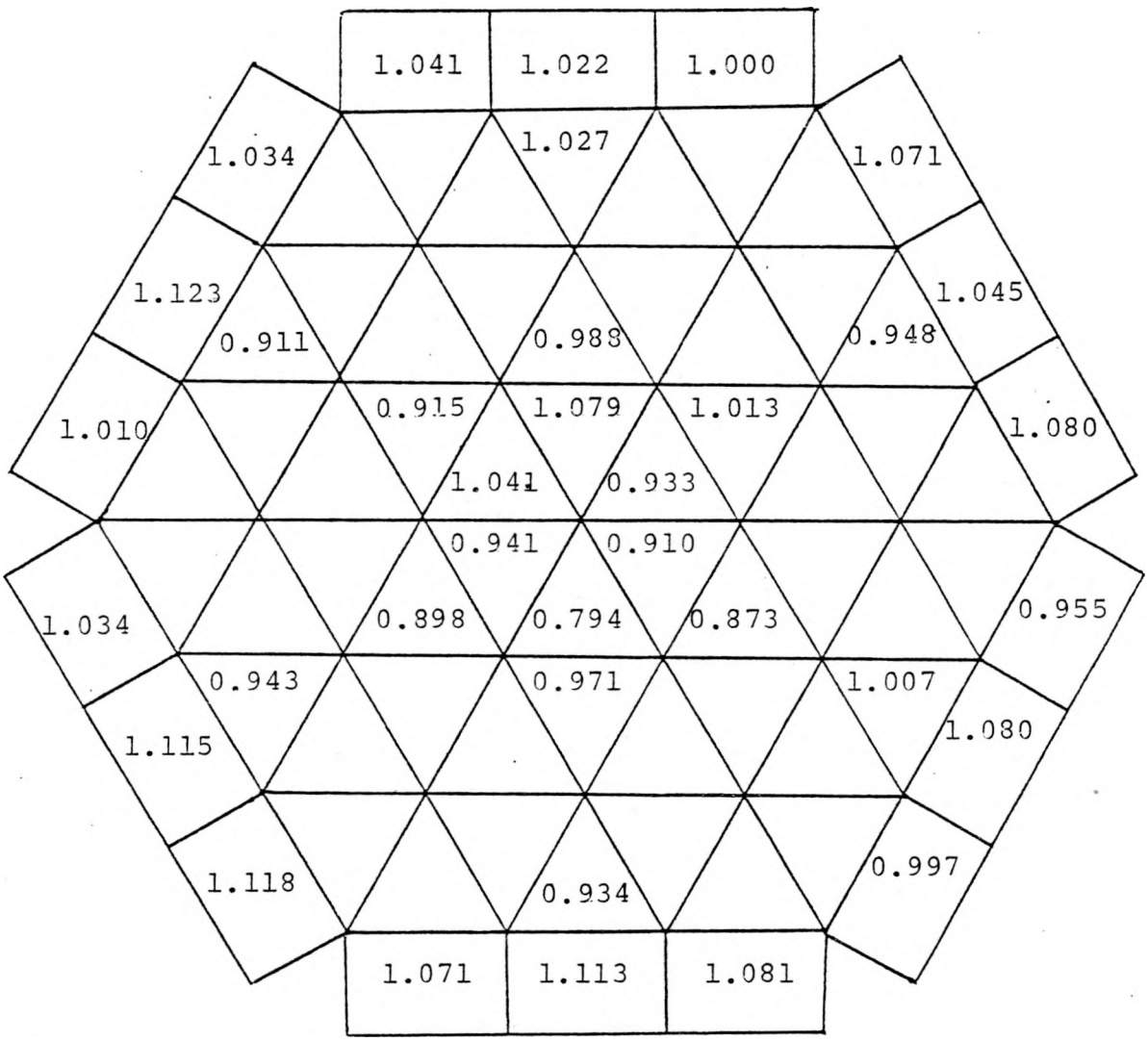

RUN 16

M_L = 215 GPM

Re_b = 26,300

X_1 = 0.967

X_2 = 1.042

Mass Balance Error = +0.9%

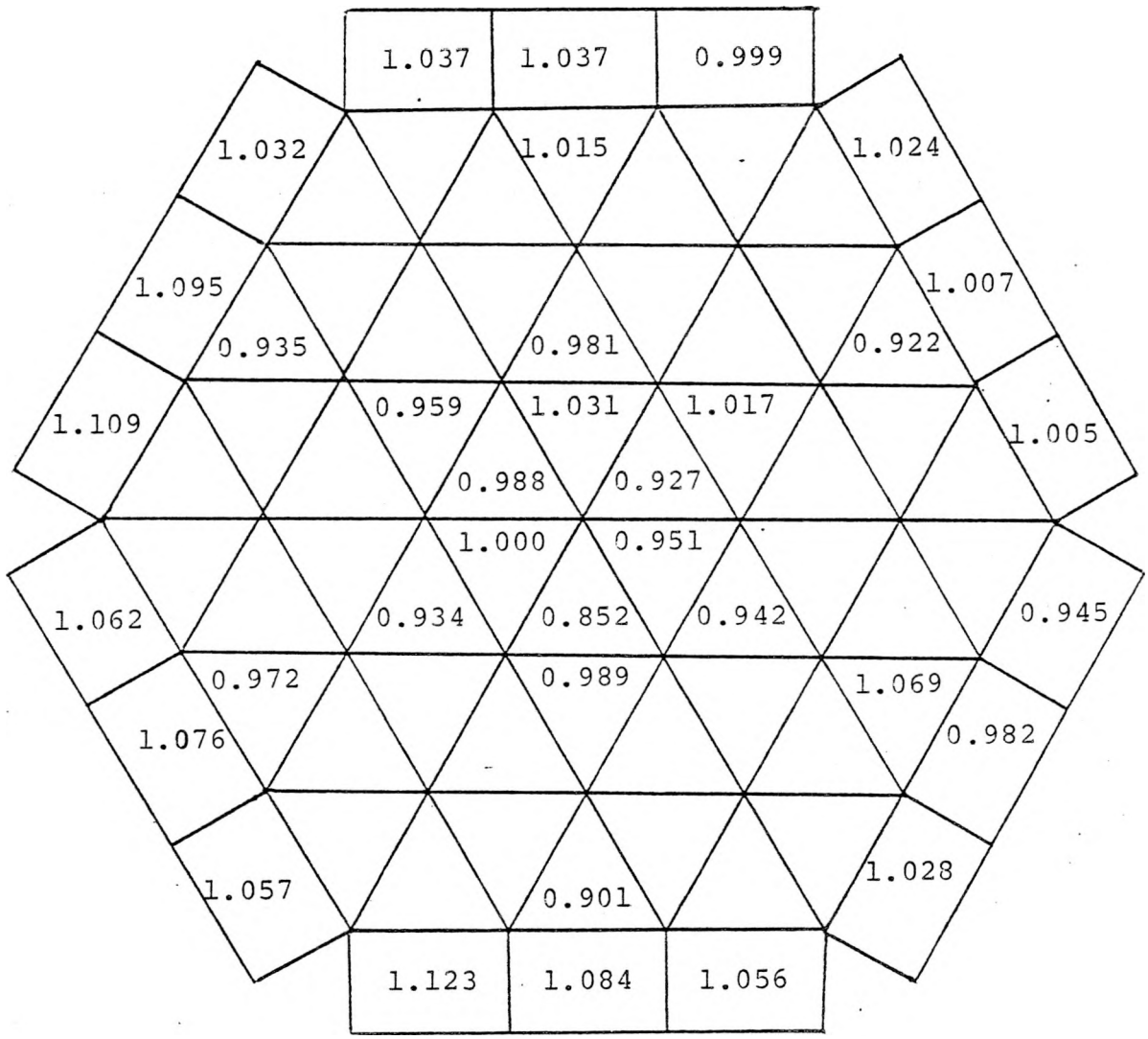

APPENDIX B

EFFECT OF DIFFERENT ASSUMPTION OF FLOW SPLIT PARAMETER FOR Re_b < 3,500 IN SUBCHANNEL FRICTION FACTORS RESULT

The isokinetic extraction method was not applicable for Re_b < 3,500; thereby no flow split data attained in this flow region. In reducing subchannel friction factors, we used the assumption that the flow split parameters are constant for Re_b < 3,500. In order to compare the difference between different assumptions, the extrapolation value of the flow split parameters were used to reduce pressure drop data to get another set of subchannel friction factors. The correct value lies between these two extremes.

Table B.1 shows the different assumed flow split parameters and the reduced subchannel friction factors up to Re_b = 3,500. Figures B.1 and B.2 illustrate these two sets of data for interior and edge subchannel friction factors, respectively.

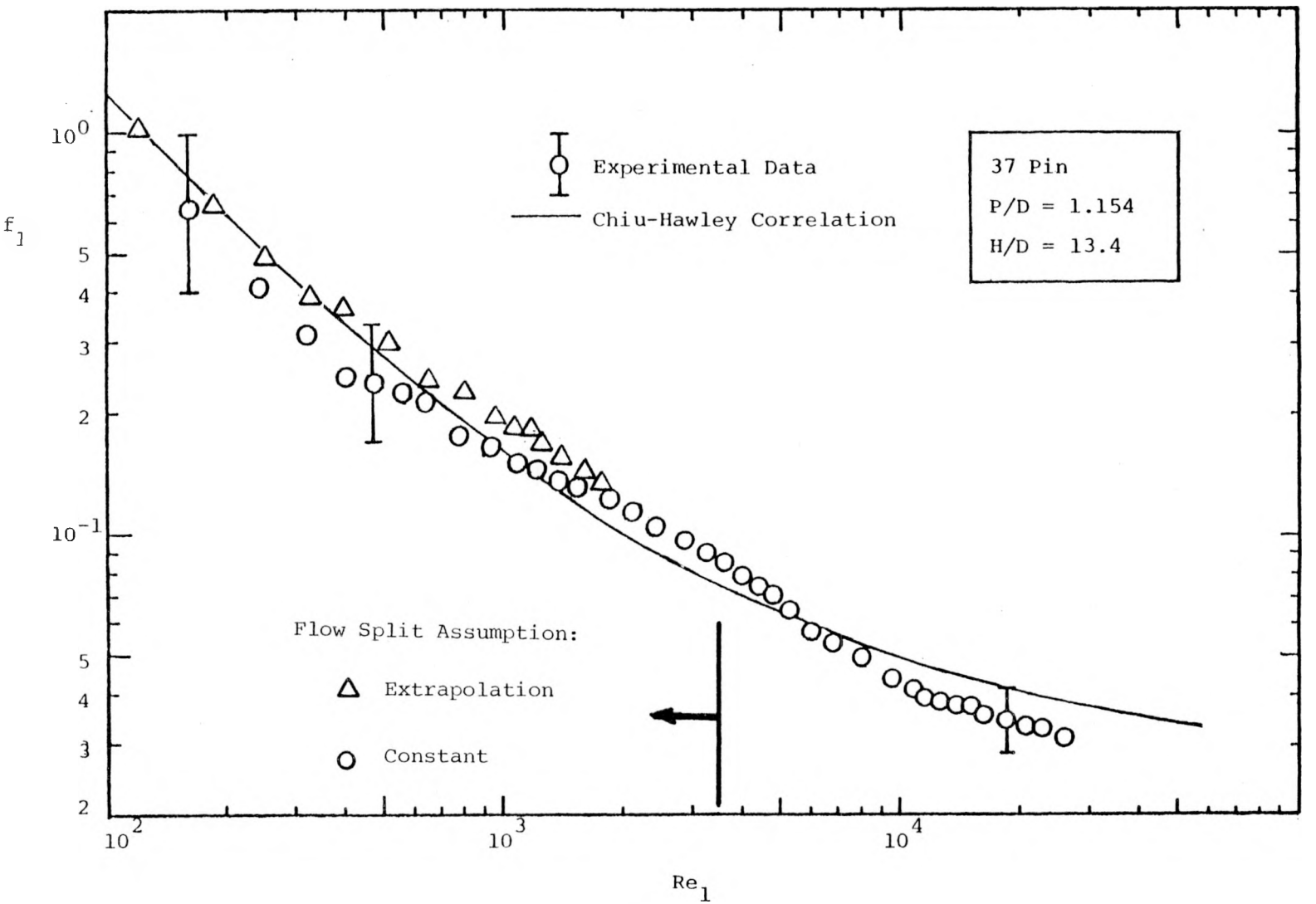

Figure B.1 Interior Subchannel Friction Factor versus Interior Subchannel Reynolds Number

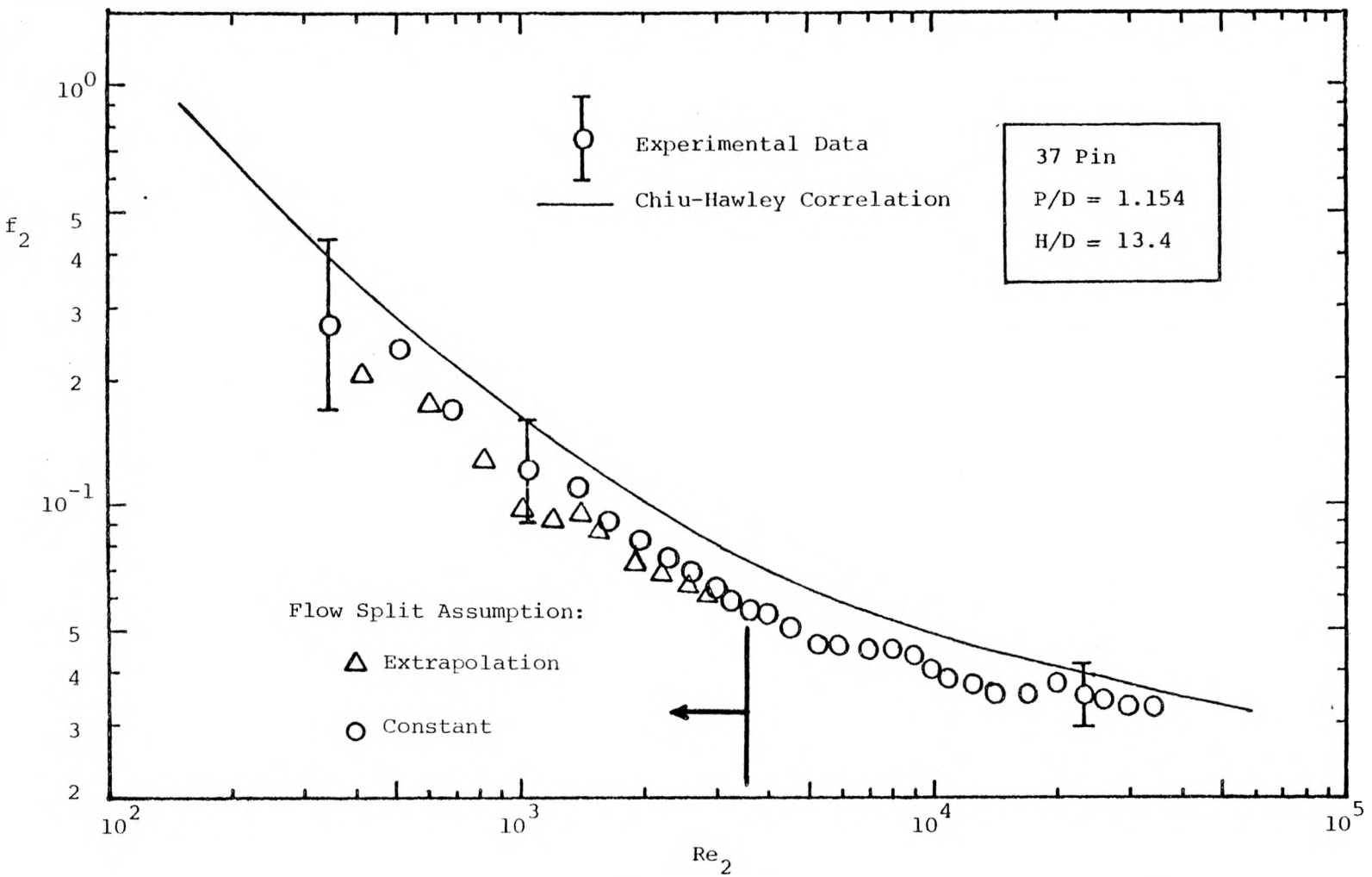

Figure B.2 Edge Subchannel Friction Factor versus Edge Subchannel Reynolds Number

Table B.1

X_1 and f_i from Extrapolation Assumption in Flow Split Parameter

Re_b	X_1	Re_1	f_1	X_2	Re_2	f_2
226	0.600	125	1.0021	1.520	402	0.1978
340	0.600	188	0.6630	1.520	605	0.1752
452	0.610	254	0.4848	1.508	797	0.1255
565	0.615	320	0.3798	1.502	992	9.68 -2*
678	0.620	387	0.3643	1.495	1,190	9.07 -2
791	0.630	459	0.3320	1.482	1,370	9.31 -2
904	0.640	533	0.3017	1.469	1,550	8.59 -2
866	0.635	507	0.3035	1.476	1,490	8.54 -2
1,080	0.650	647	0.2409	1.456	1,840	7.03 -2
1,300	0.665	796	0.2213	1.436	2,180	6.68 -2
1,520	0.675	945	0.1913	1.424	2,530	6.20 -2
1,730	0.685	1,090	0.1824	1.410	2,850	5.85 -2
1,960	0.695	1,255	0.1640	1.397	3,200	5.46 -2
2,170	0.705	1,410	0.1535	1.384	3,510	5.18 -2
2,390	0.715	1,570	0.1448	1.371	3,830	5.00 -2
2,600	0.725	1,740	0.1344	1.358	4,130	5.05 -2
3,030	0.745	2,080	0.1187	1.332	4,720	4.78 -2
3,470	0.760	2,430	0.1085	1.310	5,330	4.61 -2

* $\underline{-2} \equiv x10^{-2}$

APPENDIX C

REVISED SUPERENERGY-DRV CODE LISTING

```
c     program supdrv
c supdrv for a 78 channel, 37 pin bundle
      real length,lead
      integer calib
      common/mixin/npin,pod,hod,a(3),ncal,salt(10),calib(10,78),length(
     11),ninj,ncoe
      common/mixout/v1r(1),v2r(1),v3r(1),flow(1),ree,saltc(78)
      common/prop1/rho,cp,cond,condw,alpha
      common/geo /dr(1),dw(1),lead(1),p(1),dflat(1),gap(1),a1(1),
     1a2(1),a3(1),atotal(1),de1(1),
     2de2(1),de3(1),hp1(1),hp2(1),hp3(1),hptotl(1),
     3eta1(1),eta2(1),eta3(1),eta4(1),eta6(1),eta8(1),x1(1),x2(1),x3(3),
     4s1(1),s2(1)
      common/num /nrod(1),nring(1),nchanl(1),n1(1),n2(1),n3(1),n4(1),
     1n5(1),n6(1),n7(1),n8(1),lc(1,550,4),mrod(1,440,3)
      common/wend/y11(500)
      dimension vavg(1),v1(1),v2(1),v3(1),vswirl(1),cindi(50)
      dimension eh1(01),eh2(01),eh3(01),eh4(01),y(500)
      dimension t1(550,01),t2(550,01),t3(550,01)
      read(5,100) nrod(1),pod,hod,(a(i),i=1,3)
  100 format(i3,5f10.0)
      npin=nrod(1)
      read(5,101) dr(1),dw(1),ddw1,lead(1),p(1),dflat(1)
  101 format(6f10.0)
      read(5,200) ncal,(salt(i),i=1,ncal)
  200 format(i2,10f6.0)
      do 300 j=1,ncal
      read(5,310) (calib(j,n),n=1,78)
  310 format(16i5)
  300 continue
      k=1
      l=1
      tin=0.0
      s1(1)=0
      s2(1)=0
      tt=60.0
      call prop(tt)
      noincr=500
      call numb(k)
      call geom(k)
      m1=n1(k)
      m2=n2(k)
      m3=n3(k)
      m4=n4(k)
      m5=n5(k)
      m6=n6(k)
      m7=n7(k)
      mk1=m1+1
      mk2=m2+1
      mk3=m3+1
      mk4=m4+1
      mk5=m5+1
      mk6=m6+1
      mk7=m7+1
 1234 continue
      read(5,10,end=1235) ninj,ncoe,nset,length(1),chiua,chiuc
   10 format(3i5,3f10.3)
      call mixdata
      write(6,17)
      vavg(1)=(flow(1)*500.57/atotal(k))*144.0/rho
```

```
      v1(1)=vavg(1)*v1r(k)
      v2(1)=vavg(1)*v2r(k)
      v3(1)=vavg(1)*v3r(k)
      if(ncoe.eq.1) go to 9999
      ehsta1=chiuc
      ehsta2=chiuc
      ehsta3=chiuc
      ehsta4=chiuc
      c1=chiua
      go to 9998
 9999 continue
      c1=chiuc
      ehsta1=chiua
      ehsta2=chiua
      ehsta3=chiua
      ehsta4=chiua
 9998 continue
      jxs=0
      do 502 nexp=2,nset
      nxs=0
      adj=10.**(-1.*nexp)
 1001 continue
      jxs=jxs+1
      nxs=nxs+1
      if(jxs.eq.1) go to 998
      if(jxs.gt.30) go to 1005
      if(ncoe.eq.1) go to 999
      c1=c1-adj
      go to 998
  999 ehsta1=ehsta1-adj
      ehsta2=ehsta1
      ehsta3=ehsta1
      ehsta4=ehsta1
  998 continue
      conver=vavg(1)*de1(k)/12.
      eh1(1)=ehsta1*conver
      eh2(1)=ehsta2*conver
      eh3(1)=ehsta3*conver
      eh4(1)=ehsta4*conver
      vswirl(1)=c1*vavg(1)
      dz=length(1)/noincr
      z=dz/2.
      do 110 i=1,m4
      t2(i,1)=tin
  110 continue
      t2(ninj,1)=700.0
 1000 continue
      do 150 i=1,m1
      mm1=lc(k,i,1)
      mm2=lc(k,i,2)
      mm3=lc(k,i,3)
      t3(i,1)=t2(i,1)+((p(k)-dr(k))*dz/
     1a1(k))*((alpha+eh1(1))/v1(1))*(t2(mm1,1)+t2(mm2,1)+t2(mm3,1)-
     23*t2(i,1))/eta1(k)*12
  150 continue
      do 160 i=mk1,m2
      mm1=lc(k,i,1)
      mm2=lc(k,i,2)
      mm3=lc(k,i,3)
      r=(i-1)/6.
```

```
      n=sqrt(r)+1.0001
      iq=(i-6*(n-1)*(n-1)-1)/(2*n-1)+0.0001
      ir=i-6*(n-1)*(n-1)-iq*(2*n-1)+0.0001
      j=ir/2
      if(ir.eq.2*j) go to 1160
      eha=eh1(1)
      ehb=eh2(1)
      etaa=eta1(k)
      etab=eta2(k)
      go to 2160
 1160 continue
      eha=eh1(1)
      etaa=eta1(k)
      ehb=eh1(1)
      etab=eta1(k)
 2160 continue
      t3(i,1)=t2(i,1)+((p(k)-dr(k))*dz)/
     1(a1(k)*v1(1))*((alpha+eha)*(t2(mm1,1)+t2(mm2,1)-2*t2(i,1))/etaa+
     2(alpha+ehb)*(t2(mm3,1)-t2(i,1))/etab)*12
  160 continue
      do 170 i=mk2,m3
      mm1=lc(k,i,1)
      mm2=lc(k,i,2)
      mm3=lc(k,i,3)
      if(mm2.gt.m3) go to 1170
      etaa=eta3(k)
      eha=eh3(1)
      go to 2170
 1170 continue
      etaa=eta4(k)
      eha=eh4(1)
 2170 continue
      if(mm3.gt.m3) go to 3170
      etab=eta3(k)
      ehb=eh3(1)
      go to 4170
 3170 continue
      etab=eta4(k)
      ehb=eh4(1)
 4170 continue
      t3(i,1)=t2(i,1)+(  ddw1*dz/a2(k))*
     1(vswirl(1)/v2(1))*(t2(mm2,1)-t2( i ,1))+12*(p(k)-dr(k))*dz/a2(k)*
     2((alpha+eh2(1))/v2(1))*(t2(mm1,1)-t2(i,1))/eta2(k)+12*(  ddw1*dz/
     3(v2(1)*a2(k)))*((alpha+eha)*(t2(mm2,1)-t2(i,1))/etaa+(alpha+ehb)*
     4(t2(mm3,1)-t2(i,1))/etab)
  170 continue
      do 180 i=mk3,m4
      mm1=lc(k,i,1)
      mm2=lc(k,i,2)
      mm3=lc(k,i,3)
      t3(i,1)=t2(i,1)+(gap(k)*dz/a3(k))*
     1(vswirl(1)/v3(1))*(t2(mm1,1)-t2( i ,1))+  (gap(k)*dz/a3(k))*12*
     2((alpha+eh4(1))/v3(1))*(t2(mm1,1)+t2(mm2,1)-2*t2(i,1))/eta4(k)
  180 continue
      do 240 i=1,m4
      t2(i,1)=t3(i,1)
  240 continue
      z=z+dz
      diff=length(1)-z
      if(diff.gt.dz) go to 1000
```

```
      do 265 i=1,m4
      y(i)=((t2(i,1)-tin)/(700.0-tin))*100.0
  265 continue
      cindi(jxs)=0.0
      do 9995 i=1,m4
      cindi(jxs)=cindi(jxs)+(y(i)-saltc(i))**2
 9995 continue
      cindi(jxs)=cindi(jxs)**0.5
      write(6,40) ehsta1,c1,cindi(jxs)
   40 format(5x,'ehsta1= 'f6.3,'    c1= ',f6.3,
     1'    mean square indicator= 'f7.3)
      if(jxs.eq.1) go to 9990
      if(cindi(jxs).gt.reind) go to 7777
 9990 reind=cindi(jxs)
      ehwc1=ehsta1
      ccc1=c1
      do 7776 i=1,m4
      y11(i)=y(i)
 7776 continue
      go to 1001
 7777 continue
      ehsta1=ehwc1
      c1=ccc1
      if (nxs-2) 501,501,502
  501 adj=-1.*adj
      go to 1001
  502 continue
 1005 continue
      write(6,17)
   17 format(1h1///////)
      write(6,401)
  401 format(5x,'sup/drv results at minimum mean square indicator')
      write(6,402) ehwc1
  402 format(5x,'effective eddy diffusivity E*1 = ',f6.3)
      write(6,403)ccc1
  403 format(5x,'swirl velocity ratio C1        = ',f6.3)
      write(6,404) reind
  404 format(5x,'min. mean square indicator     = ',f6.2)
      write(6,405)
  405 format(5x,'dimensionless ratios of salt concentration*100.0:'//)
      call prin(k)
      go to 1234
 1235 continue
      stop
      end
c  ******************************************************
      subroutine prop(tt)
      common/prop1/rho,cp,cond,condw,alpha
      rho=62.40
      cp=1.00
      cond=0.0001
      alpha=cond/(rho*cp)
      condw=12.1
      return
      end
c  ******************************************************
      subroutine prin(k)
      common/wend/m(500)
      write(6,81) m(75),m(60),m(59),m(58),m(74)
      write(6,3001)
```

```
      write(6,82) m(61),m(34),m(32),m(30),m(57)
      write(6,3001)
      write(6,83) m(35),m(33),m(31),m(29)
      write(6,3001)
      write(6,84) m(62),m(36),m(12),m(10),m(28),m(56)
      write(6,3001)
      write(6,85) m(37),m(13),m(11),m(9),m(27)
      write(6,3001)
      write(6,86) m(63),m(38),m(14),m(2),m(8),m(26),m(55)
      write(6,3001)
      write(6,87) m(39),m(15),m(3),m(1),m(7),m(25)
      write(6,3001)
      write(6,90) m(76),m(73)
      write(6,3001)
      write(6,87) m(40),m(16),m(4),m(6),m(24),m(54)
      write(6,3001)
      write(6,86) m(64),m(41),m(17),m(5),m(23),m(53),m(72)
      write(6,3001)
      write(6,85) m(42),m(18),m(20),m(22),m(52)
      write(6,3001)
      write(6,84) m(65),m(43),m(19),m(21),m(51),m(71)
      write(6,3001)
      write(6,83) m(44),m(46),m(48),m(50)
      write(6,3001)
      write(6,82) m(66),m(45),m(47),m(49),m(70)
      write(6,3001)
      write(6,81) m(77),m(67),m(68),m(69),m(78)
      write(6,3001)
3001  format(' ')
81    format(1h,12x,5f6.1)
82    format(1h,12x,5f6.1)
83    format(1h,15x,4f6.1)
84    format(1h,9x,6f6.1)
85    format(1h,12x,5f6.1)
86    format(1h,6x,7f6.1)
87    format(1h,9x,6f6.1)
90    format(1h,3x,f6.1,36x,f6.1)
      return
      end
c  ******************************************************
      subroutine numb(1)
      common/num /nrod(1),nring(1),nchanl(1),n1(1),n2(1),n3(1),n4(1),
     1n5(1),n6(1),n7(1),n8(1),lc(1,550,4),mrod(1,440,3)
      nwalls=1
      norod=nrod(1)
      xnorin=(norod-1)/3.
      nring(1)=sqrt(xnorin)
      noring=nring(1)
      notrg=6*noring*noring
      notrg1=notrg+1
      notg1=6*(noring-1)*(noring-1)
      nog01=3*(noring-1)*noring
      noincr=6*(noring+1)
      lstch=notrg+noincr
      lstch1=lstch+1
      lstw=lstch-6
      lstchg=lstch+noincr
      lstwg=lstchg-6
      n1(1)=notg1
      n2(1)=notrg
```

```
      n3(l)=lstw
      n4(l)=lstch
      n5(l)=lstch+6*noring
      n6(l)=n5(l)+6
      n7(l)=n6(l)+6*noring
      n8(l)=n7(l)+6
      nchanl(l)=n4(l)
      do 7 i=1,notrg
      z=(i-1)/6.
      n=sqrt(z)+1.0001
      notr0=6*n*n
      notr1=6*(n-1)*(n-1)
      notr2=6*(n-2)*(n-2)
      not01=3*n*(n-1)
      not12=3*(n-1)*(n-2)
      iq=(i-notr1-1)/(2*n-1)+0.0001
      ir=i-notr1-iq*(2*n-1)+0.0001
      iy=1.6-1/n
      lc(l,i,4)=i
      if(i-notr1-1)901,902,901
  901 if(i.eq.notr0)go to 903
      j=ir/2
      if(ir-j*2)905,905,904
  905 iz=1.0001/(notr0-i)
      lc(l,i,1)=notr2+iq*(2*n-3)+ir-1
      lc(l,i,2)=i-1
      lc(l,i,3)=i+1
      mrod(l,i,1)=1+not12+iq*(n-1)+ir/2
      mrod(l,i,2)=mrod(l,i,1)+1-6*iz*(n-1)
      mrod(l,i,3)=not01+iq*n+ir/2+2
      go to 6
  904 lc(l,i,1)=i-1
      lc(l,i,2)=i+1
      mrod(l,i,1)=  not12+iq*(n-1)+(ir+1)/2+iy
      mrod(l,i,2)=1+not01+iq*n+(ir+1)/2
      mrod(l,i,3)=mrod(l,i,2)+1
  908 if(n.eq.noring)go to 906
      lc(l,i,3)=notr0+iq*(2*n+1)+ir+1
      go to 6
  906 lc(l,i,3)=notr0+iq*n+(ir+1)/2
      go to 6
  903 lc(l,i,1)=notr1+1
      lc(l,i,2)=notr0-1
      mrod(l,i,1)=1+iy+not12
      mrod(l,i,2)=2+not01
      mrod(l,i,3)=1+3*n*(n+1)
      go to 908
  902 lc(l,i,1)=notr1+2
      lc(l,i,2)=notr0
      mrod(l,i,1)=1+iy+not12
      mrod(l,i,2)=2+not01
      mrod(l,i,3)=mrod(l,i,2)+1
      go to 908
    6 continue
    7 continue
      do 9 i=notrg1,lstch
      mrod(l,i,3)=norod+1
      if(i.le.lstw) go to 801
      iq=i-lstch+5
      lc(l,i,2)=notrg+iq*noring+1
```

```
      lc(1,i,3)=lstchg-5+iq
      lc(1,i,4)=i
      mrod(1,i,1)=2+nog01+iq*noring
      mrod(1,i,2)=norod+1
      if(iq.eq.0) go to 802
      lc(1,i,1)=notrg+iq*noring
      go to 8
  802 lc(1,i,1)=i-1
      go to 8
  801 iz=1.0001/(lstch-5-i)
      iq=(i-notrg-1)/noring+0.0001
      ir=i-notrg-iq*noring+0.0001
      lc(1,i,1)=notg1+iq*(2*noring-1)+2*ir-1
      lc(1,i,4)=lstch+iq*noring+ir
      mrod(1,i,1)=1+nog01+iq*noring+ir
      mrod(1,i,2)=mrod(1,i,1)+1-6*iz*noring
      if(ir.eq.1) go to 803
      if(ir.eq.noring)  go to 804
      lc(1,i,2)=i-1
      lc(1,i,3)=i+1
      go to 8
  803 lc(1,i,2)=lstw+iq+1
      lc(1,i,3)=i+1
      go to 8
  804 lc(1,i,2)=i-1
      lc(1,i,3)=(1-iz)*(lstw+iq+2)+iz*(i+1)
      go to 8
    8 continue
    9 continue
      do 13 j=1,nwalls
      do 11 i=lstch1,lstchg
      if(i.le.lstwg) go to 701
      iq=i-lstwg-1
      lc(1,i,1)=lstw+1+iq
      lc(1,i,3)=lstch+iq*noring+1
      if(j.eq.nwalls) go to 12
      lc(1,i,4)=lstwg+noincr+iq+1
      go to 14
   12 continue
      lc(1,i,4)=i
   14 continue
      if(iq.eq.0) go to 702
      lc(1,i,2)=lstch+iq*noring
      go to 10
  702 lc(1,i,2)=i-1
      go to 10
  701 ix=1.0001/(lstwg+1-i)
      iq=(i-lstch-1)/noring+0.0001
      ir=i-lstch-iq*noring+0.0001
      lc(1,i,1)=notrg+iq*noring+ir
      if(j.eq.nwalls) go to 16
      lc(1,i,4)=lstchg+iq*noring+ir
      go to 18
   16 continue
      lc(1,i,4)=i
   18 continue
      if(ir.eq.1) go to 703
      if(ir.eq.noring) go to 704
      lc(1,i,2)=i-1
      lc(1,i,3)=i+1
```

```
      go to 10
  704 lc(1,i,2)=i-1
      lc(1,i,3)=(1-ix)*(lstwg+iq+2)+ix*(i+1)
      go to 10
  703 lc(1,i,2)=lstwg+iq+1
      lc(1,i,3)=i+1
      go to 10
   10 continue
   11 continue
      notrg=notrg+noincr
      lstch=lstch+noincr
      lstch1=lstch1+noincr
      lstw=lstw+noincr
      lstwg=lstwg+noincr
      lstchg=lstchg+noincr
   13 continue
      return
      end
c  ******************************************************
      subroutine geom(1)
      common/geo /dr(1),dw(1),lead(1),p(1),dflat(1),gap(1),a1(1),
     1a2(1),a3(1),atotal(1),de1(1),
     2de2(1),de3(1),hp1(1),hp2(1),hp3(1),hptot1(1),
     3eta1(1),eta2(1),eta3(1),eta4(1),eta6(1),eta8(1),x1(1),x2(1),x3(3),
     4s1(1),s2(1)
      common/num /nrod(1),nring(1),nchan1(1),n1(1),n2(1),n3(1),n4(1),
     1n5(1),n6(1),n7(1),n8(1),lc(1,550,4),mrod(1,440,3)
      n11=n2(1)
      n22=n3(1)-n2(1)
      n33=n4(1)-n3(1)
      gap(1)=(dflat(1)- 1.732* nring(1)*p(1)-dr(1))/2
      dface=dflat(1)/1.732
      pi=3.141592
      x1(1)=(dr(1)+2*gap(1))/1.732
      x2(1)=x1(1)+2*s1(1)/1.732
      x3(1)=x2(1)+s2(1)/1.732
      eta1(1)=p(1)/1.732
      eta2(1)=(eta1(1)+gap(1)+dr(1)/2)/2.
      eta3(1)=p(1)
      eta4(1)=eta3(1)/2.+x1(1)/4.
      eta6(1)=eta3(1)/2.+(x1(1)+x2(1))/4.
      eta8(1)=eta3(1)/2.+(x2(1)+x3(1))/4.
      a1(1)=1.732*p(1)**2/4.-(dr(1)**2+dw(1)**2)*pi/8.
      a2(1)=p(1)*(dr(1)/2+gap(1))-(dr(1)**2+dw(1)**2)*pi/8.
      a3(1)=(dr(1)/4+gap(1)/2)*(dface-p(1)* nring(1))-(dr(1)**2+dw(1)**2
     1)*pi/24.
      atotal(1)=n11*a1(1)+n22*a2(1)+n33*a3(1)
      wp1=(dr(1)+dw(1))*pi/2.
      wp2=p(1)+wp1
      wp3=(dr(1)+dw(1))*pi/6+dface-p(1)* nring(1)
      wp6=eta3(1)
      wp7=x2(1)
      de1(1)=4.0*a1(1)/wp1
      de2(1)=4.0*a2(1)/wp2
      de3(1)=4.0*a3(1)/wp3
      hp1(1)=dr(1)*pi/2
      hp2(1)=dr(1)*pi/2
      hp3(1)=dr(1)*pi/6
      hptot1(1)=n11*hp1(1)+n22*hp2(1)+n33*hp3(1)
      return
```

```
      end
c  ******************************************************
      subroutine mixdata
      dimension con(78)
      integer mxdata(78),calcor(78),calib
      real isaltf,isaltc,masbal,netslt,m
      common/mixin/ npin,pod,hod,a(3),ncal,salt(10),calib(10,78),depth,
     1isubch,ncoe
      common/mixout/ fsp(3),gpm,ire,m(78)
      read(5,600) gpm,ire ,(fsp(i),i=1,3)
  600 format(f6.2,i7,3f10.0)
c      read in inj. salt con. (gm/100lbm) and flow rate(gpm*10e5)
      read(5,700) isaltc,isaltf
  700 format(2f10.0)
c      read in calcorrection data and mixing data
      read(5,310) (calcor(i),i=1,78)
      read(5,310) (mxdata(i),i=1,78)
  310 format(16i5)
      do 3800 j=1,78
      mxdata(j)=mxdata(j)+calib(1,j)-calcor(j)
      ilo=0
      ihi=20000
      do 3700 n=1,ncal
      if(calib(n,j).le.mxdata(j)) go to 3701
      if(calib(n,j).ge.ihi) go to 3700
      ihi=calib(n,j)
      zi=salt(n)
      go to 3700
 3701 if(calib(n,j).le.ilo) go to 3700
      ilo=calib(n,j)
      hi=salt(n)
 3700 continue
 3710 if(ihi.ne.20000) go to 3720
      con(j)=0.
      go to 3800
 3720 if(ilo.eq.ihi) con(j)=zi
      if(ilo.eq.ihi) go to 3800
      con(j)=(zi-hi)*(mxdata(j)-ilo)/(ihi-ilo)+hi
 3800 continue
c      put average value of neighboring probe reading for bad probe 13,78,57,58
      con(13)=(con(36)+con(12)+con(14))/3.0
      con(78)=(con(69)+con(70))/2.0
      con(57)=(con(56)+con(74))/2.0
      con(58)=(con(59)+con(74))/2.0
      if (ncoe.ne.1) con(73)=(con(72)+con(55))/2.0
      vavg=gpm/5.8561
      outslt=0.0
      do 3940 n=1,54
 3940 outslt=outslt+fsp(1)*a(1)*con(n)*vavg
      do 3950 n=55,72
 3950 outslt=outslt+fsp(2)*a(2)*con(n)*vavg
      do 3960 n=73,78
 3960 outslt=outslt+fsp(3)*a(3)*con(n)*vavg
      netslt=isaltf*isaltc
      masbal=outslt*100000.0/netslt
      if(isubch.le.54) cmi=isaltf*0.00001+vavg*fsp(1)*a(1)
      if(isubch.gt.54) cmi=isaltf*0.00001+vavg*fsp(2)*a(2)
      do 4000 n=1,78
 4000 m(n)=con(n)/(outslt/cmi)*100.0
      write(6,80)
```

```
      write(6,70) npin,pod,hod
      write(6,71) isubch
      write(6,72) depth
      write(6,73) ire
      write(6,74) masbal
      write(6,75)
      write(6,81) m(75),m(60),m(59),m(58),m(74)
      write(6,81) m(61),m(34),m(32),m(30),m(57)
      write(6,83) m(35),m(33),m(31),m(29)
      write(6,84) m(62),m(36),m(12),m(10),m(28),m(56)
      write(6,81) m(37),m(13),m(11),m(9),m(27)
      write(6,86) m(63),m(38),m(14),m(2),m(8),m(26),m(55)
      write(6,84) m(39),m(15),m(3),m(1),m(7),m(25)
      write(6,90) m(76),m(73)
      write(6,84) m(40),m(16),m(4),m(6),m(24),m(54)
      write(6,86) m(64),m(41),m(17),m(5),m(23),m(53),m(72)
      write(6,81) m(42),m(18),m(20),m(22),m(52)
      write(6,84) m(65),m(43),m(19),m(21),m(51),m(71)
      write(6,83) m(44),m(46),m(48),m(50)
      write(6,81) m(66),m(45),m(47),m(49),m(70)
      write(6,81) m(77),m(67),m(68),m(69),m(78)
   70 format(5x,i2,' pin  p/d= ',f6.3,'  h/d= 'f6.2)
   71 format(4x,' inj. subchannel     = 'i5)
   72 format(4x,' inj. depth (in)     = 'f5.1)
   73 format(4x,' bundle reynolds no.= 'i5)
   74 format(4x,' mass balance ratio = 'f5.3)
   75 format(4x,' dimensionless ratios of salt concentration*100.0:'/)
   81 format(1h0,12x,5f6.1)
   80 format(1h1//////)
   83 format(1h0,15x,4f6.1)
   84 format(1h0,9x,6f6.1)
   86 format(1h0,6x,7f6.1)
   90 format(1h0,3x,f6.1,36x,f6.1)
      return
      end
```

37 pin p/d= 1.154 h/d= 13.40
inj. subchannel = 1
inj. depth (in) = 32.0
bundle reynolds no.= 220
mass balance ratio = 1.702
dimensionless ratios of salt concentration*100.0:

0.3 0.0 0.0 0.1 0.2

0.1 0.1 0.4 1.6 0.1

0.0 0.1 1.2 0.9

0.1 0.0 1.6 6.8 6.3 0.1

0.2 0.7 6.6 5.8 4.4

0.1 0.0 0.7 5.6 13.6 2.2 0.0

0.0 0.1 2.7 (5.3) 3.7 2.3

0.0 0.1

0.0 0.2 0.4 6.4 4.2 0.5

0.1 0.0 0.0 2.1 5.7 2.0 0.1

0.0 0.0 0.1 0.7 0.4

0.0 0.0 0.1 0.5 0.9 0.2

0.0 0.1 0.1 0.2

0.0 0.0 0.0 0.1 0.0

0.0 0.0 0.1 0.0 0.0

sup/drv results at minimum mean square indicator
effective eddy diffusivity E*1 = 0.049
swirl velocity ratio C1 = 0.100
min. mean square indicator = 11.92
dimensionless ratios of salt concentration*100.0:

0.0 0.0 0.1 0.1 0.1

0.0 0.2 0.6 0.6 0.1

0.2 0.8 1.3 0.8

0.0 0.4 2.0 3.3 2.0 0.2

0.2 1.3 4.4 4.4 1.2

0.0 0.2 2.0 6.9 6.9 2.0 0.1

0.1 0.8 4.4 (8.7) 4.4 0.7

0.0 0.1

0.0 0.6 3.3 6.9 3.3 0.5

0.0 0.2 1.3 4.4 4.4 1.3 0.1

0.1 0.6 2.0 2.0 0.6

0.0 0.2 0.8 1.3 0.8 0.1

0.0 0.2 0.4 0.2

0.0 0.1 0.2 0.2 0.0

0.0 0.0 0.0 0.0 0.0

37 pin p/d= 1.154 h/d= 13.40
inj. subchannel = 1
inj. depth (in) = 32.0
bundle reynolds no.= 430
mass balance ratio = 1.805
dimensionless ratios of salt concentration*100.0:

0.3 0.0 0.3 0.3 0.3

0.2 0.4 0.4 1.8 0.3

0.0 1.3 1.7 0.4

0.0 0.4 1.4 6.7 6.4 0.3

0.2 1.0 4.0 5.4 3.8

0.2 0.0 1.1 6.2 7.0 1.7 0.0

0.1 0.4 3.2 (7.7) 3.5 1.7

0.9 0.0

0.3 0.9 1.3 4.4 2.1 1.0

0.0 0.2 0.5 1.9 4.5 2.4 0.3

0.0 0.3 0.8 0.7 0.6

0.1 0.1 0.0 0.4 0.4 0.1

0.0 0.2 0.2 0.2

0.0 0.4 0.0 0.0 0.1

0.5 0.0 0.1 0.0 0.0

sup/drv results at minimum mean square indicator
effective eddy diffusivity E*1 = 0.058
swirl velocity ratio C1 = 0.100
min. mean square indicator = 8.19
dimensionless ratios of salt concentration*100.0:

0.1 0.1 0.1 0.1 0.2

0.0 0.3 0.7 0.7 0.2

0.2 0.9 1.4 0.9

0.0 0.5 2.1 3.3 2.1 0.3

0.2 1.4 4.1 4.1 1.4

0.0 0.3 2.1 6.0 6.0 2.1 0.2

0.1 0.9 4.1 (7.2) 4.1 0.9

0.0 0.1

0.1 0.7 3.3 6.0 3.3 0.7

0.0 0.2 1.5 4.1 4.1 1.4 0.1

0.1 0.7 2.1 2.1 0.7

0.0 0.2 0.9 1.4 0.9 0.1

0.1 0.3 0.5 0.3

0.0 0.1 0.2 0.2 0.0

0.0 0.0 0.0 0.0 0.0

37 pin p/d= 1.154 h/d= 13.40
inj. subchannel = 1
inj. depth (in) = 32.0
bundle reynolds no.= 860
mass balance ratio = 1.348
dimensionless ratios of salt concentration*100.0:

0.1 0.2 0.4 0.2 0.0

0.0 0.4 0.6 0.6 0.1

0.0 0.2 0.9 0.8

0.1 0.2 2.2 4.9 2.2 0.2

0.7 1.8 3.4 3.9 1.2

0.0 0.5 3.0 7.4 6.4 1.8 0.4

0.6 1.5 4.1 (6.1) 1.9 1.2

0.1 0.2

0.0 1.9 4.8 5.7 1.7 0.4

0.2 0.2 1.5 6.0 4.3 0.8 0.3

0.2 0.7 0.6 0.9 0.4

0.3 0.0 0.5 0.1 0.6 0.0

0.1 0.4 0.1 0.1

0.0 0.0 0.0 0.0 0.2

0.0 0.0 0.0 0.4 0.3

sup/drv results at minimum mean square indicator
effective eddy diffusivity E*1 = 0.058
swirl velocity ratio C1 = 0.100
min. mean square indicator = 5.64
dimensionless ratios of salt concentration*100.0:

0.1 0.1 0.1 0.1 0.2

0.0 0.3 0.7 0.7 0.2

0.2 0.9 1.4 0.9

0.0 0.5 2.1 3.3 2.1 0.3

0.2 1.4 4.1 4.1 1.4

0.0 0.3 2.1 6.0 6.0 2.1 0.2

0.1 0.9 4.1 (7.2) 4.1 0.9

0.0 0.1

0.1 0.7 3.3 6.0 3.3 0.7

0.0 0.2 1.5 4.1 4.1 1.4 0.1

0.1 0.7 2.1 2.1 0.7

0.0 0.2 0.9 1.4 0.9 0.1

0.1 0.3 0.5 0.3

0.0 0.1 0.2 0.2 0.0

0.0 0.0 0.0 0.0 0.0

37 pin p/d= 1.154 h/d= 13.40
inj. subchannel = 1
inj. depth (in) = 32.0
bundle reynolds no.= 1500
mass balance ratio = 1.393
dimensionless ratios of salt concentration*100.0:

0.0 0.0 0.5 0.3 0.2

0.1 0.2 1.2 1.0 0.3

0.4 0.5 1.5 1.1

0.2 0.6 3.1 5.0 1.3 0.3

0.8 2.3 3.6 4.3 1.6

0.0 0.8 3.2 6.5 4.3 1.5 0.0

0.6 1.9 4.2 (5.1) 3.2 0.8

0.0 0.0

0.0 2.6 3.5 4.2 1.2 0.3

0.3 0.2 1.8 5.4 3.5 0.7 0.3

0.5 0.7 0.7 0.6 0.0

0.4 0.0 0.8 0.8 0.3 0.0

0.3 0.1 0.4 0.3

0.0 0.0 0.1 0.0 0.1

0.0 0.1 0.2 0.1 0.1

sup/drv results at minimum mean square indicator
effective eddy diffusivity E*1 = 0.071
swirl velocity ratio C1 = 0.100
min. mean square indicator = 5.63
dimensionless ratios of salt concentration*100.0:

0.1 0.1 0.2 0.2 0.2

0.1 0.4 0.9 0.8 0.3

0.3 1.1 1.6 1.0

0.1 0.7 2.1 3.1 2.1 0.4

0.3 1.6 3.7 3.7 1.5

0.0 0.4 2.1 5.0 5.0 2.1 0.2

0.2 1.1 3.7 (5.8) 3.7 1.0

0.0 0.2

0.1 0.9 3.1 5.0 3.1 0.8

0.0 0.3 1.6 3.7 3.7 1.5 0.2

0.2 0.9 2.1 2.1 0.8

0.0 0.3 1.1 1.6 1.1 0.2

0.1 0.4 0.7 0.4

0.0 0.2 0.3 0.3 0.1

0.0 0.0 0.1 0.1 0.0

37 pin p/d= 1.154 h/d= 13.40
inj. subchannel = 1
inj. depth (in) = 32.0
bundle reynolds no.= 2200
mass balance ratio = 1.151
dimensionless ratios of salt concentration*100.0:

0.0 0.1 0.0 0.0 0.1
0.6 0.4 1.2 1.3 0.1
0.8 1.0 1.7 1.1
0.4 0.8 2.8 4.0 1.4 0.2
0.4 2.3 4.0 4.5 1.9
0.2 0.4 3.1 5.5 4.0 0.6 0.4
0.1 2.0 4.2 (3.7) 2.9 0.7
0.0 0.5
1.0 2.5 3.1 3.7 1.4 0.7
0.0 0.7 1.4 5.1 3.0 0.5 0.2
0.0 1.1 1.0 1.1 0.2
0.3 0.4 1.2 1.0 0.8 0.3
0.3 0.2 0.0 0.2
0.3 0.2 0.5 0.3 0.1
0.0 0.0 0.3 0.1 0.1

sup/drv results at minimum mean square indicator
effective eddy diffusivity E*1 = 0.082
swirl velocity ratio C1 = 0.200
min. mean square indicator = 5.23
dimensionless ratios of salt concentration*100.0:

0.2 0.2 0.3 0.3 0.3
0.1 0.5 0.9 0.9 0.4
0.4 1.1 1.6 1.1
0.1 0.7 2.1 2.9 2.0 0.4
0.4 1.6 3.4 3.3 1.5
0.1 0.5 2.1 4.4 4.3 2.0 0.3
0.2 1.2 3.4 (5.0) 3.3 1.0
0.1 0.2
0.2 1.0 2.9 4.4 2.9 0.9
0.0 0.4 1.6 3.4 3.4 1.6 0.2
0.2 1.0 2.1 2.1 0.9
0.0 0.4 1.2 1.6 1.1 0.2
0.2 0.5 0.7 0.5
0.0 0.2 0.4 0.4 0.1
0.0 0.0 0.1 0.1 0.1

37 pin p/d= 1.154 h/d= 13.40
inj. subchannel = 1
inj. depth (in) = 32.0
bundle reynolds no.= 3200
mass balance ratio = 1.360
dimensionless ratios of salt concentration*100.0:

0.0 0.2 0.2 0.2 0.1

0.2 0.6 1.6 1.4 0.2

0.5 1.1 1.9 0.7

0.2 1.3 2.8 3.9 1.5 0.3

0.3 2.6 3.8 4.6 1.8

0.0 0.8 3.8 5.2 3.6 0.8 0.2

0.1 1.9 4.5 (3.7) 2.8 1.0

0.0 0.7

0.3 2.7 3.2 3.5 1.4 0.1

0.3 0.8 1.8 5.1 2.7 0.9 0.2

0.1 1.1 1.0 0.9 0.2

0.1 0.6 1.5 1.1 0.7 0.1

0.3 0.5 0.0 0.0

0.2 0.4 0.4 0.4 0.0

0.0 0.0 0.1 0.3 0.2

sup/drv results at minimum mean square indicator
effective eddy diffusivity E*1 = 0.085
swirl velocity ratio C1 = 0.200
min. mean square indicator = 5.54
dimensionless ratios of salt concentration*100.0:

0.2 0.2 0.3 0.3 0.4

0.1 0.5 1.0 1.0 0.4

0.4 1.2 1.6 1.1

0.1 0.8 2.1 2.9 2.0 0.4

0.4 1.6 3.3 3.3 1.5

0.1 0.5 2.1 4.2 4.2 2.0 0.3

0.2 1.2 3.3 (4.8) 3.3 1.0

0.1 0.2

0.2 1.0 2.9 4.2 2.9 0.9

0.1 0.4 1.6 3.3 3.3 1.6 0.2

0.3 1.0 2.1 2.1 0.9

0.1 0.4 1.2 1.6 1.1 0.2

0.2 0.5 0.8 0.5

0.0 0.2 0.4 0.4 0.1

0.0 0.0 0.1 0.1 0.1

37 pin p/d= 1.154 h/d= 13.40
inj. subchannel = 1
inj. depth (in) = 32.0
bundle reynolds no.= 4300
mass balance ratio = 1.126
dimensionless ratios of salt concentration*100.0:

0.1 0.8 0.2 0.3 0.3

0.0 0.7 1.9 1.8 0.4

0.2 1.5 2.5 0.9

0.0 1.4 3.1 3.9 1.5 0.6

0.5 2.7 3.9 4.4 1.4

0.3 1.2 3.5 4.8 3.5 1.0 0.2

0.1 1.9 4.0 (4.1) 3.6 1.1

0.1 0.1

0.4 2.7 2.7 3.3 1.2 0.3

0.0 0.3 1.4 4.3 2.2 1.0 0.3

0.2 1.2 0.9 1.0 0.2

0.1 0.6 1.3 1.5 0.9 0.0

0.2 0.4 0.0 0.2

0.1 0.4 0.5 0.4 0.1

0.0 0.0 0.0 0.0 0.0

sup/drv results at minimum mean square indicator
effective eddy diffusivity E*1 = 0.095
swirl velocity ratio Ci = 0.300
min. mean square indicator = 5.27
dimensionless ratios of salt concentration*100.0:

0.3 0.3 0.4 0.4 0.4

0.2 0.6 1.0 1.0 0.5

0.5 1.2 1.6 1.1

0.2 0.8 2.0 2.8 2.0 0.4

0.5 1.6 3.2 3.1 1.5

0.1 0.6 2.1 4.0 4.0 1.9 0.3

0.3 1.2 3.2 (4.5) 3.1 1.1

0.1 0.3

0.2 1.1 2.8 4.0 2.8 0.9

0.1 0.5 1.6 3.2 3.2 1.6 0.3

0.3 1.1 2.0 2.0 0.9

0.1 0.5 1.2 1.6 1.1 0.2

0.2 0.6 0.8 0.5

0.1 0.2 0.4 0.4 0.1

0.1 0.1 0.1 0.1 0.1

37 pin p/d= 1.154 h/d= 13.40
inj. subchannel = 1
inj. depth (in) = 32.0
bundle reynolds no.= 5400
mass balance ratio = 1.307
dimensionless ratios of salt concentration*100.0:

0.1 0.2 0.3 0.2 0.1

0.0 0.7 1.8 1.6 0.2

0.4 1.1 2.3 0.8

0.2 1.1 2.9 4.2 1.5 0.3

0.5 2.6 4.0 4.3 1.2

0.0 1.1 3.9 5.8 4.0 1.0 0.0

0.4 2.3 4.1 (4.6) 3.0 0.9

0.0 0.0

0.3 3.0 3.7 4.1 1.1 0.2

0.2 0.3 2.2 5.3 2.6 1.0 0.0

0.2 1.3 1.2 0.8 0.1

0.0 0.3 1.9 2.6 1.1 0.0

0.5 0.5 0.1 0.1

0.0 0.3 0.3 0.2 0.0

0.0 0.0 0.0 0.0 0.0

sup/drv results at minimum mean square indicator
effective eddy diffusivity E*1 = 0.087
swirl velocity ratio C1 = 0.300
min. mean square indicator = 5.88
dimensionless ratios of salt concentration*100.0:

0.2 0.3 0.3 0.4 0.4

0.2 0.5 0.9 0.9 0.4

0.4 1.1 1.6 1.1

0.1 0.7 2.1 3.0 2.0 0.4

0.4 1.6 3.5 3.4 1.5

0.1 0.5 2.1 4.5 4.5 2.0 0.3

0.2 1.1 3.5 (5.2) 3.4 1.0

0.1 0.2

0.2 1.0 3.0 4.5 3.0 0.9

0.1 0.4 1.6 3.5 3.5 1.6 0.2

0.2 1.0 2.1 2.1 0.9

0.1 0.4 1.1 1.6 1.1 0.2

0.2 0.5 0.7 0.5

0.0 0.2 0.4 0.4 0.1

0.0 0.0 0.1 0.1 0.1

37 pin p/d= 1.154 h/d= 13.40
inj. subchannel = 1
inj. depth (in) = 32.0
bundle reynolds no.= 6500
mass balance ratio = 1.444
dimensionless ratios of salt concentration*100.0.

0.6 0.2 0.5 0.4 0.4

0.4 0.8 1.9 0.9 0.2

1.0 1.4 2.5 1.4

0.0 1.2 3.7 4.6 1.4 0.1

1.0 2.8 4.6 3.9 0.8

0.3 0.7 3.6 5.4 3.8 1.0 0.2

0.5 1.4 3.9 (4.2) 3.0 0.3

0.2 0.1

0.3 2.1 3.6 3.8 0.9 0.6

0.0 0.4 2.0 4.5 2.4 1.7 0.1

0.7 0.7 0.3 0.4 0.3

0.0 0.7 1.2 1.0 0.6 0.0

0.3 0.5 0.2 0.3

0.0 0.4 0.2 0.2 0.0

0.5 0.2 0.3 0.0 0.0

sup/drv results at minimum mean square indicator
effective eddy diffusivity E*1 = 0.094
swirl velocity ratio C1 = 0.300
min. mean square indicator = 5.93
dimensionless ratios of salt concentration*100.0:

0.3 0.3 0.4 0.4 0.4

0.2 0.6 1.0 1.0 0.4

0.4 1.2 1.6 1.1

0.2 0.8 2.1 2.9 2.0 0.4

0.4 1.6 3.3 3.3 1.5

0.1 0.5 2.1 4.3 4.3 2.0 0.3

0.2 1.2 3.3 (4.9) 3.3 1.0

0.1 0.2

0.2 1.0 2.9 4.3 2.9 0.9

0.1 0.4 1.6 3.3 3.3 1.6 0.2

0.3 1.0 2.1 2.1 0.9

0.1 0.4 1.2 1.6 1.1 0.2

0.2 0.5 0.7 0.5

0.1 0.2 0.4 0.4 0.1

0.0 0.1 0.1 0.1 0.1

37 pin p/d= 1.154 h/d= 13.40
inj. subchannel = 1
inj. depth (in) = 32.0
bundle reynolds no.= 9400
mass balance ratio = 1.584
dimensionless ratios of salt concentration*100.0:

0.1 0.1 0.6 0.5 0.4

0.1 0.6 2.4 1.4 0.2

0.2 1.2 2.0 1.9

0.1 0.7 3.6 3.8 0.9 0.1

0.9 2.7 4.4 3.7 1.2

0.2 1.2 3.9 5.6 4.0 1.3 0.1

0.2 2.1 4.4 (4.9) 3.0 1.0

0.0 0.0

0.1 2.9 4.0 3.6 1.1 0.5

0.1 0.2 2.4 4.6 2.6 1.2 0.0

0.3 1.1 1.1 0.9 0.2

0.1 0.2 1.6 1.3 0.9 0.0

0.3 0.2 0.1 0.0

0.0 0.4 0.0 0.0 0.0

0.1 0.0 0.0 0.0 0.0

sup/drv results at minimum mean square indicator
effective eddy diffusivity E*1 = 0.095
swirl velocity ratio C1 = 0.300
min. mean square indicator = 5.89
dimensionless ratios of salt concentration*100.0:

0.3 0.3 0.4 0.4 0.4

0.2 0.5 1.0 1.0 0.4

0.4 1.1 1.6 1.1

0.2 0.7 2.1 3.0 2.1 0.4

0.4 1.6 3.4 3.4 1.5

0.1 0.5 2.1 4.5 4.5 2.0 0.3

0.2 1.1 3.4 (5.1) 3.4 1.0

0.1 0.2

0.2 1.0 3.0 4.5 3.0 0.9

0.1 0.4 1.6 3.4 3.4 1.6 0.2

0.2 1.0 2.1 2.1 0.9

0.1 0.4 1.1 1.6 1.1 0.2

0.2 0.5 0.7 0.5

0.1 0.2 0.4 0.4 0.1

0.0 0.0 0.1 0.1 0.1

37 pin p/d= 1.154 h/d= 13.40
inj. subchannel = 1
inj. depth (in) = 32.0
bundle reynolds no.= 12200
mass balance ratio = 1.566
dimensionless ratios of salt concentration*100.0:

0.2 0.4 0.8 0.7 0.6

0.1 0.8 2.9 1.6 0.4

0.2 1.3 2.1 2.4

0.1 1.0 3.7 4.2 0.9 0.1

1.0 2.8 4.4 4.1 1.2

0.2 1.2 3.6 5.4 4.1 1.5 0.2

0.2 1.2 3.6 (4.0) 2.9 0.8

0.4 0.2

0.2 2.9 3.2 3.3 1.1 0.5

0.1 0.3 1.9 4.2 2.3 1.1 0.1

0.2 1.0 0.3 0.9 0.2

0.2 0.2 1.3 0.8 0.8 0.0

0.1 0.3 0.4 0.1

0.0 0.3 0.3 0.1 0.1

0.6 0.0 0.1 0.0 0.0

sup/drv results at minimum mean square indicator
effective eddy diffusivity E*1 = 0.107
swirl velocity ratio C1 = 0.300
min. mean square indicator = 6.13
dimensionless ratios of salt concentration*100.0:

0.4 0.4 0.5 0.5 0.5

0.3 0.6 1.0 1.0 0.5

0.5 1.2 1.6 1.1

0.2 0.8 2.1 2.9 2.0 0.5

0.5 1.6 3.3 3.2 1.5

0.2 0.6 2.1 4.1 4.1 2.0 0.4

0.3 1.2 3.3 (4.7) 3.2 1.1

0.1 0.3

0.2 1.0 2.9 4.1 2.8 0.9

0.1 0.5 1.6 3.3 3.2 1.6 0.3

0.3 1.0 2.1 2.1 0.9

0.1 0.4 1.2 1.6 1.1 0.2

0.2 0.6 0.8 0.5

0.1 0.2 0.4 0.4 0.1

0.1 0.1 0.1 0.1 0.1

37 pin p/d= 1.154 h/d= 13.40
inj. subchannel = 1
inj. depth (in) = 32.0
bundle reynolds no.= 14800
mass balance ratio = 1.672
dimensionless ratios of salt concentration*100.0:

0.0 0.3 0.5 0.5 0.5
0.1 0.7 1.7 1.1 0.3
0.2 1.2 1.8 1.5
0.1 0.9 3.2 3.7 0.9 0.1
0.9 2.6 4.4 3.4 1.3
0.3 1.3 3.7 5.6 3.8 1.6 0.3
0.6 2.7 3.8 (4.1) 3.1 0.6
0.1 0.2
0.7 3.0 3.9 3.4 1.1 0.5
0.1 0.4 2.2 4.4 2.2 1.3 0.0
0.5 1.2 0.8 0.8 0.1
0.1 0.3 1.9 1.6 1.1 0.1
0.4 0.3 0.0 0.1
0.2 0.4 0.5 0.3 0.0
0.0 0.0 0.2 0.0 0.0

sup/drv results at minimum mean square indicator
effective eddy diffusivity E*1 = 0.109
swirl velocity ratio C1 = 0.300
min. mean square indicator = 5.71
dimensionless ratios of salt concentration*100.0:

0.4 0.4 0.5 0.5 0.5
0.3 0.6 1.0 1.0 0.5
0.5 1.2 1.6 1.2
0.2 0.8 2.1 2.9 2.0 0.5
0.5 1.6 3.3 3.2 1.5
0.2 0.6 2.1 4.2 4.1 2.0 0.4
0.3 1.2 3.3 (4.7) 3.2 1.1
0.2 0.3
0.2 1.0 2.9 4.1 2.9 0.9
0.1 0.4 1.6 3.3 3.3 1.6 0.3
0.3 1.0 2.1 2.1 0.9
0.1 0.4 1.2 1.6 1.1 0.2
0.2 0.6 0.8 0.5
0.1 0.2 0.4 0.4 0.2
0.1 0.1 0.1 0.1 0.1

37 pin p/d= 1.154 h/d= 13.40
inj. subchannel = 1
inj. depth (in) = 32.0
bundle reynolds no.= 18600
mass balance ratio = 1.583
dimensionless ratios of salt concentration*100.0:

0.4 0.7 0.6 0.6 0.5
0.2 0.7 2.5 1.8 0.3
0.7 1.5 2.3 1.9
0.1 1.5 3.7 4.6 0.9 0.1
1.0 3.0 5.2 3.9 1.4
0.0 1.3 3.7 5.2 4.0 1.7 0.1
0.5 1.7 3.6 (3.2) 3.0 0.6
0.3 0.0
0.9 2.5 3.2 3.1 0.9 0.3
0.1 0.3 2.0 3.8 1.9 0.9 0.0
0.4 0.9 0.7 0.8 0.2
0.2 0.3 1.4 1.2 0.7 0.2
0.2 0.4 0.2 0.0
0.1 0.8 0.1 0.0 0.0
0.3 0.0 0.0 0.1 0.0

sup/drv results at minimum mean square indicator
effective eddy diffusivity E*1 = 0.115
swirl velocity ratio C1 = 0.300
min. mean square indicator = 6.39
dimensionless ratios of salt concentration*100.0:

0.4 0.5 0.5 0.5 0.5
0.3 0.7 1.1 1.1 0.6
0.5 1.2 1.6 1.2
0.3 0.8 2.1 2.8 2.0 0.5
0.5 1.6 3.1 3.1 1.5
0.2 0.6 2.0 3.9 3.9 2.0 0.4
0.3 1.2 3.1 (4.4) 3.1 1.1
0.2 0.3
0.3 1.1 2.8 3.9 2.8 1.0
0.1 0.5 1.6 3.1 3.1 1.6 0.3
0.3 1.1 2.0 2.0 1.0
0.1 0.5 1.2 1.6 1.2 0.3
0.2 0.6 0.8 0.5
0.1 0.3 0.4 0.4 0.2
0.1 0.1 0.1 0.1 0.1

37 pin p/d= 1.154 h/d= 13.40
inj. subchannel = 1
inj. depth (in) = 32.0
bundle reynolds no.= 22100
mass balance ratio = 1.423
dimensionless ratios of salt concentration*100.0:

0.3 0.5 0.8 0.6 0.4
0.1 0.8 2.8 1.4 0.2
0.5 1.3 2.3 1.7
0.3 1.3 3.8 4.2 1.0 0.0
1.0 3.1 4.4 4.0 1.5
0.1 1.3 4.2 5.5 3.7 1.3 0.3
0.4 1.6 3.6 (3.9) 2.8 0.7
0.2 0.0
0.5 2.7 4.1 3.2 0.9 0.1
0.0 0.1 2.1 4.0 2.2 0.9 0.0
0.6 1.3 0.9 0.7 0.0
0.0 0.3 1.5 1.2 0.5 0.1
0.0 0.2 0.3 0.2
0.1 0.1 0.4 0.0 0.0
0.1 0.1 0.1 0.0 0.0

sup/drv results at minimum mean square indicator
effective eddy diffusivity E*1 = 0.111
swirl velocity ratio C1 = 0.300
min. mean square indicator = 6.44
dimensionless ratios of salt concentration*100.0:

0.4 0.4 0.5 0.5 0.5
0.3 0.6 1.0 1.0 0.5
0.5 1.2 1.6 1.2
0.3 0.8 2.1 2.8 2.0 0.5
0.5 1.6 3.2 3.2 1.5
0.2 0.6 2.1 4.1 4.1 2.0 0.4
0.3 1.2 3.2 (4.6) 3.2 1.1
0.2 0.3
0.2 1.0 2.8 4.1 2.8 1.0
0.1 0.5 1.6 3.2 3.2 1.6 0.3
0.3 1.0 2.1 2.1 1.0
0.1 0.5 1.2 1.6 1.2 0.3
0.2 0.6 0.8 0.5
0.1 0.2 0.4 0.4 0.2
0.1 0.1 0.1 0.1 0.1

37 pin p/d= 1.154 h/d= 13.40
inj. subchannel = 1
inj. depth (in) = 32.0
bundle reynolds no.= 26000
mass balance ratio = 1.415
dimensionless ratios of salt concentration*100.0:

0.2 0.6 1.0 0.8 0.5

0.2 0.8 2.6 1.2 0.3

0.5 1.7 2.3 1.6

0.4 1.3 3.9 4.2 1.0 0.1

0.8 3.0 4.8 3.9 1.7

0.4 1.3 3.8 5.4 3.7 1.2 0.1

0.3 1.5 3.4 (3.9) 2.8 0.8

0.0 0.0

0.8 2.7 3.3 3.1 0.9 0.3

0.2 0.3 2.1 3.4 2.1 1.0 0.1

0.5 0.8 0.7 0.7 0.0

0.1 0.2 1.0 0.8 0.8 0.1

0.1 0.2 0.0 0.0

0.0 0.4 0.5 0.0 0.1

0.0 0.3 0.2 0.0 0.0

sup/drv results at minimum mean square indicator
effective eddy diffusivity E*1 = 0.114
swirl velocity ratio C1 = 0.300
min. mean square indicator = 6.28
dimensionless ratios of salt concentration*100.0:

0.4 0.4 0.5 0.5 0.5

0.3 0.7 1.1 1.1 0.6

0.5 1.2 1.6 1.2

0.3 0.8 2.1 2.8 2.0 0.5

0.5 1.6 3.2 3.1 1.5

0.2 0.6 2.1 4.0 4.0 2.0 0.4

0.3 1.2 3.2 (4.5) 3.1 1.1

0.2 0.3

0.2 1.1 2.8 4.0 2.8 1.0

0.1 0.5 1.6 3.2 3.2 1.6 0.3

0.3 1.1 2.0 2.0 1.0

0.1 0.5 1.2 1.6 1.2 0.3

0.2 0.6 0.8 0.5

0.1 0.3 0.4 0.4 0.2

0.1 0.1 0.1 0.1 0.1

37 pin p/d= 1.154 h/d= 13.40
inj. subchannel = 1
inj. depth (in) = 32.0
bundle reynolds no.= 29600
mass balance ratio = 1.430
dimensionless ratios of salt concentration*100.0:

0.5 0.1 0.5 0.3 0.0

0.3 1.0 2.5 0.5 0.0

0.7 2.0 2.5 0.2

0.0 1.5 3.3 3.9 1.1 0.0

0.7 3.1 4.9 4.6 1.4

0.4 1.4 4.6 5.3 3.7 1.3 0.1

0.3 1.6 4.0 (3.8) 3.8 0.9

0.0 0.0

0.2 2.7 2.9 3.7 1.2 0.6

0.0 0.5 1.2 2.9 2.2 1.2 0.0

0.5 0.9 0.6 0.9 0.6

0.5 0.7 0.9 1.4 0.5 0.0

0.6 0.6 0.1 0.0

0.3 0.1 0.3 0.0 0.0

0.7 0.6 0.5 0.0 0.0

sup/drv results at minimum mean square indicator
effective eddy diffusivity E*1 = 0.108
swirl velocity ratio C1 = 0.300
min. mean square indicator = 6.44
dimensionless ratios of salt concentration*100.0:

0.4 0.4 0.5 0.5 0.5

0.3 0.6 1.0 1.0 0.5

0.5 1.2 1.6 1.2

0.2 0.8 2.1 2.9 2.0 0.5

0.5 1.6 3.3 3.3 1.5

0.2 0.6 2.1 4.2 4.2 2.0 0.4

0.3 1.2 3.3 (4.7) 3.3 1.1

0.1 0.3

0.2 1.0 2.9 4.2 2.9 0.9

0.1 0.4 1.6 3.3 3.3 1.6 0.3

0.3 1.0 2.1 2.1 0.9

0.1 0.4 1.2 1.6 1.1 0.2

0.2 0.6 0.8 0.5

0.1 0.2 0.4 0.4 0.1

0.1 0.1 0.1 0.1 0.1

37 pin p/d= 1.154 h/d= 13.40
inj. subchannel = 71
inj. depth (in) = 32.0
bundle reynolds no.= 430
mass balance ratio = 2.007
dimensionless ratios of salt concentration*100.0:

1.0 0.2 0.0 9.2 18.3

0.0 0.6 1.3 1.1 15.7

0.4 0.7 1.2 7.2

0.5 1.1 0.0 0.0 4.5 13.1

0.9 0.5 0.0 1.4 3.5

1.1 0.2 0.5 0.2 2.8 16.8 7.7

0.2 0.0 0.0 0.3 2.3 12.7

0.2 7.7

0.7 0.0 0.0 0.0 1.0 14.9

0.8 0.9 0.0 0.0 0.0 9.6 7.8

0.0 0.1 0.6 1.0 9.6

0.0 0.9 0.7 0.0 1.0 (1.7)

0.2 1.1 0.5 2.4

0.0 1.2 0.9 2.6 0.1

2.7 0.6 0.5 0.5 0.3

sup/drv results at minimum mean square indicator
effective eddy diffusivity E*1 = 0.060
swirl velocity ratio C1 = 0.225
min. mean square indicator = 18.69
dimensionless ratios of salt concentration*100.0:

1.9 2.6 4.9 8.4 11.9

0.9 0.6 1.4 3.8 12.7

0.3 0.4 1.3 5.6

0.3 0.1 0.1 0.6 4.0 14.1

0.1 0.0 0.2 1.4 7.8

0.1 0.0 0.0 0.2 1.4 6.7 12.7

0.0 0.0 0.1 0.6 3.5 10.5

0.1 8.7

0.0 0.0 0.1 0.8 4.0 9.4

0.0 0.0 0.0 0.3 2.1 6.9 7.0

0.0 0.0 0.4 2.2 5.4

0.0 0.0 0.1 1.0 3.6 (3.0)

0.0 0.1 0.6 2.0

0.0 0.0 0.2 0.9 0.8

0.0 0.0 0.0 0.1 0.2

37 pin p/d= 1.154 h/d= 13.40
inj. subchannel = 71
inj. depth (in) = 32.0
bundle reynolds no.= 860
mass balance ratio = 1.532
dimensionless ratios of salt concentration*100.0:

0.0 0.0 7.6 12.5 17.3

0.0 0.3 0.3 3.7 14.1

0.0 0.4 0.7 7.7

0.0 0.0 0.0 0.4 2.6 10.8

0.5 0.1 0.0 0.0 6.5

0.0 0.0 0.2 0.0 1.5 8.9 7.5

0.4 0.2 0.2 0.2 1.1 10.5

0.0 6.3

0.2 0.0 0.2 0.3 4.2 11.4

0.0 0.0 0.0 0.2 0.0 9.3 5.0

0.2 0.6 0.4 3.9 7.3

0.0 0.0 0.0 1.5 7.3 (4.2)

1.1 0.2 0.5 5.9

0.0 2.9 0.0 1.6 0.9

0.0 0.0 0.2 0.0 0.5

sup/drv results at minimum mean square indicator
effective eddy diffusivity E*1 = 0.060
swirl velocity ratio C1 = 0.248
min. mean square indicator = 13.36
dimensionless ratios of salt concentration*100.0:

2.8 3.6 6.2 9.6 12.6

1.4 0.9 1.9 4.5 13.0

0.4 0.6 1.6 6.2

0.6 0.1 0.2 0.7 4.3 13.3

0.1 0.0 0.2 1.6 7.8

0.2 0.0 0.0 0.2 1.4 6.7 11.0

0.0 0.0 0.1 0.6 3.5 9.9

0.1 7.0

0.0 0.0 0.1 0.8 3.8 8.6

0.1 0.0 0.0 0.3 2.0 6.4 5.6

0.0 0.0 0.4 2.1 4.9

0.0 0.0 0.1 0.9 3.3 (2.3)

0.0 0.1 0.6 1.8

0.0 0.0 0.2 0.8 0.6

0.0 0.0 0.0 0.1 0.2

37 pin p/d= 1.154 h/d= 13.40
inj. subchannel = 71
inj. depth (in) = 32.0
bundle reynolds no.= 1500
mass balance ratio = 1.051
dimensionless ratios of salt concentration*100.0:

0.4 4.9 11.9 10.3 8.7

0.0 0.0 0.0 4.9 9.2

0.3 0.6 0.3 6.7

0.0 0.0 0.0 0.0 8.8 9.7

0.0 0.3 0.0 1.3 7.6

0.0 0.0 1.0 0.0 1.2 8.9 7.4

0.3 0.0 0.0 0.3 1.9 11.7

0.0 6.6

0.0 0.0 0.0 0.2 3.5 11.0

0.0 0.7 0.0 0.0 0.8 7.0 5.8

0.3 0.0 0.0 4.5 9.3

0.3 0.0 0.7 0.4 5.8 (2.1)

1.2 0.9 1.3 4.8

0.0 1.5 1.7 1.9 1.1

0.0 0.4 0.0 0.3 0.7

sup/drv results at minimum mean square indicator
effective eddy diffusivity E*1 = 0.070
swirl velocity ratio C1 = 0.258
min. mean square indicator = 13.51
dimensionless ratios of salt concentration*100.0:

3.1 3.9 6.5 9.7 12.2

1.6 1.2 2.2 5.0 12.4

0.6 0.8 2.0 6.6

0.7 0.2 0.2 1.0 4.8 12.4

0.2 0.1 0.3 2.0 8.0

0.3 0.0 0.0 0.3 1.8 7.1 10.1

0.1 0.0 0.1 0.8 4.0 9.5

0.2 6.5

0.0 0.0 0.1 1.0 4.1 8.2

0.1 0.0 0.0 0.4 2.3 6.3 5.2

0.0 0.1 0.5 2.2 4.6

0.0 0.0 0.2 1.1 3.3 (2.2)

0.0 0.1 0.7 1.8

0.0 0.0 0.2 0.9 0.7

0.0 0.0 0.0 0.1 0.2

37 pin p/d= 1.154 h/d= 13.40
inj. subchannel = 71
inj. depth (in) = 32.0
bundle reynolds no.= 2200
mass balance ratio = 1.265
dimensionless ratios of salt concentration*100.0:

2.2 7.3 11.2 10.4 9.6
0.0 0.5 2.1 6.5 9.0
0.9 0.5 0.8 7.3
0.0 0.0 0.0 1.0 6.9 8.4
0.0 0.0 0.0 0.3 6.1
0.0 0.0 0.0 0.5 3.5 10.4 7.4
0.0 0.0 0.3 1.1 2.5 8.9
0.0 6.9
0.0 0.0 0.0 0.2 4.2 9.0
0.0 0.0 0.0 0.0 1.7 9.6 6.4
0.0 0.0 0.3 3.2 4.6
0.0 0.0 0.3 0.9 6.8 (2.7)
0.0 0.5 0.8 4.3
0.3 0.0 0.0 1.6 0.2
0.0 0.0 0.3 0.3 0.2

sup/drv results at minimum mean square indicator
effective eddy diffusivity E*1 = 0.080
swirl velocity ratio C1 = 0.278
min. mean square indicator = 11.51
dimensionless ratios of salt concentration*100.0:

3.8 4.6 7.2 10.0 11.8
2.1 1.6 2.8 5.7 11.8
0.9 1.1 2.6 7.1
1.0 0.3 0.4 1.4 5.4 11.1
0.3 0.1 0.5 2.5 8.1
0.5 0.1 0.1 0.4 2.2 7.2 8.7
0.1 0.0 0.2 1.1 4.3 8.8
0.3 5.5
0.0 0.0 0.2 1.2 4.3 7.5
0.1 0.0 0.1 0.6 2.5 5.9 4.4
0.0 0.1 0.6 2.3 4.2
0.0 0.0 0.2 1.2 3.1 (2.0)
0.0 0.2 0.8 1.7
0.0 0.0 0.3 0.9 0.6
0.0 0.0 0.0 0.2 0.2

37 pin p/d= 1.154 h/d= 13.40
inj. subchannel = 71
inj. depth (in) = 32.0
bundle reynolds no.= 3200
mass balance ratio = 1.335
dimensionless ratios of salt concentration*100.0:

4.5 10.6 9.1 9.8 10.5

2.1 0.8 2.7 7.6 8.7

0.8 1.5 2.0 7.9

0.5 0.3 0.0 1.0 3.4 6.9

0.0 0.1 0.0 1.9 6.8

0.3 0.0 0.0 0.2 1.7 8.4 5.7

0.0 0.0 0.3 0.0 0.6 8.2

0.5 5.5

0.7 0.0 0.0 2.6 3.0 8.3

1.0 0.0 0.0 0.0 1.0 9.4 5.4

0.3 0.0 1.9 3.1 5.4

0.0 0.5 0.3 1.1 5.1 (1.4)

1.0 0.0 2.1 3.6

0.0 0.3 0.3 1.5 0.0

1.2 0.3 1.0 0.2 0.1

sup/drv results at minimum mean square indicator
effective eddy diffusivity E*1 = 0.090
swirl velocity ratio C1 = 0.311
min. mean square indicator = 11.38
dimensionless ratios of salt concentration*100.0:

5.0 5.8 8.2 10.3 11.1

3.1 2.3 3.6 6.4 10.7

1.4 1.6 3.3 7.5

1.7 0.5 0.6 1.9 5.8 9.4

0.5 0.3 0.8 3.0 7.8

0.8 0.2 0.1 0.6 2.6 7.0 7.0

0.2 0.1 0.3 1.3 4.5 7.8

0.6 4.3

0.1 0.0 0.3 1.4 4.2 6.4

0.3 0.0 0.1 0.7 2.6 5.3 3.4

0.0 0.1 0.7 2.3 3.7

0.1 0.0 0.3 1.2 2.8 (1.6)

0.0 0.2 0.8 1.6

0.0 0.1 0.3 0.9 0.6

0.0 0.0 0.1 0.2 0.2

37 pin p/d= 1.154 h/d= 13.40
inj. subchannel = 71
inj. depth (in) = 32.0
bundle reynolds no.= 4300
mass balance ratio = 0.939
dimensionless ratios of salt concentration*100.0:

4.3 9.1 9.6 9.0 8.4

0.3 0.6 0.9 6.8 7.3

0.7 1.0 1.0 7.4

0.3 0.0 0.3 1.6 5.1 6.1

0.0 1.3 0.0 1.0 6.0

0.0 0.0 3.7 0.3 4.4 11.3 5.2

0.3 0.0 0.3 0.8 2.0 6.2

0.7 5.0

0.0 0.0 0.0 0.3 3.4 9.0

1.0 0.0 0.0 0.2 2.7 8.1 4.9

0.0 0.0 0.3 3.3 3.0

0.0 0.0 0.0 0.7 5.4 (2.2)

0.0 0.0 1.7 4.1

0.3 0.0 0.0 1.2 1.1

0.0 0.4 1.6 1.6 1.3

sup/drv results at minimum mean square indicator
effective eddy diffusivity E*1 = 0.100
swirl velocity ratio C1 = 0.287
min. mean square indicator = 12.66
dimensionless ratios of salt concentration*100.0:

4.6 5.3 7.5 9.4 10.2

2.9 2.2 3.5 6.1 10.0

1.3 1.6 3.3 7.1

1.6 0.5 0.7 1.9 5.6 8.9

0.5 0.3 0.8 3.0 7.4

0.8 0.2 0.1 0.7 2.7 6.8 6.8

0.2 0.1 0.3 1.4 4.5 7.5

0.6 4.4

0.1 0.1 0.3 1.5 4.2 6.2

0.3 0.0 0.1 0.7 2.6 5.2 3.5

0.0 0.1 0.7 2.3 3.7

0.1 0.1 0.3 1.3 2.8 (1.7)

0.0 0.2 0.8 1.6

0.0 0.1 0.4 0.9 0.7

0.0 0.0 0.1 0.2 0.3

37 pin p/d= 1.154 h/d= 13.40
inj. subchannel = 71
inj. depth (in) = 32.0
bundle reynolds no.= 5400
mass balance ratio = 1.383
dimensionless ratios of salt concentration*100.0:

4.5 7.4 8.2 7.8 7.4

1.6 0.7 2.4 6.5 6.7

1.0 2.7 2.4 5.9

0.2 1.5 0.0 2.2 7.1 6,0

1.4 0.5 0.6 1.9 4.9

0.5 0.5 0.0 0.2 2.3 8.3 6.0

0.4 0.4 2.0 1.1 2.5 7.2

0.2 4.8

0.0 2.6 0.2 1.2 2.9 7.1

0.2 0.7 0.0 0.0 1.8 7.6 3.5

1.2 0.2 0.4 2.7 4.1

0.5 0.7 0.9 2.8 5.5 (1.7)

0.2 0.9 2.3 4.2

0.2 1.3 0.0 3.0 1.1

0.0 0.0 1.3 0.9 1.0

sup/drv results at minimum mean square indicator
effective eddy diffusivity E*1 = 0.100
swirl velocity ratio C1 = 0.297
min. mean square indicator = 10.57
dimensionless ratios of salt concentration*100.0:

4.9 5.6 7.7 9.4 10.0

3.2 2.3 3.6 6.1 9.6

1.5 1.7 3.2 7.0

1.8 0.5 0.7 1.9 5.5 8.4

0.6 0.3 0.8 2.9 7.2

0.9 0.2 0.1 0.6 2.5 6.5 6.3

0.3 0.1 0.3 1.3 4.3 7.2

0.7 4.0

0.1 0.1 0.3 1.3 4.0 6.0

0.3 0.0 0.1 0.7 2.5 5.0 3.2

0.0 0.1 0.6 2.2 3.5

0.1 0.0 0.3 1.2 2.7 (1.6)

0.0 0.2 0.8 1.5

0.1 0.1 0.3 0.9 0.6

0.0 0.0 0.1 0.2 0.2

37 pin p/d= 1.154 h/d= 13.40
inj. subchannel = 71
inj. depth (in) = 32.0
bundle reynolds no.= 6500
mass balance ratio = 1.112
dimensionless ratios of salt concentration*100.0:

5.0 8.4 9.3 8.5 7.8

1.0 1.2 0.7 7.4 7.2

0.8 1.0 2.4 8.2

0.5 0.3 0.7 1.0 8.0 6.6

0.0 0.3 0.9 2.6 7.4

0.0 0.0 0.0 0.2 2.5 7.2 6.4

0.0 0.0 0.0 1.2 3.4 7.5

0.0 5.2

0.0 0.2 0.0 1.5 3.4 7.6

0.0 0.0 0.0 1.1 2.2 8.6 4.1

0.0 0.0 0.5 3.0 4.3

0.0 0.0 0.0 0.8 4.7 (2.8)

0.0 0.0 0.5 3.7

0.3 0.0 0.0 1.8 0.6

0.0 0.0 0.5 0.0 0.3

sup/drv results at minimum mean square indicator
effective eddy diffusivity E*1 = 0.100
swirl velocity ratio C1 = 0.281
min. mean square indicator = 9.31
dimensionless ratios of salt concentration*100.0:

4.5 5.2 7.3 9.2 9.9

2.8 2.1 3.3 5.8 9.7

1.3 1.5 3.0 6.8

1.6 0.4 0.6 1.7 5.3 8.6

0.5 0.2 0.7 2.8 7.2

0.8 0.2 0.1 0.6 2.4 6.5 6.6

0.2 0.1 0.2 1.2 4.2 7.3

0.6 4.3

0.1 0.0 0.3 1.3 4.0 6.2

0.3 0.0 0.1 0.6 2.5 5.1 3.5

0.0 0.1 0.6 2.2 3.6

0.1 0.0 0.3 1.2 2.7 (1.7)

0.0 0.2 0.8 1.6

0.0 0.1 0.3 0.9 0.7

0.0 0.0 0.1 0.2 0.3

37 pin p/d= 1.154 h/d= 13.40
inj. subchannel = 71
inj. depth (in) = 32.0
bundle reynolds no.= 9400
mass balance ratio = 1.197
dimensionless ratios of salt concentration*100.0:

6.4 7.5 8.8 8.0 7.2

2.4 0.7 3.1 7.7 6.7

1.0 1.9 2.5 8.3

0.0 0.0 0.0 0.9 7.6 6.2

0.2 0.0 0.9 1.2 6.8

0.3 0.0 0.0 0.6 0.7 6.6 5.3

0.0 0.2 0.0 0.4 2.8 6.4

0.0 4.8

0.0 0.0 0.0 1.1 3.4 6.8

0.0 0.0 0.0 0.0 1.3 8.7 4.3

0.0 0.0 0.9 2.4 4.1

0.2 0.0 0.0 1.1 4.3 (0.7)

0.2 0.0 1.2 3.8

0.7 0.0 0.0 2.8 0.4

0.4 0.5 0.0 1.6 1.0

sup/drv results at minimum mean square indicator
effective eddy diffusivity E*1 = 0.100
swirl velocity ratio C1 = 0.284
min. mean square indicator = 9.41
dimensionless ratios of salt concentration*100.0:

5.0 5.6 7.5 8.9 9.2

3.3 2.2 3.4 5.7 8.9

1.5 1.6 3.0 6.5

1.9 0.5 0.6 1.7 5.0 7.7

0.6 0.3 0.7 2.6 6.6

1.0 0.2 0.1 0.5 2.2 6.0 5.7

0.3 0.1 0.2 1.1 3.9 6.7

0.8 3.7

0.1 0.0 0.2 1.2 3.7 5.7

0.4 0.0 0.1 0.6 2.3 4.8 3.0

0.0 0.1 0.6 2.0 3.4

0.2 0.0 0.2 1.1 2.5 (1.5)

0.0 0.2 0.7 1.5

0.1 0.1 0.3 0.8 0.6

0.1 0.0 0.1 0.2 0.2

37 pin p/d= 1.154 h/d= 13.40
inj. subchannel = 71
inj. depth (in) = 32.0
bundle reynolds no.= 9400
mass balance ratio = 1.197
dimensionless ratios of salt concentration*100.0:

6.4 7.5 8.8 8.0 7.2
2.4 0.7 3.1 7.7 6.7
1.0 1.9 2.5 8.3
0.0 0.0 0.0 0.9 7.6 6.2
0.2 0.0 0.9 1.2 6.8
0.3 0.0 0.0 0.6 0.7 6.6 5.3
0.0 0.2 0.0 0.4 2.8 6.4
0.0 4.8
0.0 0.0 0.0 1.1 3.4 6.8
0.0 0.0 0.0 0.0 1.3 8.7 4.3
0.0 0.0 0.9 2.4 4.1
0.2 0.0 0.0 1.1 4.3 (0.7)
0.2 0.0 1.2 3.8
0.7 0.0 0.0 2.8 0.4
0.4 0.5 0.0 1.6 1.0

sup/drv results at minimum mean square indicator
effective eddy diffusivity E*1 = 0.100
swirl velocity ratio C1 = 0.284
min. mean square indicator = 9.41
dimensionless ratios of salt concentration*100.0:

5.0 5.6 7.5 8.9 9.2
3.3 2.2 3.4 5.7 8.9
1.5 1.6 3.0 6.5
1.9 0.5 0.6 1.7 5.0 7.7
0.6 0.3 0.7 2.6 6.6
1.0 0.2 0.1 0.5 2.2 6.0 5.7
0.3 0.1 0.2 1.1 3.9 6.7
0.8 3.7
0.1 0.0 0.2 1.2 3.7 5.7
0.4 0.0 0.1 0.6 2.3 4.8 3.0
0.0 0.1 0.6 2.0 3.4
0.2 0.0 0.2 1.1 2.5 (1.5)
0.0 0.2 0.7 1.5
0.1 0.1 0.3 0.8 0.6
0.1 0.0 0.1 0.2 0.2

37 pin p/d= 1.154 h/d= 13.40
inj. subchannel = 71
inj. depth (in) = 32.0
bundle reynolds no.= 12200
mass balance ratio = 1.620
dimensionless ratios of salt concentration*100.0:

7.4 6.9 7.5 6.7 5.8

2.4 1.6 3.4 6.4 5.5

1.2 3.1 1.8 7.2

0.2 1.4 0.2 0.7 6.8 5.2

0.4 0.5 0.2 2.3 6.2

0.0 0.0 0.0 1.0 2.2 6.6 5.1

0.0 0.3 0.0 0.1 2.3 6.1

0.4 4.2

0.2 0.4 0.3 1.0 3.6 6.2

0.0 0.4 0.4 0.3 1.4 7.2 3.4

0.2 0.2 0.9 3.8 4.1

0.2 0.4 0.2 2.1 5.6 (2.7)

0.4 2.0 2.0 3.1

0.6 0.2 0.6 0.0 0.8

0.9 0.0 0.2 1.1 0.9

sup/drv results at minimum mean square indicator
effective eddy diffusivity E*1 = 0.110
swirl velocity ratio C1 = 0.289
min. mean square indicator = 9.43
dimensionless ratios of salt concentration*100.0:

5.1 5.6 7.2 8.4 8.5

3.5 2.4 3.5 5.7 8.1

1.6 1.8 3.2 6.3

2.1 0.6 0.7 1.8 5.0 6.9

0.7 0.3 0.8 2.7 6.3

1.2 0.2 0.1 0.6 2.4 5.8 5.2

0.3 0.1 0.2 1.2 3.9 6.2

0.9 3.4

0.2 0.1 0.3 1.2 3.7 5.3

0.5 0.1 0.1 0.6 2.3 4.5 2.8

0.1 0.1 0.6 2.0 3.2

0.2 0.0 0.3 1.1 2.4 (1.4)

0.0 0.2 0.7 1.4

0.1 0.1 0.3 0.8 0.6

0.1 0.0 0.1 0.2 0.3

37 pin p/d= 1.154 h/d= 13.40
inj. subchannel = 71
inj. depth (in) = 32.0
bundle reynolds no.= 14800
mass balance ratio = 1.402
dimensionless ratios of salt concentration*100.0:

8.4 8.2 8.1 7.2 6.3

3.4 0.9 1.8 6.5 5.8

1.1 1.6 1.7 7.2

0.2 0.0 0.2 0.8 6.6 5.4

0.0 0.1 0.2 2.5 6.1

0.2 0.4 0.0 0.0 2.2 5.5 5.3

0.0 0.0 0.0 0.5 2.7 5.6

0.0 4.5

0.0 0.2 0.5 1.1 3.3 6.1

0.2 0.0 0.0 0.0 1.1 7.7 3.6

0.0 0.0 0.9 3.0 3.6

0.4 0.0 0.0 1.3 4.2 (1.7)

0.2 0.4 1.0 3.3

0.2 0.2 0.0 1.7 1.0

0.0 1.1 0.2 0.6 0.8

sup/drv results at minimum mean square indicator
effective eddy diffusivity E*1 = 0.110
swirl velocity ratio C1 = 0.285
min. mean square indicator = 8.96
dimensionless ratios of salt concentration*100.0:

5.1 5.6 7.1 8.2 8.2

3.6 2.4 3.5 5.6 7.8

1.7 1.7 3.1 6.1

2.2 0.6 0.7 1.8 4.9 6.7

0.7 0.3 0.8 2.6 6.1

1.3 0.2 0.1 0.5 2.3 5.7 5.0

0.4 0.1 0.2 1.1 3.8 6.1

1.0 3.3

0.2 0.1 0.2 1.2 3.6 5.2

0.5 0.1 0.1 0.6 2.2 4.4 2.7

0.1 0.1 0.6 1.9 3.1

0.2 0.0 0.2 1.0 2.4 (1.4)

0.0 0.2 0.7 1.4

0.1 0.1 0.3 0.8 0.6

0.1 0.0 0.1 0.2 0.3

37 pin p/d= 1.154 h/d= 13.40
inj. subchannel = 71
inj. depth (in) = 32.0
bundle reynolds no.= 18600
mass balance ratio = 1.502
dimensionless ratios of salt concentration*100.0:

7.9 6.7 7.3 6.7 6.1

3.7 1.3 1.3 7.1 5.7

2.1 1.9 2.4 7.2

1.0 0.2 0.0 0.9 6.4 5.4

1.2 0.3 0.4 2.0 5.3

0.0 0.0 0.8 1.9 2.0 7.4 4.3

0.2 0.2 0.0 0.2 3.1 5.4

0.0 3.6

0.6 0.2 0.2 1.3 3.2 6.1

0.4 0.0 0.0 0.0 1.2 6.9 3.0

0.2 0.2 0.9 4.0 3.5

0.0 0.0 0.4 1.7 5.6 (0.7)

0.2 0.6 2.1 3.2

0.0 0.2 0.6 2.5 0.5

0.0 0.0 0.6 1.5 1.0

sup/drv results at minimum mean square indicator
effective eddy diffusivity E*1 = 0.110
swirl velocity ratio C1 = 0.291
min. mean square indicator = 9.22
dimensionless ratios of salt concentration*100.0:

5.3 5.8 7.2 8.2 8.1

3.7 2.5 3.6 5.6 7.7

1.8 1.8 3.2 6.1

2.4 0.7 0.7 1.8 4.9 6.5

0.8 0.3 0.8 2.7 6.1

1.4 0.3 0.1 0.6 2.3 5.6 4.8

0.4 0.1 0.2 1.1 3.8 6.0

1.1 3.1

0.2 0.1 0.2 1.2 3.5 5.0

0.6 0.1 0.1 0.6 2.2 4.3 2.6

0.1 0.1 0.6 1.9 3.1

0.3 0.0 0.2 1.0 2.3 (1.3)

0.0 0.2 0.7 1.4

0.1 0.1 0.3 0.8 0.6

0.1 0.1 0.1 0.2 0.2

37 pin p/d= 1.154 h/d= 13.40
inj. subchannel = 71
inj. depth (in) = 32.0
bundle reynolds no.= 22100
mass balance ratio = 1.222
dimensionless ratios of salt concentration*100.0:

7.6 7.8 6.8 7.4 8.0

3.6 1.1 1.5 6.2 6.2

1.7 1.3 0.9 5.8

1.6 1.0 0.2 3.2 7.4 4.4

0.0 0.5 0.8 3.0 6.6

0.5 0.0 0.2 0.2 3.3 5.8 3.6

0.0 0.4 0.0 0.9 3.0 5.8

0.5 3.0

0.0 0.0 0.6 1.9 3.4 6.0

0.0 0.0 0.0 0.3 1.7 7.5 2.5

0.0 0.4 1.3 4.3 4.1

0.0 0.0 0.0 1.7 4.5 (1.4)

0.0 0.9 1.8 5.0

0.0 0.0 0.7 1.9 0.6

0.0 0.0 0.0 0.0 0.3

sup/drv results at minimum mean square indicator
effective eddy diffusivity E*1 = 0.110
swirl velocity ratio C1 = 0.291
min. mean square indicator = 9.29
dimensionless ratios of salt concentration*100.0:

5.3 5.8 7.2 8.2 8.1

3.7 2.5 3.6 5.6 7.7

1.8 1.8 3.2 6.1

2.4 0.7 0.7 1.8 4.9 6.5

0.8 0.3 0.8 2.7 6.1

1.4 0.3 0.1 0.6 2.3 5.6 4.8

0.4 0.1 0.2 1.1 3.8 6.0

1.1 3.1

0.2 0.1 0.2 1.2 3.5 5.0

0.6 0.1 0.1 0.6 2.2 4.3 2.6

0.1 0.1 0.6 1.9 3.1

0.3 0.0 0.2 1.0 2.3 (1.3)

0.0 0.2 0.7 1.4

0.1 0.1 0.3 0.8 0.6

0.1 0.1 0.1 0.2 0.2

37 pin p/d= 1.154 h/d= 13.40
inj. subchannel = 71
inj. depth (in) = 32.0
bundle reynolds no.= 26000
mass balance ratio = 1.310
dimensionless ratios of salt concentration*100.0:

9.6 7.5 6.9 6.3 5.7

4.2 0.6 0.8 6.0 5.4

2.0 2.1 2.4 5.2

2.3 0.5 0.0 1.4 5.1 5.2

0.0 0.2 1.2 2.6 6.0

0.4 0.0 0.0 0.2 3.1 6.8 4.1

0.0 0.0 0.2 0.0 2.8 6.1

0.4 3.6

0.0 0.0 0.2 2.1 2.6 4.4

0.0 0.0 0.4 0.0 1.2 5.3 3.1

0.0 0.2 0.8 3.1 4.9

0.0 0.0 0.0 3.0 4.6 (1.5)

0.2 1.2 2.7 3.7

0.9 0.0 1.1 1.7 1.0

0.0 0.0 1.4 0.4 0.7

sup/drv results at minimum mean square indicator
effective eddy diffusivity E*1 = 0.110
swirl velocity ratio C1 = 0.305
min. mean square indicator = 9.53
dimensionless ratios of salt concentration*100.0:

5.7 6.1 7.4 8.1 7.7

4.2 2.8 3.8 5.7 7.3

2.0 2.0 3.3 6.1

2.7 0.8 0.8 1.9 4.8 6.0

0.9 0.4 0.8 2.7 5.9

1.7 0.3 0.2 0.6 2.3 5.4 4.4

0.5 0.1 0.2 1.1 3.7 5.6

1.4 2.8

0.3 0.1 0.2 1.2 3.4 4.8

0.8 0.1 0.1 0.6 2.1 4.1 2.3

0.1 0.1 0.5 1.8 2.9

0.4 0.1 0.2 1.0 2.2 (1.2)

0.1 0.2 0.7 1.3

0.2 0.1 0.3 0.7 0.5

0.1 0.1 0.1 0.2 0.2

APPENDIX E

ERROR ANALYSIS OF MIXING PARAMETERS RESULTS

E.1 Overview

The final objective of this appendix is to estimate the error associated with the results of mixing parameters. The error analysis of the salt mixing experiments has been discussed in detail in Chapter 5 of Reference 12. However, some modification and correction were invoked after careful investigation.

The total error inherent in the determination of the mixing parameter ε^*_{1L} and C_{1L} is comprised of three parts: 1) the error involved in obtaining the dimensionless salt concentration, C^*_i; 2) the error involved in the code calibration; and 3) the error involved by using this reduced value as the sodium heat mixing parameter.

E.2 Error Involved in C^*_i: Experimental Error

The dimensionless salt concentration is defined by

$$C_i^* \equiv \frac{C_i}{\frac{1}{m_o}\left[\sum_{j=\text{interior}} m_j C_j + \sum_{k=\text{edge}} m_k c_k\right]} \qquad \text{(E.1)}$$

where

m_j, m_k = interior and edge subchannel flow rates

m_o = injection subchannel flow rate

= m_j for interior injection

= m_k for edge injection

C_i, C_j, C_k = detected subchannel salt concentrations

For interior injection, since almost all the salt tracer is confined in the interior region at the bundle exit level, C_i^* can be expressed as

$$C_i^* \simeq \frac{C_i}{\sum_{j=\text{interior}} C_j} \qquad \text{(E.2)}$$

Therefore,

$$\frac{\delta C_i^*}{C_i} = \frac{\delta C_i}{C_i} ,$$

the error associated with C_i^*, is caused by the uncertainty in determining C_i only.

For edge injection, approximately half the amount of injected salt diffused into the central region, then since

$$\sum_j C_j = \sum_k C_k$$

$$C_i^* = \frac{C_i}{\sum_j \frac{m_j}{m_o} C_j + \sum_k C_k} = \frac{C_i}{\frac{X_1}{X_2} \sum_j C_j + \sum_k C_k}$$

$$\simeq \frac{C_T}{(1 + \frac{X_1}{X_2}) \sum_j C_j} \qquad \text{(E.3)}$$

Therefore,

$$\frac{\delta C_i^*}{C_i^*} = \frac{\delta C_i}{C_i} + \frac{\delta\left(\frac{X_1}{X_2}\right)}{1 + \frac{X_1}{X_2}} \simeq \frac{\delta C_i}{C_i} + \frac{\delta\left(\frac{X_1}{X_2}\right)}{2} \qquad \text{(E.4)}$$

since in general $X_1 \simeq X_2$.

Eq. (E.4) shows that the error associated with $\frac{X_1}{X_2}$ will induce error in C_i^*. However, since Eq. (E.3) shows that this error influences all the C_i^* in the same direction, it is systematic in nature.

E.2.1 Error Caused by Misdetermination of C_i

The error associated with C_i is caused by two parts: the fluctuation in the data and the spatial nonuniformity of subchannel concentration. Both of these are random errors and should be combined in a statistical manner.

The standard deviation of the probe resistance after combining calibration and mixing data was estimated to be 12. The nominal value of the difference between the calibration correction and mixing data, which were used to reduce to salt concentration, was about 100 for most subchannels that is important in this experiment. Therefore, the error associated with C_i is 12/100 = 12%. Note that in Reference 12, the mean probe resistance of 1200 was used as the nominal value which is now not considered to be correct.

The nonuniformity of subchannel concentration would cause at most 5% error when the detected value was used as the real

average value [12]. The total error involved in determining C_i is then $\sqrt{(5)^2+(12)^2}$ = 13%.

To investigate how this error affected the reduced mixing parameters, the prediction maps by DRV with different mixing parameters input, e.g., map A calculated by ε_1^* = 0.10 and map B calculated by ε_1^* = 0.11, were compared. It was found that the percentage difference of the dimensionless concentration in most subchannels between these two maps were about the same as the percentage difference of the mixing parameters input, i.e., the difference in most subchannels between map A and map B is about 10%. The random nature of these experimental errors in different subchannels would mitigate their effect in reducing mixing parameters. So we can conservatively assume the error of mixing parameters in this part to be the same as the error associated with salt concentration, 13%.

E.2.2 Error Caused by Misdetermination of Flow Split Parameters

As discussed in the beginning of this section, only in the edge injection case would the C_i^* be affected by this flow split parameters misdetermination. The error associated with X_i are 5% in the turbulent flow regime and 10% in the transition/laminar flow regime, as described in Section 3.1. By Eq. (E.4), this would give 5% and 10% error in C_i^*, respectively.

Reference 12 had studied this kind of systematic error. The conclusion is about half the percentage error was induced

in reducing them to mixing parameters. Hence, 3% and 5% error were imposed on C_{1L} by this misdetermination, respectively.

E.3 Error Involved in the Code Calibration

The maldistribution of the concentration map caused by the injection flow disturbance and the strong local sweeping flow near the injection position will introduce uncertainty in the determination of ε^*_{1L} and C_{1L} as reduced by the DRV code

E.3.1 Interior Injection Case: ε^*_{1L}

In this case, all except the two lowest flow rate runs showed the peak concentration in subchannel 2 instead of subchannel 1. This implied that the maldistribution was caused by the strong local sweeping flow at the injection position rather than the injection disturbance. To investigate this effect, DRV was run with the same sets of data with injection subchannel set to be 2. Table E.1 shows the comparison of the induced ε^*_1 and the minimum mean square indicator between injection subchannels set to be 2 and 1. Appendix F illustrates detail concentration maps predicted by DRV with the injection subchannel set to be 2 together with the experimental dimensionless map for all 16 runs of interior injection.

Table E.1 shows the differences between these two results are about 10%. The real value should be between these two

results; hence, we conclude the error caused by maldistribution is about 5%.

E.3.2 Edge Injection Case: C_{1L}

In contrast to the ε^*_{1L} case, since the strong swirl flow is a characteristic of the edge region, the injection disturbance was expected to be dominant in this case. Since the injection flow was in the same direction as the swirl flow direction, it would increase the swirl effect, thereby increasing the reduced value of C_{1L}. Reference 17 studied this effect, and the total error was believed to be less than 5%.

Note that in our work the injection depth was 32" longer than all the previous similiar works. The longer the injection depth, the less the data reduction error because the disturbance effect is mitigated. However, the injection depth should not be too long; otherwise, too flat salt concentration distrubution might cause large uncertainty in data reduction. The 32" length of our choice here is believed to be near optimum.

E.4 Error Involved by Methodology

In the LMFBR, sodium instead of water is used as a coolant, and heat mixing instead of salt tracer mixing occurs. Chapter 2 of Reference 12 had derived and discussed the validity of the mixing parameters reduced by this method. The conclusion was that ε^*_{1L} obtained from this salt injection method can be taken as sodium's heat mixing parameter within 5% error.

Since swirl flow is not a property of the specific coolant, the value of C_{1L} derived from salt tracer experiments is directly applicable to heated sodium assemblies.

Note that all the errors that have been discussed are associated with the local mixing parameters ε^*_{1L} and C_{1L}, rather than ε^*_1 and C_1. This is because DRV calibrates ε^*_{1L} and C_{1L}, although its outputs are ε^*_1 and C_1. To make this point clear, let's investigate the subchannel energy equations used in the SUPERENERGY code.

For interior subchannel,

$$\rho V_1 A_1 C_p \frac{dT}{dz} = (P-D)(\rho C_p \varepsilon + Kk)\nabla T + Q_1 A_1 \qquad (E.5)$$

For edge subchannel,

$$\rho V_2 A_2 C_p \frac{dT}{dz} = (\rho C_p \varepsilon + Kk)[(P-D)\nabla T + D_g \nabla T]$$

$$+ \rho C_p V_T D_g (T_j - T_i) + Q_2 A_2 \qquad (E.6)$$

In DRV, $\frac{k}{\rho C_p}$ is replaced by α which is very small compared to ε, and can be neglected here. The heat source is zero in salt injection simulation, hence $Q_i = 0$. Reaarranging these equations and substituting the ε^*_1 and C_1 by their definitions, $\varepsilon/V_b De_1$ and V_2/V_b , respectively, Equations (E.5) and (E.6) become

$$\frac{dT}{dz} = \frac{(P-D)De_1}{A_1} \frac{\varepsilon_1^*}{X_1} \nabla T \qquad (E.7a)$$

$$= \frac{(P-D)De_1}{A_1} \varepsilon^*_{1L} \nabla T \qquad (E.7b)$$

and

$$\frac{dT}{dz} = \frac{\varepsilon_1^*}{X_2} \frac{De_1}{A_2} [(P-D)\nabla T + D_g \nabla T] + \frac{C_1}{X_2} \frac{D_g}{A_2} (T_j - T_i) \qquad (E.8a)$$

$$= \varepsilon^*_{1L} \frac{X_1}{X_2} \frac{De_1}{A_2} [(P-D)\nabla T + D_g \nabla T] + C_{1L} \frac{D_g}{A_2} (T_j - T_i) \qquad (E.8b)$$

To reduce one parameter (ε_1^* or C_1), the other parameter (C_1 or ε_1^*), the flow split parameters (X_1 and X_2) and dimensionless salt concentrations are input to DRV. The best fit mixing parameter (ε_1^* or C_1) will be output, and it is divided by the flow split parameter (X_1 or X_2) to get the local parameter (ε^*_{1L} or C_{1L}). It is apparent from Equations (E.7) and (E.8) that actually the local parameter (ε^*_{1L} or C_{1L}) is calibrated; the code just separates them into the forms ε_1^*/X_1 and C_1/X_2.

The total error for ε^*_{1L} and C_{1L} are then

for ε^*_{1L}: 13% (experimental) + 5% (maldistribution)
+ 5% (methodology) = 23%

for C_{1L}: 13% (experimental) + 5% (maldistribution)

$$+ \begin{cases} 5\% \text{ (flow split maldetermination, for } Re_b < 6{,}000) = 23\% \\ 3\% \text{ (flow split maldetermination, for } Re_b > 6{,}000) = 21\% \end{cases}$$

Since ε_1^* and C_1 are calculated by $\varepsilon_{1L}^* \cdot X_1$ and $C_{1L} \cdot X_2$, respectively, the additional error caused by flow split parameters misdetermination must be added to ε_1^* and C_1, i.e., 5% for $Re_b \geq 6{,}000$ and 10% for $Re_b < 6{,}000$. However, the errors associated with the flow split parameters were random in nature. Hence, they should be combined into the total error determination statistically.

$Re_b < 6{,}000$ $\quad \varepsilon_1^*$: $\sqrt{23^2+10^2} = 25\%$

$\quad C_1$: $\sqrt{23^2+10^2} = 25\%$

$Re_b \geq 6{,}000$ $\quad \varepsilon_1^*$: $\sqrt{23^2+5^2} = 24\%$

$\quad C_1$: $\sqrt{21^2+5^2} = 22\%$

Table E.2 summarizes these error estimates.

Table E.1

Comparison Between Injection Subchannels 1 and 2

Re_b	Injection Subchannel = 1		Injection Subchannel = 2		$\frac{\varepsilon^*_{1,2}-\varepsilon^*_{1,1}}{\varepsilon^*_{1,1}}$
	min. MSI	$\varepsilon^*_{1,1}$	min. MSI	$\varepsilon^*_{1,2}$	
220	11.92	0.049	16.26	0.067	-37%
430	8.19	0.058	10.99	0.074	-28%
860	5.64	0.058	7.28	0.065	-12%
1,500	5.63	0.071	5.25	0.072	-1%
2,200	5.23	0.082	4.74	0.081	1%
3,200	5.54	0.085	4.41	0.082	4%
4,300	5.27	0.095	3.97	0.090	5%
5,400	5.88	0.087	4.72	0.084	3%
6,500	5.93	0.094	3.97	0.087	7%
9,400	5.89	0.095	4.07	0.089	6%
12,200	6.13	0.107	4.72	0.099	8%
14,800	5.71	0.109	4.08	0.101	7%
18,600	6.39	0.115	4.33	0.102	11%
22,100	6.44	0.111	3.92	0.101	9%
26,000	6.28	0.114	4.17	0.099	13%
29,600	6.44	0.108	4.45	0.099	9%

Table E.2

Summarization of Errors Associated with Mixing Parameters

Cause	$\delta C_i^*/C_i^*$				Maldis-tribution	Method-ology	Total		Error in X_1 and X_2	Total
	$\delta C_i/C_i$			$\frac{\delta(X_1/X_2)}{2}$						
	Data fluctuation	Non-uniformity	Total							
ε_{1L}^*	12%	5%	13%	--	5%	5%	23%	ε_1^*	10% (Re<6,000) 5% (Re>6,000)	25% 24%
C_{1L}	12%	5%	13%	5% (Re<6,000) 3% (Re>6,000)	5%	--	23% (Re<6,000) 21% (Re>6,000)	C_1	10% (Re<6,000) 5% (Re>6,000)	25% 22%

APPENDIX F

EXPERIMENTAL DIMENSIONLESS SALT CONCENTRATION MAPS AND DRV PREDICTED MAPS AT MINIMUM MEAN SQUARE INDICATOR WITH INJECTION SUBCHANNEL SET TO 2

37 pin p/d= 1.154 h/d= 13.40
inj. subchannel = 1
inj. depth (in) = 32.0
bundle reynolds no.= 220
mass balance ratio = 1.702
dimensionless ratios of salt concentration*100.0:

0.3 0.0 0.0 0.1 0.2
0.1 0.1 0.4 1.6 0.1
0.0 0.1 1.2 0.9
0.1 0.0 1.6 6.8 6.3 0.1
0.2 0.7 6.6 5.8 4.4
0.1 0.0 0.7 (5.6) 13.6 2.2 0.0
0.0 0.1 2.7 5.3 3.7 2.3
0.0 0.1
0.0 0.2 0.4 6.4 4.2 0.5
0.1 0.0 0.0 2.1 5.7 2.0 0.1
0.0 0.0 0.1 0.7 0.4
0.0 0.0 0.1 0.5 0.9 0.2
0.0 0.1 0.1 0.2
0.0 0.0 0.0 0.1 0.0
0.0 0.0 0.1 0.0 0.0

sup/drv results at minimum mean square indicator
effective eddy diffusivity E*1 = 0.067
swirl velocity ratio C1 = 0.100
min. mean square indicator = 16.26
dimensionless ratios of salt concentration*100.0

0.2 0.3 0.3 0.2 0.1
0.2 1.0 1.4 1.0 0.2
0.8 2.1 2.1 0.8
0.2 1.5 3.8 3.8 1.5 0.1
0.8 3.2 5.2 3.2 0.8
0.1 1.0 3.8 (6.2) 3.8 1.0 0.1
0.4 2.1 5.3 5.3 2.1 0.4
0.1 0.0
0.3 1.5 3.8 3.8 1.5 0.3
0.1 0.6 2.1 3.2 2.1 0.6 0.0
0.3 1.0 1.6 1.0 0.3
0.1 0.4 0.9 0.9 0.4 0.0
0.1 0.3 0.3 0.1
0.0 0.1 0.2 0.1 0.0
0.0 0.0 0.0 0.0 0.0

37 pin p/d= 1.154 h/d= 13.40
inj. subchannel = 1
inj. depth (in) = 32.0
bundle reynolds no.= 430
mass balance ratio = 1.805
dimensionless ratios of salt concentration*100.0:

0.3 0.0 0.3 0.3 0.3

0.2 0.4 0.4 1.8 0.3

0.0 1.3 1.7 0.4

0.0 0.4 1.4 6.7 6.4 0.3

0.2 1.0 4.0 5.4 3.8

0.2 0.0 1.1 (6.2) 7.0 1.7 0.0

0.1 0.4 3.2 7.7 3.5 1.7

0.9 0.0

0.3 0.9 1.3 4.4 2.1 1.0

0.0 0.2 0.5 1.9 4.5 2.4 0.3

0.0 0.3 0.8 0.7 0.6

0.1 0.1 0.0 0.4 0.4 0.1

0.0 0.2 0.2 0.2

0.0 0.4 0.0 0.0 0.1

0.5 0.0 0.1 0.0 0.0

sup/drv results at minimum mean square indicator
effective eddy diffusivity E*1 = 0.074
swirl velocity ratio C1 = 0.100
min. mean square indicator = 10.99
dimensionless ratios of salt concentration*100.0

0.3 0.3 0.4 0.3 0.2

0.2 1.0 1.5 1.0 0.2

0.9 2.1 2.1 0.9

0.2 1.6 3.6 3.6 1.6 0.2

0.9 3.1 4.8 3.1 0.9

0.1 1.1 3.6 (5.5) 3.6 1.1 0.1

0.5 2.1 4.8 4.8 2.1 0.4

0.1 0.1

0.3 1.6 3.6 3.6 1.6 0.3

0.1 0.7 2.1 3.1 2.1 0.7 0.1

0.3 1.1 1.6 1.1 0.3

0.1 0.5 0.9 0.9 0.5 0.1

0.2 0.4 0.4 0.2

0.0 0.1 0.2 0.1 0.0

0.0 0.0 0.0 0.0 0.0

37 pin p/d= 1.154 h/d= 13.40
inj. subchannel = 2
inj. depth (in) = 32.0
bundle reynolds no.= 860
mass balance ratio = 1.348
dimensionless ratios of salt concentration*100.0:

0.1 0.2 0.4 0.2 0.0

0.0 0.4 0.6 0.6 0.1

0.0 0.2 0.9 0.8

0.1 0.2 2.2 4.9 2.2 0.2

0.7 1.8 3.4 3.9 1.2

0.0 0.5 3.0 (7.4) 6.4 1.8 0.4

0.6 1.5 4.1 6.1 1.9 1.2

0.1 0.2

0.0 1.9 4.8 5.7 1.7 0.4

0.2 0.2 1.5 6.0 4.3 0.8 0.3

0.2 0.7 0.6 0.9 0.4

0.3 0.0 0.5 0.1 0.6 0.0

0.1 0.4 0.1 0.1

0.0 0.0 0.0 0.0 0.2

0.0 0.0 0.0 0.4 0.3

sup/drv results at minimum mean square indicator
effective eddy diffusivity E*1 = 0.065
swirl velocity ratio C1 = 0.100
min. mean square indicator = 7.28
dimensionless ratios of salt concentration*100.0

0.2 0.3 0.3 0.2 0.1

0.2 1.0 1.4 0.9 0.2

0.8 2.1 2.1 0.8

0.2 1.5 3.9 3.8 1.5 0.1

0.8 3.2 5.4 3.2 0.8

0.1 1.0 3.9 (6.4) 3.9 1.0 0.1

0.4 2.1 5.4 5.4 2.1 0.4

0.1 0.0

0.3 1.5 3.9 3.9 1.5 0.3

0.1 0.6 2.1 3.2 2.1 0.6 0.0

0.3 1.0 1.5 1.0 0.3

0.0 0.4 0.8 0.8 0.4 0.0

0.1 0.3 0.3 0.1

0.0 0.1 0.1 0.1 0.0

0.0 0.0 0.0 0.0 0.0

37 pin p/d= 1.154 h/d= 13.40
inj. subchannel = 1
inj. depth (in) = 32.0
bundle reynolds no.= 1500
mass balance ratio = 1.393
dimensionless ratios of salt concentration*100.0:

0.0 0.0 0.5 0.3 0.2

0.1 0.2 1.2 1.0 0.3

0.4 0.5 1.5 1.1

0.2 0.6 3.1 5.0 1.3 0.3

0.8 2.3 3.6 4.3 1.6

0.0 0.8 3.2 (6.5) 4.3 1.5 0.0

0.6 1.9 4.2 5.1 3.2 0.8

0.0 0.0

0.0 2.6 3.5 4.2 1.2 0.3

0.3 0.2 1.8 5.4 3.5 0.7 0.3

0.5 0.7 0.7 0.6 0.0

0.4 0.0 0.8 0.8 0.3 0.0

0.3 0.1 0.4 0.3

0.0 0.0 0.1 0.0 0.1

0.0 0.1 0.2 0.1 0.1

sup/drv results at minimum mean square indicator
effective eddy diffusivity E*1 = 0.072
swirl velocity ratio C1 = 0.100
min. mean square indicator = 5.25
dimensionless ratios of salt concentration*100.0

0.2 0.3 0.4 0.2 0.2

0.2 1.0 1.5 1.0 0.2

0.8 2.1 2.1 0.8

0.2 1.6 3.6 3.6 1.6 0.2

0.9 3.1 4.9 3.1 0.8

0.1 1.1 3.6 (5.7) 3.6 1.1 0.1

0.4 2.1 4.9 4.9 2.1 0.4

0.1 0.0

0.3 1.6 3.7 3.7 1.6 0.3

0.1 0.7 2.1 3.1 2.1 0.7 0.1

0.3 1.1 1.6 1.1 0.3

0.1 0.5 0.9 0.9 0.5 0.1

0.2 0.3 0.3 0.2

0.0 0.1 0.2 0.1 0.0

0.0 0.0 0.0 0.0 0.0

37 pin p/d= 1.154 h/d= 13.40
inj. subchannel = 1
inj. depth (in) = 32.0
bundle reynolds no.= 2200
mass balance ratio = 1.151
dimensionless ratios of salt concentration*100.0:

0.0 0.1 0.0 0.0 0.1

0.6 0.4 1.2 1.3 0.1

0.8 1.0 1.7 1.1

0.4 0.8 2.8 4.0 1.4 0.2

0.4 2.3 4.0 4.5 1.9

0.2 0.4 3.1 (5.5) 4.0 0.6 0.4

0.1 2.0 4.2 3.7 2.9 0.7

0.0 0.5

1.0 2.5 3.1 3.7 1.4 0.7

0.0 0.7 1.4 5.1 3.0 0.5 0.2

0.0 1.1 1.0 1.1 0.2

0.3 0.4 1.2 1.0 0.8 0.3

0.3 0.2 0.0 0.2

0.3 0.2 0.5 0.3 0.1

0.0 0.0 0.3 0.1 0.1

sup/drv results at minimum mean square indicator
effective eddy diffusivity E*1 = 0.081
swirl velocity ratio C1 = 0.200
min. mean square indicator = 4.74
dimensionless ratios of salt concentration*100.0

0.3 0.4 0.4 0.3 0.2

0.3 1.1 1.5 1.0 0.2

0.9 2.0 2.0 0.9

0.3 1.6 3.4 3.4 1.6 0.2

0.9 2.9 4.4 2.9 0.9

0.2 1.1 3.4 (5.0) 3.4 1.1 0.1

0.5 2.1 4.4 4.4 2.1 0.5

0.2 0.1

0.4 1.6 3.4 3.4 1.6 0.4

0.1 0.7 2.1 3.0 2.1 0.7 0.1

0.4 1.2 1.6 1.1 0.4

0.1 0.5 1.0 1.0 0.5 0.1

0.2 0.4 0.4 0.2

0.1 0.2 0.2 0.2 0.0

0.1 0.0 0.0 0.0 0.0

37 pin p/d= 1.154 h/d= 13.40
inj. subchannel = 2
inj. depth (in) = 32.0
bundle reynolds no.= 3200
mass balance ratio = 1.360
dimensionless ratios of salt concentration*100.0:

0.0 0.2 0.2 0.2 0.1

0.2 0.6 1.6 1.4 0.2

0.5 1.1 1.9 0.7

0.2 1.3 2.8 3.9 1.5 0.3

0.3 2.6 3.8 4.6 1.8

0.0 0.8 3.8 (5.2) 3.6 0.8 0.2

0.1 1.9 4.5 3.7 2.8 1.0

0.0 0.7

0.3 2.7 3.2 3.5 1.4 0.1

0.3 0.8 1.8 5.1 2.7 0.9 0.2

0.1 1.1 1.0 0.9 0.2

0.1 0.6 1.5 1.1 0.7 0.1

0.3 0.5 0.0 0.0

0.2 0.4 0.4 0.4 0.0

0.0 0.0 0.1 0.3 0.2

sup/drv results at minimum mean square indicator
effective eddy diffusivity E*1 = 0.082
swirl velocity ratio C1 = 0.200
min. mean square indicator = 4.41
dimensionless ratios of salt concentration*100.0

0.3 0.4 0.4 0.3 0.2

0.3 1.1 1.5 1.0 0.2

0.9 2.0 2.0 0.9

0.3 1.6 3.3 3.3 1.6 0.2

0.9 2.9 4.3 2.9 0.9

0.2 1.1 3.4 (5.0) 3.4 1.1 0.1

0.5 2.1 4.4 4.4 2.1 0.5

0.2 0.1

0.4 1.6 3.4 3.4 1.6 0.4

0.1 0.7 2.1 2.9 2.1 0.7 0.1

0.4 1.2 1.6 1.2 0.4

0.1 0.5 1.0 1.0 0.5 0.1

0.2 0.4 0.4 0.2

0.1 0.2 0.2 0.2 0.0

0.1 0.0 0.0 0.0 0.0

37 pin p/d= 1.154 h/d= 13.40
inj. subchannel = 1
inj. depth (in) = 32.0
bundle reynolds no.= 4300
mass balance ratio = 1.126
dimensionless ratios of salt concentration*100.0:

0.1 0.8 0.2 0.3 0.3

0.0 0.7 1.9 1.8 0.4

0.2 1.5 2.5 0.9

0.0 1.4 3.1 3.9 1.5 0.6

0.5 2.7 3.9 4.4 1.4

0.3 1.2 3.5 (4.8) 3.5 1.0 0.2

0.1 1.9 4.0 4.1 3.0 1.1

0.1 0.1

0.4 2.7 2.7 3.3 1.2 0.3

0.0 0.3 1.4 4.3 2.2 1.0 0.3

0.2 1.2 0.9 1.0 0.2

0.1 0.6 1.3 1.5 0.9 0.0

0.2 0.4 0.0 0.2

0.1 0.4 0.5 0.4 0.1

0.0 0.0 0.0 0.0 0.0

sup/drv results at minimum mean square indicator
effective eddy diffusivity E*1 = 0.090
swirl velocity ratio C1 = 0.200
min. mean square indicator = 3.97
dimensionless ratios of salt concentration*100.0

0.4 0.5 0.4 0.3 0.3

0.4 1.1 1.5 1.1 0.3

1.0 2.0 2.0 0.9

0.4 1.6 3.3 3.3 1.6 0.2

1.0 2.9 4.2 2.9 0.9

0.3 1.2 3.3 (4.7) 3.3 1.1 0.1

0.6 2.1 4.2 4.2 2.1 0.5

0.2 0.1

0.4 1.6 3.3 3.3 1.6 0.4

0.2 0.8 2.1 2.9 2.1 0.8 0.1

0.4 1.2 1.6 1.2 0.4

0.1 0.6 1.0 1.0 0.5 0.1

0.2 0.4 0.4 0.2

0.1 0.2 0.3 0.2 0.1

0.1 0.1 0.1 0.1 0.0

37 pin p/d= 1.154 h/d= 13.40
inj. subchannel = 1
inj. depth (in) = 32.0
bundle reynolds no.= 5400
mass balance ratio = 1.307
dimensionless ratios of salt concentration*100.0:

```
          0.1   0.2   0.3   0.2   0.1
          0.0   0.7   1.8   1.6   0.2
             0.4   1.1   2.3   0.8
       0.2   1.1   2.9   4.2   1.5   0.3
          0.5   2.6   4.0   4.3   1.2
    0.0   1.1   3.9  (5.8)  4.0   1.0   0.0
       0.4   2.3   4.1   4.6   3.0   0.9
 0.0                                     0.0
       0.3   3.0   3.7   4.1   1.1   0.2
    0.2   0.3   2.2   5.3   2.6   1.0   0.0
          0.2   1.3   1.2   0.8   0.1
       0.0   0.3   1.9   2.6   1.1   0.0
             0.5   0.5   0.1   0.1
          0.0   0.3   0.3   0.2   0.0
          0.0   0.0   0.0   0.0   0.0
```

sup/drv results at minimum mean square indicator
effective eddy diffusivity E*1 = 0.084
swirl velocity ratio C1 = 0.200
min. mean square indicator = 4.72
dimensionless ratios of salt concentration*100.0

```
          0.4   0.4   0.4   0.3   0.2
          0.3   1.1   1.5   1.0   0.2
             0.9   2.1   2.0   0.9
       0.3   1.6   3.5   3.5   1.6   0.2
          0.9   3.0   4.7   3.0   0.9
    0.2   1.1   3.5  (5.4)  3.5   1.1   0.1
       0.5   2.1   4.7   4.7   2.1   0.5
 0.2                                     0.1
       0.4   1.6   3.5   3.5   1.6   0.4
    0.1   0.7   2.1   3.0   2.1   0.7   0.1
          0.4   1.1   1.6   1.1   0.4
       0.1   0.5   0.9   0.9   0.5   0.1
             0.2   0.4   0.4   0.2
          0.1   0.2   0.2   0.2   0.0
          0.1   0.0   0.0   0.0   0.0
```

37 pin p/d= 1.154 h/d= 13.40
inj. subchannel = 1
inj. depth (in) = 32.0
bundle reynolds no.= 6500
mass balance ratio = 1.444
dimensionless ratios of salt concentration*100.0

0.6 0.2 0.5 0.4 0.4

0.4 0.8 1.9 0.9 0.2

1.0 1.4 2.5 1.4

0.0 1.2 3.7 4.6 1.4 0.1

1.0 2.8 4.6 3.9 0.8

0.3 0.7 3.6 (5.4) 3.8 1.0 0.2

0.5 1.4 3.9 4.2 3.0 0.3

0.2 0.1

0.3 2.1 3.6 3.8 0.9 0.6

0.0 0.4 2.0 4.5 2.4 1.7 0.1

0.7 0.7 0.3 0.4 0.3

0.0 0.7 1.2 1.0 0.6 0.0

0.3 0.5 0.2 0.3

0.0 0.4 0.2 0.2 0.0

0.5 0.2 0.3 0.0 0.0

sup/drv results at minimum mean square indicator
effective eddy diffusivity E*1 = 0.087
swirl velocity ratio C1 = 0.200
min. mean square indicator = 3.97
dimensionless ratios of salt concentration*100.0

0.4 0.4 0.4 0.3 0.2

0.3 1.1 1.5 1.0 0.2

0.9 2.1 2.0 0.9

0.3 1.6 3.5 3.5 1.6 0.2

0.9 3.0 4.6 3.0 0.9

0.2 1.1 3.5 (5.3) 3.5 1.1 0.1

0.5 2.1 4.6 4.6 2.1 0.5

0.2 0.1

0.4 1.6 3.5 3.5 1.6 0.4

0.1 0.7 2.1 3.0 2.1 0.7 0.1

0.4 1.1 1.6 1.1 0.4

0.1 0.5 1.0 1.0 0.5 0.1

0.2 0.4 0.4 0.2

0.1 0.2 0.2 0.2 0.0

0.1 0.0 0.0 0.0 0.0

37 pin p/d= 1.154 h/d= 13.40
inj. subchannel = 1
inj. depth (in) = 32.0
bundle reynolds no.= 9400
mass balance ratio = 1.584
dimensionless ratios of salt concentration*100.0:

0.1 0.1 0.6 0.5 0.4
0.1 0.6 2.4 1.4 0.2
0.2 1.2 2.0 1.9
0.1 0.7 3.6 3.8 0.9 0.1
0.9 2.7 4.4 3.7 1.2
0.2 1.2 3.9 (5.6) 4.0 1.3 0.1
0.2 2.1 4.4 4.9 3.0 1.0
0.0 0.0
0.1 2.9 4.0 3.6 1.1 0.5
0.1 0.2 2.4 4.6 2.6 1.2 0.0
0.3 1.1 1.1 0.9 0.2
0.1 0.2 1.6 1.3 0.9 0.0
0.3 0.2 0.1 0.0
0.0 0.4 0.0 0.0 0.0
0.1 0.0 0.0 0.0 0.0

sup/drv results at minimum mean square indicator
effective eddy diffusivity E*1 = 0.089
swirl velocity ratio C1 = 0.200
min. mean square indicator = 4.07
dimensionless ratios of salt concentration*100.0

0.4 0.4 0.4 0.3 0.2
0.4 1.1 1.5 1.0 0.2
0.9 2.1 2.1 0.9
0.3 1.6 3.6 3.6 1.6 0.2
0.9 3.1 4.8 3.1 0.9
0.2 1.1 3.6 (5.5) 3.6 1.1 0.1
0.5 2.1 4.8 4.8 2.1 0.4
0.2 0.1
0.4 1.6 3.6 3.6 1.6 0.3
0.2 0.7 2.1 3.1 2.1 0.7 0.1
0.4 1.1 1.6 1.1 0.3
0.1 0.5 0.9 0.9 0.5 0.1
0.2 0.4 0.4 0.2
0.1 0.2 0.2 0.2 0.0
0.1 0.0 0.0 0.0 0.0

37 pin p/d= 1.154 h/d= 13.40
inj. subchannel = 1
inj. depth (in) = 32.0
bundle reynolds no.= 12200
mass balance ratio = 1.566
dimensionless ratios of salt concentration*100.0:

0.2 0.4 0.8 0.7 0.6

0.1 0.8 2.9 1.6 0.4

0.2 1.3 2.1 2.4

0.1 1.0 3.7 4.2 0.9 0.1

1.0 2.8 4.4 4.1 1.2

0.2 1.2 3.6 (5.4) 4.1 1.5 0.2

0.2 1.2 3.6 4.0 2.9 0.8

0.4 0.2

0.2 2.9 3.2 3.3 1.1 0.5

0.1 0.3 1.9 4.2 2.3 1.1 0.1

0.2 1.0 0.3 0.9 0.2

0.2 0.2 1.3 0.8 0.8 0.0

0.1 0.3 0.4 0.1

0.0 0.3 0.3 0.1 0.1

0.6 0.0 0.1 0.0 0.0

sup/drv results at minimum mean square indicator
effective eddy diffusivity E*1 = 0.099
swirl velocity ratio C1 = 0.200
min. mean square indicator = 4.72
dimensionless ratios of salt concentration*100.0

0.5 0.5 0.5 0.4 0.3

0.4 1.1 1.5 1.1 0.3

1.0 2.1 2.0 0.9

0.4 1.6 3.4 3.4 1.6 0.2

1.0 3.0 4.4 3.0 0.9

0.3 1.1 3.4 (5.1) 3.4 1.1 0.1

0.5 2.1 4.5 4.5 2.1 0.5

0.3 0.1

0.4 1.6 3.4 3.4 1.6 0.4

0.2 0.7 2.1 3.0 2.1 0.7 0.1

0.4 1.1 1.6 1.1 0.4

0.2 0.5 1.0 1.0 0.5 0.1

0.2 0.4 0.4 0.2

0.1 0.2 0.2 0.2 0.1

0.1 0.1 0.1 0.1 0.0

37 pin p/d= 1.154 h/d= 13.40
inj. subchannel = 1
inj. depth (in) = 32.0
bundle reynolds no.= 14800
mass balance ratio = 1.672
dimensionless ratios of salt concentration*100.0:

0.0 0.3 0.5 0.5 0.5

0.1 0.7 1.7 1.1 0.3

0.2 1.2 1.8 1.5

0.1 0.9 3.2 3.7 0.9 0.1

0.9 2.6 4.4 3.4 1.3

0.3 1.3 3.7 5.6 3.8 1.6 0.3

0.6 2.7 3.8 4.1 3.1 0.6

0.1 0.2

0.7 3.0 3.9 3.4 1.1 0.5

0.1 0.4 2.2 4.4 2.2 1.3 0.0

0.5 1.2 0.8 0.8 0.1

0.1 0.3 1.9 1.6 1.1 0.1

0.4 0.3 0.0 0.1

0.2 0.4 0.5 0.3 0.0

0.0 0.0 0.2 0.0 0.0

sup/drv results at minimum mean square indicator
effective eddy diffusivity E*1 = 0.101
swirl velocity ratio C1 = 0.200
min. mean square indicator = 4.08
dimensionless ratios of salt concentration*100.0

0.5 0.5 0.5 0.4 0.3

0.4 1.1 1.5 1.1 0.3

1.0 2.1 2.0 0.9

0.4 1.6 3.4 3.4 1.6 0.2

1.0 3.0 4.5 3.0 0.9

0.3 1.1 3.4 5.1 3.4 1.1 0.1

0.5 2.1 4.5 4.5 2.1 0.5

0.3 0.1

0.4 1.6 3.4 3.4 1.6 0.4

0.2 0.7 2.1 3.0 2.1 0.7 0.1

0.4 1.1 1.6 1.1 0.4

0.2 0.5 1.0 1.0 0.5 0.1

0.2 0.4 0.4 0.2

0.1 0.2 0.2 0.2 0.1

0.1 0.1 0.1 0.1 0.0

37 pin p/d= 1.154 h/d= 13.40
inj. subchannel = 1
inj. depth (in) = 32.0
bundle reynolds no.= 18600
mass balance ratio = 1.583
dimensionless ratios of salt concentration*100.0:

0.4 0.7 0.6 0.6 0.5

0.2 0.7 2.5 1.8 0.3

0.7 1.5 2.3 1.9

0.1 1.5 3.7 4.6 0.9 0.1

1.0 3.0 5.2 3.9 1.4

0.0 1.3 3.7 (5.2) 4.0 1.7 0.1

0.5 1.7 3.6 3.2 3.0 0.6

0.3 0.0

0.9 2.5 3.2 3.1 0.9 0.3

0.1 0.3 2.0 3.8 1.9 0.9 0.0

0.4 0.9 0.7 0.8 0.2

0.2 0.3 1.4 1.2 0.7 0.2

0.2 0.4 0.2 0.0

0.1 0.8 0.1 0.0 0.0

0.3 0.0 0.0 0.1 0.0

sup/drv results at minimum mean square indicator
effective eddy diffusivity E*1 = 0.102
swirl velocity ratio C1 = 0.200
min. mean square indicator = 4.33
dimensionless ratios of salt concentration*100.0

0.5 0.5 0.5 0.4 0.3

0.5 1.1 1.5 1.1 0.3

1.0 2.1 2.0 0.9

0.4 1.6 3.4 3.4 1.6 0.2

1.0 3.0 4.4 2.9 0.9

0.3 1.2 3.4 (5.0) 3.4 1.1 0.1

0.6 2.1 4.4 4.4 2.1 0.5

0.3 0.1

0.4 1.6 3.4 3.4 1.6 0.4

0.2 0.8 2.1 3.0 2.1 0.7 0.1

0.4 1.2 1.6 1.1 0.4

0.2 0.5 1.0 1.0 0.5 0.1

0.2 0.4 0.4 0.2

0.1 0.2 0.2 0.2 0.1

0.1 0.1 0.1 0.1 0.0

37 pin p/d= 1.154 h/d= 13.40
inj. subchannel = 1
inj. depth (in) = 32.0
bundle reynolds no.= 22100
mass balance ratio = 1.423
dimensionless ratios of salt concentration*100.0:

0.3 0.5 0.8 0.6 0.4
0.1 0.8 2.8 1.4 0.2
0.5 1.3 2.3 1.7
0.3 1.3 3.8 4.2 1.0 0.0
1.0 3.1 4.4 4.0 1.5
0.1 1.3 4.2 5.5 3.7 1.3 0.3
0.4 1.6 3.6 3.9 2.8 0.7
0.2 0.0
0.5 2.7 4.1 3.2 0.9 0.1
0.0 0.1 2.1 4.0 2.2 0.9 0.0
0.6 1.3 0.9 0.7 0.0
0.0 0.3 1.5 1.2 0.5 0.1
0.0 0.2 0.3 0.2
0.1 0.1 0.4 0.0 0.0
0.1 0.1 0.1 0.0 0.0

sup/drv results at minimum mean square indicator
effective eddy diffusivity E*1 = 0.099
swirl velocity ratio C1 = 0.200
min. mean square indicator = 4.17
dimensionless ratios of salt concentration*100.0

0.5 0.5 0.5 0.4 0.3
0.4 1.1 1.5 1.1 0.3
1.0 2.1 2.1 0.9
0.4 1.6 3.5 3.5 1.6 0.2
1.0 3.0 4.5 3.0 0.9
0.3 1.1 3.5 5.2 3.5 1.1 0.1
0.5 2.1 4.5 4.5 2.1 0.5
0.3 0.1
0.4 1.6 3.5 3.5 1.6 0.4
0.2 0.7 2.1 3.0 2.1 0.7 0.1
0.4 1.1 1.6 1.1 0.4
0.2 0.5 1.0 1.0 0.5 0.1
0.2 0.4 0.4 0.2
0.1 0.2 0.2 0.2 0.1
0.1 0.1 0.1 0.1 0.0

37 pin p/d= 1.154 h/d= 13.40
inj. subchannel = 1
inj. depth (in) = 32.0
bundle reynolds no.= 26000
mass balance ratio = 1.415
dimensionless ratios of salt concentration*100.0:

0.2 0.6 1.0 0.8 0.5

0.2 0.8 2.6 1.2 0.3

0.5 1.7 2.3 1.6

0.4 1.3 3.9 4.2 1.0 0.1

0.8 3.0 4.8 3.9 1.7

0.4 1.3 3.8 (5.4) 3.7 1.2 0.1

0.3 1.5 3.4 3.9 2.8 0.8

0.0 0.0

0.8 2.7 3.3 3.1 0.9 0.3

0.2 0.3 2.1 3.4 2.1 1.0 0.1

0.5 0.8 0.7 0.7 0.0

0.1 0.2 1.0 0.8 0.8 0.1

0.1 0.2 0.0 0.0

0.0 0.4 0.5 0.0 0.1

0.0 0.3 0.2 0.0 0.0

sup/drv results at minimum mean square indicator
effective eddy diffusivity E*1 = 0.101
swirl velocity ratio C1 = 0.200
min. mean square indicator = 3.92
dimensionless ratios of salt concentration*100.0

0.5 0.5 0.5 0.4 0.3

0.4 1.1 1.5 1.1 0.3

1.0 2.1 2.0 0.9

0.4 1.6 3.4 3.4 1.6 0.2

1.0 3.0 4.5 3.0 0.9

0.3 1.1 3.4 (5.1) 3.4 1.1 0.1

0.5 2.1 4.5 4.5 2.1 0.5

0.3 0.1

0.4 1.6 3.4 3.4 1.6 0.4

0.2 0.7 2.1 3.0 2.1 0.7 0.1

0.4 1.1 1.6 1.1 0.4

0.2 0.5 1.0 1.0 0.5 0.1

0.2 0.4 0.4 0.2

0.1 0.2 0.2 0.2 0.1

0.1 0.1 0.1 0.1 0.0

37 pin p/d= 1.154 h/d= 13.40
inj. subchannel = 1
inj. depth (in) = 32.0
bundle reynolds no.= 29600
mass balance ratio = 1.430
dimensionless ratios of salt concentration*100.0:

0.5 0.1 0.5 0.3 0.0
0.3 1.0 2.5 0.5 0.0
0.7 2.0 2.5 0.2
0.0 1.5 3.3 3.9 1.1 0.0
0.7 3.1 4.9 4.6 1.4
0.4 1.4 4.6 (5.3) 3.7 1.3 0.1
0.3 1.6 4.0 3.8 3.8 0.9
0.0 0.0
0.2 2.7 2.9 3.7 1.2 0.6
0.0 0.5 1.2 2.9 2.2 1.2 0.0
0.5 0.9 0.6 0.9 0.6
0.5 0.7 0.9 1.4 0.5 0.0
0.6 0.6 0.1 0.0
0.3 0.1 0.3 0.0 0.0
0.7 0.6 0.5 0.0 0.0

sup/drv results at minimum mean square indicator
effective eddy diffusivity E*1 = 0.099
swirl velocity ratio C1 = 0.200
min. mean square indicator = 4.45
dimensionless ratios of salt concentration*100.0

0.5 0.5 0.5 0.4 0.3
0.4 1.1 1.5 1.1 0.3
1.0 2.1 2.1 0.9
0.4 1.6 3.5 3.5 1.6 0.2
1.0 3.0 4.5 3.0 0.9
0.3 1.1 3.5 (5.2) 3.5 1.1 0.1
0.5 2.1 4.5 4.5 2.1 0.5
0.3 0.1
0.4 1.6 3.5 3.5 1.6 0.4
0.2 0.7 2.1 3.0 2.1 0.7 0.1
0.4 1.1 1.6 1.1 0.4
0.2 0.5 1.0 1.0 0.5 0.1
0.2 0.4 0.4 0.2
0.1 0.2 0.2 0.2 0.1
0.1 0.1 0.1 0.1 0.0